

Copyright Undertaking

This thesis is protected by copyright, with all rights reserved.

By reading and using the thesis, the reader understands and agrees to the following terms:

1. The reader will abide by the rules and legal ordinances governing copyright regarding the use of the thesis.
2. The reader will use the thesis for the purpose of research or private study only and not for distribution or further reproduction or any other purpose.
3. The reader agrees to indemnify and hold the University harmless from and against any loss, damage, cost, liability or expenses arising from copyright infringement or unauthorized usage.

IMPORTANT

If you have reasons to believe that any materials in this thesis are deemed not suitable to be distributed in this form, or a copyright owner having difficulty with the material being included in our database, please contact lbsys@polyu.edu.hk providing details. The Library will look into your claim and consider taking remedial action upon receipt of the written requests.

The Hong Kong Polytechnic University

Interdisciplinary Division of Biomedical Engineering

**Development of an Arthroscopy-based Water-jet Ultrasound
Indentation System for the Morphological, Acoustic and
Mechanical Assessment of Articular Cartilage Degeneration**

Yan-Ping HUANG

A thesis submitted in partial fulfilment of the requirements for the degree of Doctor
of Philosophy

September 2012

CERTIFICATE OF ORIGINALITY

I hereby declare that this thesis is my own work and that, to the best of my knowledge and belief, it reproduces no material previously published or written, nor material that has been accepted for the award of any other degree or diploma, except where due acknowledgement has been made in the text.

Yan-Ping HUANG

Abstract

Osteoarthritis (OA) is a common disease related to the joints. Millions of patients especially the elderly in the world are suffering both physically and economically from this disease. Cartilage is one of the main tissues that are significantly affected by this disease. Traditionally, plain X-ray radiography and arthroscopy can be used for the diagnosis of cartilage degeneration. However, significant thinning and erosion observed in X-ray imaging and arthroscopy are symptoms of the cartilage degeneration at an advanced stage when currently no effective treatment is available. In contrast, it is much more potential to treat the cartilage degeneration diagnosed at the early stage. Therefore, detection of the early cartilage degeneration is of critical importance but related instruments are still lacking in the field.

The water-jet ultrasound indentation test is a specific technique that has been developed to use an ultrasound-based measurement to obtain morphological, acoustic and mechanical properties from the articular cartilage. These properties are potential indicators of the degeneration of cartilage with osteoarthritic change. In order to make this technique available for clinical applications, this study targets at developing an arthroscopy-based water-jet ultrasound indentation system, mainly a new arthroscopic probe, and corresponding measurement procedure for the purpose of quantitative assessment of the cartilage degeneration in intra-articular measurement. To achieve this goal, a two-step realization scheme was adopted in the study and corresponding experiments were conducted on phantom and cartilage samples to test the utility of the newly developed probe and measurement technique.

For the first step development, a miniaturized probe was realized in an aluminous rod of 12 mm in diameter with the use of a small single element ultrasound transducer. At the second step, a real arthroscopy channel-based probe was successfully designed and fabricated with the aid of intra-articular ultrasound (IAUS) catheter transducer. The main design was realized at the tip of an arthroscopic trochar of 5.5 mm in diameter so that an intra-articular operation is possible for its operation in intact knee joints.

Validation experiments were conducted on 28 silicone phantoms, 40 bovine patellar cartilage samples before and after enzymatic digestions, 40 opened rabbit

knees sacrificed at different time points after the anterior cruciate ligament (ACL) transection surgery and 10 intact porcine knees before and after enzymatic digestion. The measured parameters mainly included the thickness, surface roughness, integrated reflection coefficient (IRC), stiffness and energy dissipation ratio (EDR) of the cartilage. These parameters were compared between normal and degenerated groups or among different groups with different severity of degeneration. Results from the validation experiments showed that the developed probe could be successfully applied in an intra-articular operation with the guide of arthroscopy and the ultrasound-based measurement was effective to differentiate the degeneration of articular cartilage.

In conclusion, in this study an arthroscopy-based water-jet ultrasound indentation probe has been successfully designed and fabricated through a two-step development scheme. This newly developed probe could be used to detect the degeneration of articular cartilage in different models of cartilage degeneration. Future research may include the optimization of the probe design, tests on human cadaver cartilage samples in vitro and clinical trials on human subjects in vivo.

Related Publications

The following is a list of author-related publications or manuscripts in preparation or under review in the study period.

Directly related to the current thesis:

Huang YP, Cheung JCW, Zheng YP. Miniaturization of a water-jet ultrasound indentation probe for detection of articular cartilage degeneration. *Med Eng Phys*, under review.

Huang YP, Zheng YP. Development of an arthroscopy-based water-jet ultrasound indentation probe for detection of articular cartilage degeneration: a preliminary validation study. *Ultrasound Med Biol*, in preparation.

Wang YX, **Huang YP**, Zheng YP. Ultrasound-based measurement for detection of degeneration of articular cartilage in a rabbit knee model of osteoarthritis. *Osteoarthritis Cartilage*, in preparation.

Huang YP, Zheng YP. Intravascular ultrasound (IVUS): a potential arthroscopic tool for quantitative assessment of articular cartilage. *Open Biomed Eng J* 2009;3:13-20.

Wang SZ, **Huang YP**, Saarakkala S, Zheng YP. Quantitative assessment of articular cartilage with morphologic, acoustic and mechanical properties obtained using high frequency ultrasound. *Ultrasound Med Biol* 2010;36:512-27.

Zheng YP, **Huang YP**. More intrinsic parameters should be used in assessing degeneration of articular cartilage with quantitative ultrasound. *Arthritis Res Ther* 2008;10:125.

Huang YP, Zheng YP. Development of a miniaturized water-jet ultrasound indentation probe for detection of articular cartilage degeneration. The 10th International Tissue Elasticity Conference. Arlington, Texas, USA, 2011. p. 93.

Huang YP, Zheng YP. Development and phantom test of a minimized water-jet ultrasound indentation system for arthroscopic measurement of articular cartilage

integrity. In: Lim CT, Goh JCH, editors. IFMBE Proceedings on 6th World Congress on Biomechanics. Singapore: Springer; 2010. p. 903-6.

Huang YP, Zheng YP. Miniaturized water-jet ultrasound indentation probe for assessing the degeneration of articular cartilage. BME 2010, Biomedical Engineering International Conference, 2-5 Nov. Hong Kong, 2010. p. B-8.

Zheng YP, **Huang YP**. Quantitative arthroscopic ultrasonic assessment of articular cartilage - the potential of intravascular ultrasound. IEEE International Ultrasonics Symposium (IUS) 2009. p. 2264-7.

Other related publications generated during the study period:

Huang YP, Saarakkala S, Toyraas J, Wang LK, Jurvelin JS, Zheng YP. Effects of optical beam angle on quantitative optical coherence tomography (OCT) in normal and surface degenerated bovine articular cartilage. Phys Med Biol 2011;56:491-509.

Huang YP, Wang SZ, Saarakkala S, Zheng YP. Quantification of stiffness change in degenerated articular cartilage using optical coherence tomography-based air-jet indentation. Connect Tissue Res 2011;52:433-43.

Huang YP, Zheng YP, Wang SZ, Chen ZP, Huang QH, He YH. An optical coherence tomography (OCT)-based air jet indentation system for measuring the mechanical properties of soft tissues. Meas Sci Technol 2009;20:015805.

Virén T, **Huang YP**, Saarakkala S, Pulkkinen H, Tiitu V, Linjama A, et al. Comparison of ultrasound and optical coherence tomography techniques for evaluation of integrity of spontaneously repaired horse cartilage. J Med Eng Technol 2012;36:185-92.

Saarakkala S, Wang SZ, **Huang YP**, Jurvelin JS, Zheng YP. Characterization of center frequency and bandwidth of broadband ultrasound reflected by the articular cartilage to subchondral bone interface. Ultrasound Med Biol 2011;37:112-21.

Wang SZ, **Huang YP**, Wang Q, Zheng YP, He YH. Assessment of depth and degeneration dependences of articular cartilage refractive index using optical coherence tomography in vitro. Connect Tissue Res 2010;51:36-47.

Wang Q, Zheng YP, Wang XY, **Huang YP**, Liu MQ, Wang SZ, et al. Ultrasound evaluation of site-specific effect of simulated microgravity on articular cartilage. *Ultrasound Med Biol* 2010;36:1089-97.

Nieminen HJ, Zheng YP, Saarakkala S, Wang Q, Toyras J, **Huang YP**, et al. Quantitative assessment of articular cartilage using high-frequency ultrasound: research findings and diagnostic prospects. *Crit Rev Biomed Eng* 2009;37:461-94.

Saarakkala S, Wang SZ, **Huang YP**, Zheng YP. Quantification of optical surface reflection and surface roughness of articular cartilage using optical coherence tomography. *Phys Med Biol* 2009;54:6837-52.

Acknowledgements

I would like to sincerely thank my supervisor, Prof. Yong-Ping Zheng for his supervision of my study during the past several years. Although he was very busy every day, he squeezed some time out of his work to discuss with me every week and gave his professional, insightful and practical suggestions on how to move forward my research project. This study would not have been possible without his patient guidance. In addition to specialty knowledge, he also tried in all opportunities to train me to gain the caliber of leadership and have a broad and high vision for predicting the trend of future technology in my field. In short, Prof. Zheng is an excellent example for me and there are still a lot of virtues for me to learn from him in my future life.

I would also like to thank the help from all the current and previous colleagues in the Biomedical Ultrasound Solution (BUS) group of the BME Division. Among them, Zheng-Ming Huang and William Chiu spent a lot of time in solving the hardware and software problems encountered in integrating the IAUS into my probe design. Special thank is given to them. There were also a lot of great efforts made by Dr. Jun Shi, Dr. Qing-Hua Huang and Dr. Xin Chen in developing the custom-designed software that I used in my study and therefore I also thank them for providing me such a good tool which my study was based on. Li-Ke Wang and James Cheung helped me in fabricating the arthroscopy-based probe and the miniaturized probe. Jun-Feng He was responsible for the fabrication of the custom-designed mechanical indentation system which I used for the silicone phantom test. Shu-Zhe Wang and Dr. Qing Wang together with Xiao-Yun Wang (Rehabilitation Science Department) taught me how to conduct the histological staining of the articular cartilage. To learn the procedure of cartilage histological analysis was interesting and I thanked them for their professional support. I thank Sally Ding for her precious time in checking the grammatical errors of my thesis. She was always so kind to help my group members in writing a good thesis. I would like to thank all other colleagues, including Man Mak, Louis Lee, Yen Law, Patrick Yip, Guang-Quan Zhou, Wei-Wei Jiang, Dr. Tian-Jie Li, Dr. Yong-Jin Zhou, Dr. Cong-Zhi Wang, Dr. Jing-Yi Guo and Jia-Wei Li in working around me as a big team which had brought a lot of fun to me during the past five years.

I would like to thank Dr. William Hau and Eddie for providing me the intravascular ultrasound machine as a tool of IAUS imaging which I used in my project. William especially spent a lot of efforts in trying to solve the problem of radiofrequency signal collection from the machine. I also learned a lot from his expertise in the IVUS and its cardiovascular applications.

I would like to thank Dr. Yue-Xiang Wang from Beijing 301 Hospital in the collaboration of animal study of cartilage degeneration. The rabbit samples provided me a precious opportunity to study the natural degeneration of cartilage in addition to the enzymatic digestion model, which was frequently used in previous investigations.

I also thank the help from the general staff of the BME Division and also previously of the HTI Department. Their miscellaneous support for issues such as expense reimbursement, activity registrations and component fabrication in workshop could let me have more energy focusing on my own project and pushed forward the progress of my study.

I would like to thank all members in my families, including my wife Amy, my parents in hometown and my wife's parents in supporting me to complete the current study. They gave me tremendous support in helping me to get along with difficulties that I encountered during the study. This study would not have been possible without their support.

Finally, I would like to thank the financial support from various grants of the Hong Kong government, the Hong Kong Polytechnic University and other related industrial organizations.

Table of Contents

Abstract.....	ii
Related Publications	iv
Acknowledgements.....	vii
Table of Contents	ix
List of Figures.....	xiii
List of Tables	xx
List of Abbreviations	xxi
 1. Introduction.....	 1
1.1. Osteoarthritis and cartilage.....	1
1.2. Clinical methods for diagnosis of cartilage degeneration	4
1.2.1. Histological and histochemical grading schemes	4
1.2.2. Radiographic assessment	4
1.2.3. Arthroscopic diagnosis.....	5
1.3. Potential methods for detecting early cartilage lesions	7
1.3.1. Conventional mechanical tests.....	7
1.3.2. MRI and CT method	10
1.3.3. Optical methods	12
1.4. Potential method: ultrasound-based techniques	14

1.4.1.	Sonographic examination.....	14
1.4.2.	Quantitative ultrasound.....	16
1.4.2.1.	Morphological properties.....	16
1.4.2.2.	Acoustical properties.....	19
1.4.3.	Ultrasound indentation and water-jet ultrasound indentation.....	23
1.5.	Arthroscopic instrumentation.....	26
1.6.	Objectives of the current study.....	30
2.	Methodology.....	34
2.1.	Development of arthroscopy-based water-jet indentation probe.....	34
2.1.1.	Miniaturized probe with a single-element ultrasound transducer.....	34
2.1.2.	Arthroscopy-based probe with IAUS catheter.....	37
2.2.	Experimental validation studies.....	41
2.2.1.	Experiments on silicone phantoms.....	42
2.2.1.1.	Phantoms preparation.....	42
2.2.1.2.	Phantom tests.....	42
2.2.1.3.	Extraction of parameters.....	43
2.2.1.4.	Statistical analysis.....	44
2.2.2.	Experiments on bovine cartilage in vitro.....	44
2.2.2.1.	Cartilage specimen preparation and histology.....	44
2.2.2.2.	Cartilage tests.....	46
2.2.2.3.	Extraction of parameters.....	48
2.2.2.4.	Statistical analysis.....	52
2.2.3.	Experiments on rabbit cartilage in situ.....	54
2.2.3.1.	Animal model and specimen preparation.....	54
2.2.3.2.	Experimental tests.....	55
2.2.3.2.1.	High frequency ultrasound measurement.....	55
2.2.3.2.2.	Water-jet indentation and contact indentation test.....	58
2.2.3.2.3.	Histology and grading.....	59

2.2.3.3. Extraction of parameters	60
2.2.3.4. Statistical analysis	63
2.2.4. Experiments on cartilage in intact porcine knees.....	64
2.2.4.1. Feasibility of IAUS for detection of cartilage degeneration	64
2.2.4.1.1. Measurement system.....	64
2.2.4.1.2. Specimens and experimental tests	66
2.2.4.1.3. Data processing method.....	67
2.2.4.1.4. Statistical analysis.....	70
2.2.4.2. Arthroscopic tests on cartilage in intact porcine knees.....	70
2.2.4.2.1. Samples, experimental setup and tests.....	71
2.2.4.2.2. Data processing and statistical analysis	73
3. Results	74
3.1. Results of experiments on phantoms.....	74
3.2. Results of experiments on bovine cartilage in vitro	75
3.2.1. Reproducibility study	75
3.2.2. Enzymatic digestion effect.....	75
3.2.3. Comparisons with reference methods	77
3.3. Results of experiments on rabbit cartilage in situ	79
3.3.1. Histological results.....	79
3.3.2. Changes of parameters with post-surgery time.....	80
3.3.3. Changes of parameters with pathology	83
3.3.4. Inter-correlations among measured parameters	89
3.4. Results of tests using the arthroscopy-based probe.....	91
3.4.1. Results of IAUS for detection of cartilage degeneration	91
3.4.2. Results of tests on cartilage in intact porcine knees.....	94
4. Discussion	95
4.1. Instrumental development	95

4.1.1.	Development of miniaturized probe.....	95
4.1.2.	Limitations and future development of the arthroscopic probe	97
4.2.	Experimental validation studies	99
4.2.1.	Phantom tests	99
4.2.2.	Tests on bovine cartilage in vitro	100
4.2.3.	Tests on rabbit cartilage in situ	105
4.2.3.1.	Change of various parameters with post-surgery time.....	105
4.2.3.2.	Association of parameters with histology and inter-correlations.....	107
4.2.4.	Arthroscopic tests on cartilage in intact porcine knees.....	110
4.2.5.	Limitations of experimental studies and future research directions....	111
5.	Conclusions and Suggestions on Future Work	115
	References	116

List of Figures

Figure 1-1	Zonal structure of the articular cartilage (Herzog 2006).....	2
Figure 1-2	X-ray of normal knee (left) and knee with cartilage degeneration as showed by narrowed joint space (right).....	5
Figure 1-3	Typical arthroscopic surgery. (a) A general view of the operation and (b) a specific view of the use of instruments (Treuting 2000).....	6
Figure 1-4	Mechanical testing methods for the articular cartilage. (a) Unconfined compression; (b) Confined compression; (c) Indentation (Knecht et al. 2006).....	9
Figure 1-5	(a) The near infrared reflection spectroscopy (NIRS) system with a conventional arthroscopic hook; (b) The operation of the probe with the arthroscopic observation; (c) Probe under the arthroscopic view; (d) The front view of the probe with light source fibers from the surroundings and the center fiber which can collect the optical signal (Spahn et al. 2007).....	13
Figure 1-6	Sonographic grading of cartilage degeneration (from grade 1 to grade 6) using the B-mode images obtained through transcutaneous ultrasound. The grading is made by descriptions of surface sharpness, layer clarity, thickness and uniformity of the thickness and etc (Lee et al. 2008).....	14
Figure 1-7	(a) The compact tissue ultrasound palpation system with a probe and the main control box; (b) A typical indentation process and the load/indentation, i.e., force/deformation, curve for calculating the tissue stiffness.	24
Figure 1-8	The water-jet ultrasound indentation system developed for measuring the mechanical properties of soft tissues. (a) The probe for water-jet indentation and (b) the data collection schematics of the system (Lu et al. 2005).....	24
Figure 1-9	(a) A schematics showing the principle of an arthroscopic indentation device for the testing of articular cartilage stiffness; (b) The ArtScan probe; (c) A side view and bottom view of the head of the indentation probe (Lyyra et al. 1995).....	28

Figure 1-10	Improved arthroscopic indentation system for mechano-acoustical measurement of articular cartilage. (a) Principle (b) Indentation operation and (c) acoustical reflection measurement (Laasanen et al. 2002).....	29
Figure 1-11	A water-jet indentation system incorporating an optical measurement for the measurement of mechanical properties of cartilage (Duda et al. 2004).	30
Figure 2-1	(a) A schematic diagram of the probe in Step-1 design; (b) A real picture of the probe. “1” and “2” indicate rotation or orientation of the probe for an optimal reception of the ultrasound signal during operation; (c) A comparison with the previous prototype of the water-jet ultrasound indentation probe.	35
Figure 2-2	A schematics of the data collection system for the miniaturized water-jet ultrasound indentation probe.....	36
Figure 2-3	Software interface for the data collection of the water-jet ultrasound indentation system. The main two parameters acquired in the software are ultrasound A-line signal from the tissue and the water pressure signal. A-line signals were further processed to obtain the deformation.	37
Figure 2-4	(a) A real picture of the IAUS probe; (b) An overall view of the aluminous adaptor for incorporation of the IAUS transducer used in arthroscopic channel; (c) A sectioned view of the internal structure of the adaptor. The black part of the IAUS transducer indicates the active elements which transmit and receive ultrasound signals; (d) A real picture of the arthroscopy channel-based water-jet ultrasound indentation probe.....	38
Figure 2-5	A schematics showing the main components of the arthroscopy-based water-jet ultrasound indentation system.	39
Figure 2-6	Software interface for the data collection of the arthroscopy-based water-jet ultrasound indentation system. The two parameters acquired in the software are ultrasound A-line signal from the cartilage tissue and the water pressure signal Compared to the software version of the single element transducer-based miniaturized	

probe, a B-mode image is shown in this software interface and a target line is selected for the signal display and data storage.	40
Figure 2-7 A flowchart of the experimental validation studies for the developed arthroscopy-based water-jet ultrasound indentation system.	41
Figure 2-8 The test of phantom under (a) the miniaturized water-jet indentation probe and (b) a custom-designed indentation device.	43
Figure 2-9 (a) A typical picture of a bovine patella; (b) Embedding of an osteochondral disk in a sample holder.	45
Figure 2-10 (a) The experimental setup for the miniaturized water-jet indentation probe. “1” indicates the flexible adjustment for the distance between probe and sample, and “2” indicates adjustment of orientation of the probe; (b) A typical loading profile as shown by the force and deformation curves along with time	47
Figure 2-11 Mechanical indentation test for the articular cartilage. Details of the indenter on the specimen are enlarged as shown on the right side.	48
Figure 2-12 The measurement of cartilage thickness by the time of flight calculated from the two reflections indicating the cartilage surface and cartilage-bone interface. The red rectangular window indicates where to apply the Hamming windowing in order to calculate the integrated reflection coefficient (IRC) of the cartilage surface.	49
Figure 2-13 Typical force/deformation curves for the cartilage specimen before and after the trypsin digestion. A symbolic curve is also shown on the right to indicate how to calculate the energy dissipation ratio (EDR) from one cycle of loading and unloading.	52
Figure 2-14 Preparation of the rabbit knee samples for the test of cartilage. Left: the tibial side; Right: the femoral side. Typical positions for the assessment are indicated by arrows.	54

Figure 2-15	(a) The high frequency ultrasound imaging system (Vevo 770); (b) The RMV708 ultrasound probe.	56
Figure 2-16	(a) The scanning of the rabbit cartilage using the high frequency ultrasound; (b) The patten of the scanning directions for the ultrasound measurement at one point. The scanning width is ~ 1.5 mm for each direction.	57
Figure 2-17	(a) A typical software interface showing the B-mode image for the knee rabbit cartilage at the femoral lateral condyle. The cartilage layer can be seen where two bright lines indicate the cartilage surface and the cartilage-bone interface; (b) A typical software interface showing the collection of RF signals. A region of interest (ROI) was selected at the B-mode images where 100 RF lines were collected without saturation of the amplitude. The single line RF signal and its spectrum coming from the dotted line are shown on the right lower corner of the image.	58
Figure 2-18	(a) The fixation of the knee sample for an indentation test in a sample holder. The two white arrows indicate the two arms can be adjusted by the knob to clamp the sample for a firm fixation; (b) The indentation test of cartilage sample with the water-jet ultrasound indentation probe.	59
Figure 2-19	The fixation of the rabbit knee sample for an indentation test using the Instron mechanical testing machine.	60
Figure 2-20	Matlab GUI interface for processing the data from the acoustic measurement. Thickness, roughness index and acoustic parameters were calculated in this GUI. For thickness, two cursors were used to indicate the two interfaces of the cartilage layer; For URI, a cartilage surface region was selected to indicate where to extract the surface profile and then the roughness index; for integrated reflection coefficient, the cartilage surface region was also used.	61
Figure 2-21	(a) The catheter tip which included the ultrasound array elements in the IAUS system. The diameter of the catheter is about 1.2 mm. The core part of the ultrasound transducer is shown as the yellow part of the catheter tip; (b) A typical IAUS B-mode image of articular cartilage. The two interfaces of the cartilage are shown. Arrowhead: the cartilage-saline solution interface; arrow: the cartilage-	

subchondral bone interface. The rectangular window shows where the average was taken (~ 1 mm in width) for obtaining the parameters of the articular cartilage; (c) Typical interface echoes after spatial averaging in the selected rectangular region. Arrowhead: the cartilage-saline solution interface; arrow: the cartilage-subchondral bone interface; diamond: the center of the image.	64
Figure 2-22 (a) A typical B-mode image of articular cartilage obtained from the Vevo ultrasound imaging system. The two interfaces of the cartilage are shown. Arrowhead: the cartilage-saline solution interface; arrow: the cartilage-subchondral bone interface. The rectangular window shows where the average was taken (~ 1 mm in width) for calculating the parameters of the articular cartilage; (b) Typical interface echoes after spatial averaging in the selected region. Arrowhead: the cartilage-saline solution interface; arrow: the cartilage-subchondral bone interface.	66
Figure 2-23 The processing of (a) the image data from IAUS system and (b) the RF signals from Vevo 770 imaging system using custom-designed GUI in Matlab..	68
Figure 2-24 The change of normalized factor F_c according to distance to the transducer surface.....	69
Figure 2-25 (a) The test of intra-articular cartilage using the developed water-jet ultrasound indentation probe with the help of the arthroscopy; (b) A typical view of the water-jet indentation probe under arthroscopy.....	71
Figure 2-26 (a) The arthroscopic system used for guiding the tested position of the water-jet ultrasound indentation probe; (b) Enlarged view of the camera tip and the developed water-jet indentation probe.....	72
Figure 2-27 (a) An IAUS imaging of the articular cartilage obtained through the water-jet channel of the developed probe; (b) In the custom-designed software, a typical A-line signal of the cartilage layer is shown.....	72
Figure 3-1 The correlation between the two f/d coefficients measured from the water-jet ultrasound indentation and the Instron indentation.....	74

- Figure 3-2 The changes of various parameters measured by the water-jet ultrasound indentation system after the trypsin and collagenase digestions: (a) Thickness; (b) IRC; (c) Stiffness coefficient; (d) Young's modulus; (e) EDR obtained from the water-jet indentation; and (f) EDR obtained from the Instron indentation. . 76
- Figure 3-3 The relationship between the stiffness coefficient (SC) from the water-jet indentation and the Young's modulus (E) from the rigid Instron indentation. 78
- Figure 3-4 The relationship between EDR from the water-jet indentation and that from the rigid Instron indentation. 78
- Figure 3-5 Typical histological pictures showing the Safranin O and fast green staining for the (a) normal (b) collagenase-digested and (c) trypsin-digested cartilage. It was typically observed that in collagenase-digested cartilage, there was partial loss of proteoglycans (red color) while they were completely depleted in trypsin-digested samples. Arrows indicate the cartilage-bone interfaces. 79
- Figure 3-6 Typical histological images showing the Safranin O red and fast green staining for different cartilage samples. (a) Normal cartilage mainly stained with Safranin O red; (b) Grade 1 with uneven surface and loss of Safranin O staining in the superficial layer of cartilage; (c) Grade 2 with surface fibrillation and loss of Safranin O staining in the superficial and middle layers of cartilage; (d) Grade 3 with defect of partial cartilage thickness and loss of Safranin O staining in the superficial and middle layers of cartilage. The arrow indicates the cartilage-bone interface. 80
- Figure 3-7 The change of various parameters: (a) Pathological grade, (b) thickness, (c) URI, (d) IRC, (e) Stiffness coefficient, (f) Young's modulus E along with the post-surgery time. 82
- Figure 3-8 Distribution of the pathological grade of cartilage lesions (a) at the femoral side and (b) at the tibial side. An overall increase of the histological grades from Week-0 to Week-9 for the cartilage lesion could be observed in the figure, which indicated the progression of OA in the rabbit knee. 83

Figure 3-9	Comparisons of various measured parameters among groups classified according to the pathological grade. (a) Thickness; (b) URI; (c) IRC; (d) Stiffness coefficient and (e) Young's modulus E . The number of tested points was 18, 25, 24, 9 and 4 for the 5 groups at the femoral side and 37, 15, 17, 9, 2 for the 5 groups at the tibial side, respectively.	86
Figure 3-10	The correlations among different parameters measured in the current study. (a) Thickness vs. URI; (b) Thickness vs. IRC; (c) Thickness vs. SC; (d) URI vs. IRC; (e) SC vs. URI and (f) SC vs. IRC. “*” represents $p < 0.05$, “**” represents $p < 0.01$ and “***” represents $p < 0.001$	90
Figure 3-11	The correlation between Young's modulus (E) from the Instron indentation and stiffness coefficient from the water-jet indentation (the total sample number for correlation analysis: $n = 160$).	91
Figure 3-12	The correlation of thickness measured from IAUS and Vevo ultrasound imaging for cartilage specimens before enzyme digestion ($n = 16$).	92
Figure 3-13	A comparison of (a) thickness and (b) stiffness coefficient for the cartilage before and after the trypsin digestion in the intact porcine knee. No significant change of thickness ($p > 0.05$), but significant decrease of the cartilage stiffness ($p < 0.001$) were detected after the trypsin digestion.	94
Figure 4-1	(a) A 3D scatter plot of three parameters IRC, stiffness and EDR in normal and degenerated cartilage before and after trypsin and collagenase digestion. The corresponding projection of the 3D data sets into 2-D plane in terms of mean and standard deviation of different groups is also plotted in (b) IRC vs. stiffness, (c) IRC vs. EDR and (d) stiffness vs. EDR. Normal cartilages included all those samples before trypsin digestion and before collagenase digestion. NOR: normal, AFT_TRY: trypsin-digested samples, AFT-COL: collagenase-digested samples.	103
Figure 4-2	A simple demonstration of the arthroscopic operation of the developed probe in the human knee test in vivo.	114

List of Tables

Table 3-1	Changes of various parameters after enzymatic digestions.	77
Table 3-2	The various parameters among different post-surgery groups and comparisons at the femoral side.	84
Table 3-3	The various parameters among different post-surgery groups and comparisons at the tibial side.	85
Table 3-4	The comparison of parameters for samples with different pathological grades at the femoral side.	87
Table 3-5	The comparison of parameters for samples with different pathological grades at the tibial side.	88
Table 3-6	The correlations among different parameters measured in the study of rabbit cartilage.	89
Table 3-7	Effect of trypsin treatment on cartilage measured by IAUS.	93
Table 3-8	Effect of collagenase treatment on cartilage measured by IAUS.	93

List of Abbreviations

2D: two-dimensional

3D: three-dimensional

ACL: anterior cruciate ligament

CT: computed tomography

CV: coefficient of variation

dGEMRIC: delayed gadolinium-enhanced MRI of cartilage

EDR: energy dissipation ratio

EDTA: ethylenediaminetetraacetic acid

FEM: finite element method

GAG: glycosaminoglycan

GUI: graphic user interface

IAUS: Intra-articular ultrasound

ICRS: International Cartilage Repair Society

IRC: integrated reflection coefficient

IAUS: intra-articular ultrasound

IVUS: intravascular ultrasound

LVDT: linear variable differential transformer

MRI: magnetic resonance imaging

NIR: near infrared

OA: osteoarthritis

OARSI: Osteoarthritis Research Society International

OCT: optical coherence tomography

PCL: posterior cruciate ligament

PG: proteoglycan

QUS: quantitative ultrasound

RF: radiofrequency

ROI: region of interest

SC: stiffness coefficient

SCV: standardized coefficient of variation

SEM: scanning electron microscopy

SD: standard deviation

SNR: signal-to-noise ratio

SOS: speed of sound

TUPS: tissue ultrasound palpation system

URI: ultrasound roughness index

US: ultrasound

YM: Young's modulus

1. Introduction

1.1. Osteoarthritis and cartilage

Arthritis is a common disease affecting the joints in the musculoskeletal system of the human body. According to previous epidemiological survey and prediction, the number of persons associated with arthritis would rise from 40 million (15% of the total population) in 1995, to 59 million (18% of the population) by 2020 in the United States (Lawrence et al. 1998). Osteoarthritis (OA) is the most common type of arthritis and the number of people who have clinical signs and symptoms of OA was conservatively estimated to be as large as nearly 21 million (12% of the population) in the late 1990s in USA (Lawrence et al. 1998). According to a study conducted in France, the cost for OA in 2002 was about 1.6 billion Euros, which contributed about 1.7% of expense of the French health insurance system (Le Pen et al. 2005). In Hong Kong, according to a survey conducted by the Chinese University of Hong Kong in 2000 (<http://www.cuhk.edu.hk/ipro/010306e.htm>, successfully accessed on Apr 4, 2012), for Hong Kong Chinese over 50 years old, 7% men and 13% women could be diagnosed to have knee OA. The annual direct cost (excluding joint replacement) for treating OA for Hong Kong Chinese was from HK\$ 11,690 to 40,180, with an indirect cost being HK\$ 3,300-6,640. The total cost is about 0.28% of gross national product (GNP) of Hong Kong (Woo et al. 2003). The annual cost is also increasing with an increasing number of aging people and with the increased prevalence of risk factors such as obesity. Therefore, OA has brought a big financial burden to both society and individuals. It deserves special efforts to have systematic and complete management of this disease, which can reduce the social and economic burden through studying the epidemiology, risk factors and developing new diagnostic and intervention methods for this disease (Sharma et al. 2006).

Osteoarthritis, according to the American College of Rheumatology (ACR), is defined as “a heterogeneous group of conditions that lead to joint symptoms and signs which are associated with defective integrity of articular cartilage, in addition to related changes in the underlying bone and at the joint margins” (Altman et al. 1986). Another consensus definition of OA was “a result of both mechanical and biologic

events that destabilize the normal coupling of degradation and synthesis of articular cartilage chondrocytes and extracellular matrix, and subchondral bone...Ultimately, OA diseases are manifested by morphological, biochemical, molecular, and biomechanical changes of both cells and matrix which lead to softening, fibrillation, ulceration, loss of articular cartilage, sclerosis and eburnation of subchondral bone, osteophytes, and subchondral cysts..." (Kuettnner and Goldberg 1995). From the above descriptions, it can be seen that one significant change associated with OA is related to a thin, but very important tissue – articular cartilage.

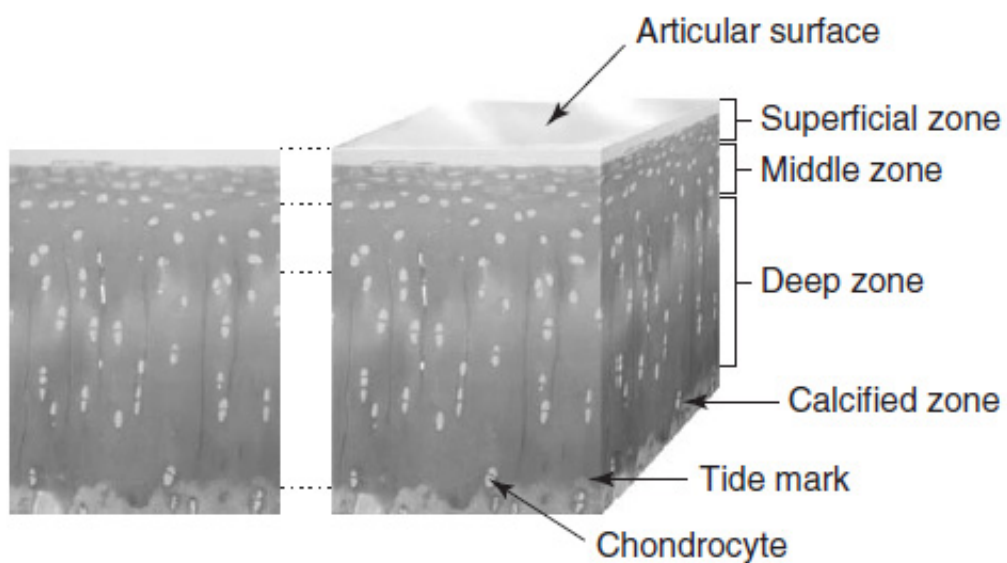


Figure 1-1 Zonal structure of the articular cartilage (Herzog 2006).

Articular cartilage is a mechanically functional and lubricative fibrous connective tissue covering the bone surface in the joint, acting as a cushion during the joint movement. In normal status, the tissue will look bluish white and glistening. For its chemical compositions, it mainly includes a large portion (> 90%) of water, collagen, proteoglycans, and non-collagenous protein (Buckwalter and Mankin 1997). The articular cartilage is structurally composed of extracellular matrix and only a sparse portion of special cell – chondrocytes. No vasculature, nerve and lymph tissue exists in articular cartilage. Although the density of chondrocytes is low, they play an important role in establishing the balance between matrix degradation and synthesis, thus maintaining the function of the articular cartilage. With aging, the capability of the chondrocytes to synthesize the matrix macromolecule and their response to

stimuli, including growth factors, will decrease and this has been thought to contribute to the articular cartilage degeneration. The extracellular matrix is a collagenous fibril network that includes macromolecular aggregates of proteoglycans. It is the collagen fibrils, proteoglycan network, their interactions and water that mainly contribute to the mechanical properties of the cartilage. According to the morphology and distribution of the collagen fibrils and chondrocytes, articular cartilage is normally divided into four layers, i.e., starting from the surface, the superficial zone, middle zone, deep zone and the calcified zone (Figure 1-1) (Herzog 2006).

Complete reasons for the initiation of osteoarthritis are not so clear yet. However, risk factors that have been proposed include the generic factors, injury, occupational physical activities, aging and obesity (Sharma et al. 2006). Early changes in the OA process may include the cartilage swelling, chondrocyte proliferation and surface fibrillation. Then the cartilage becomes softened with proteoglycan degradation. Associated with the progression of OA, clefts develop deep into the cartilage. Ultimately, total erosion of the cartilage may ensue (Pelletier et al. 2001). Conventional methods and some recently proposed approaches for the diagnosis of the articular cartilage degeneration are introduced as in the following subsections.

The Introduction part is organized as follows. Firstly in Subsection 1.2, clinical methods for diagnosis of cartilage degeneration are given. Currently these methods are used routinely in clinics but they are either inappropriate or impossible for the early detection of cartilage degeneration in vivo. Then potential methods for the early detection of cartilage degeneration or for assessment of cartilage treatment efficacy are introduced in Subsection 1.3. They include the mechanical testing methods, MRI and CT methods, optical methods, except that the ultrasound-based method which is described separately in Subsection 1.4 as the most pertinent part of the current study. Then, some techniques related to the arthroscopic instrumentation are briefly introduced in Subsection 1.5 because the goal of the current study is to develop such an arthroscopic probe. Finally the objectives of my study are summarized in Subsection 1.6.

1.2. Clinical methods for diagnosis of cartilage degeneration

The degeneration of articular cartilage can be classified into different stages. However, different classification schemes are existent up to date and there is no consensus on selecting a universal scheme for the purpose of degeneration classification. In general, the grading system can be divided into the following categories according to the sample preparation methods and techniques used.

1.2.1. Histological and histochemical grading schemes

When histology is available, the lesion of cartilage can be classified based on the examination of several histological and histochemical factors, which mainly include structure, cell, staining and tidemark integrity, as used in one of the most famous grading systems - the Mankin scoring system (Mankin et al. 1971). A grade ranging from 0 to 6 can be given to rate the condition of each factor and a summation of the marks for each factor will be used to represent the overall cartilage degeneration. Although the histological and histochemical grading systems have been demonstrated to be significantly correlated with the tissue physiology such as the content of polysaccharide of cartilage and can be effectively used to grade the severity of cartilage lesions, they can never be used for the assessment of living tissues because thin and regular sections of samples should be prepared for microscopic analysis. Therefore, non-dissection grading schemes are necessary for clinical applications.

1.2.2. Radiographic assessment

Radiographic assessment through the X-ray imaging has been used as a conventional method to confirm the severe degeneration of articular cartilage. Normally the cartilage cannot be seen in the radiographic image but a thin and dark space with a universal thickness between the femoral condyles and the tibial plateaus will indicate a normal cartilage. In the situation of osteoarthritis, the degeneration of cartilage makes the joint space become narrower and therefore a phenomenon of joint space narrowing may indicate the existence of cartilage degeneration. Figure 1-2 shows the typical X-ray photograph of normal knee and knee with obvious joint space narrowing due to cartilage degeneration. Grading scales were also suggested to

differentiate the severity of osteoarthritis based on the condition of joint space. For example, Scott et al. used a four-point scale from 0 to 3 to define the severity of joint space narrowing and studied the measurement reliability (Scott et al. 1993). The problem of this kind of grading based on joint space width is that it is hard to detect the early degeneration of articular cartilage, because the width is just an indirect reflection of the cartilage thickness. Furthermore, the X-ray radiograph is just a plane projection of mainly the bone structure, and therefore the results can be easily affected by the angle of projection in real practice (Le Graverand et al. 2006), which may increase the variation of measurement and reduce the reliability of results. In general, the plane radiography is not enough to specifically detect the lesion of articular cartilage in the joint. Even when the cartilage degeneration is detected by the radiographic method, it is usually at the very late stage and the degeneration at this stage is nearly impossible to be cured. Therefore, it is necessary to seek the help of other techniques for the specific detection of cartilage lesions.

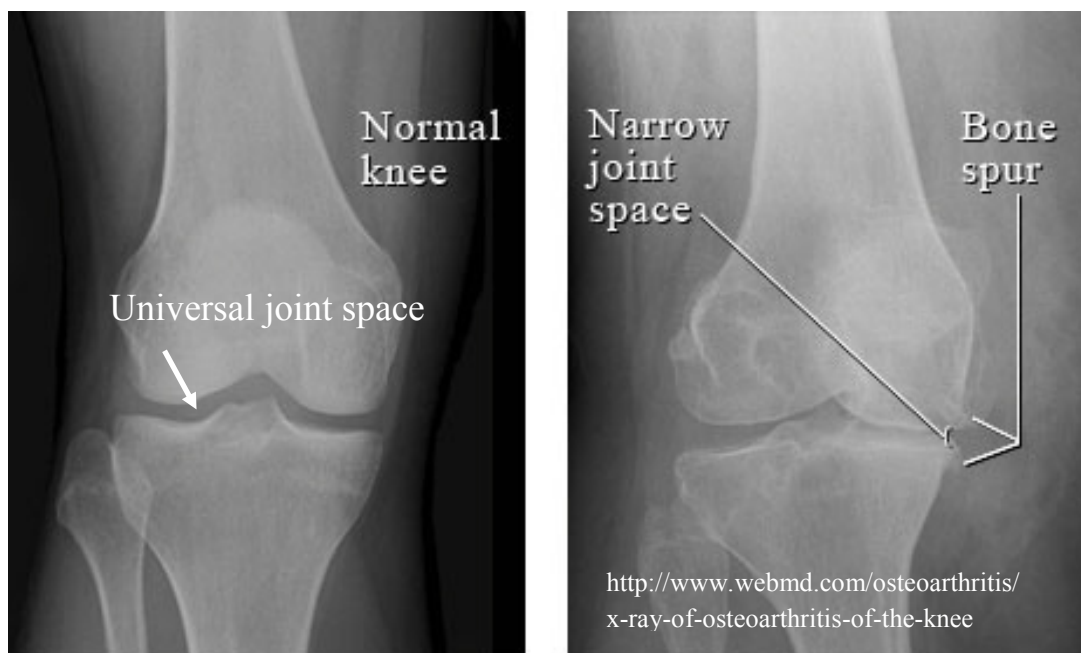


Figure 1-2 X-ray of normal knee (left) and knee with cartilage degeneration as showed by narrowed joint space (right).

1.2.3. Arthroscopic diagnosis

Arthroscopy is a specific type of endoscopy used for the inspection of joint situation. The use of arthroscopy for the assessment of articular cartilage is mainly

based on the visual observation from the cartilage surface, i.e., the morphology of the lesion. A typical arthroscopic operation is shown in Figure 1-3. Two to three channels will be used in the process with one used for the injection of irrigation fluid and observation and the other for the specific operation such as surgery. The lesion of the cartilage can be directly observed under the arthroscopic view, which can be video-taped for off-line processing.

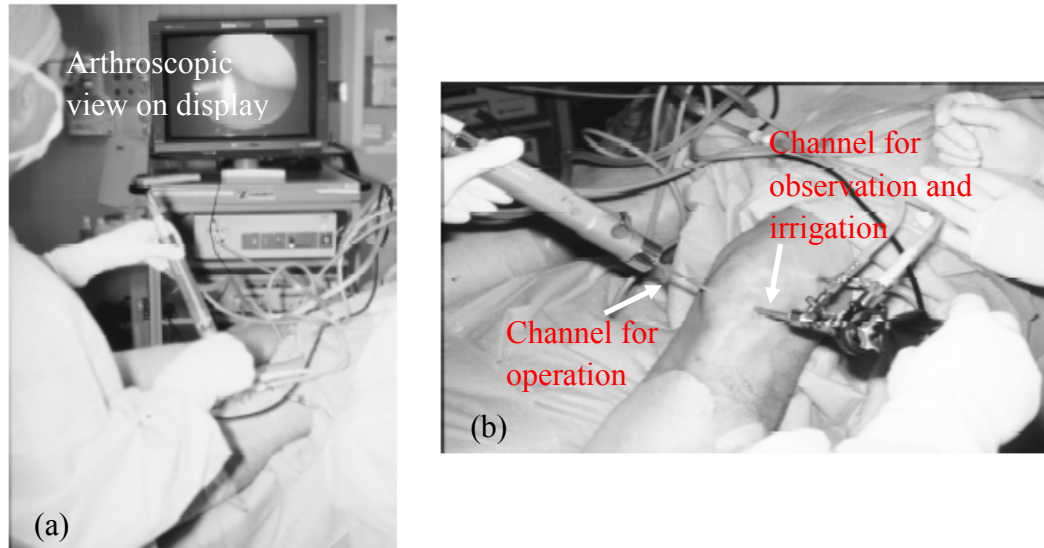


Figure 1-3 Typical arthroscopic surgery. (a) A general view of the operation and (b) a specific view of the use of instruments (Treuting 2000).

A lot of grading methods have been developed for the arthroscopic evaluation of cartilage lesions and have been well reviewed in past studies (Giurea et al. 1998; Oakley and Lassere 2003). For example, the most famous and earliest grading method – the Outerbridge scale divides the cartilage lesions into four stages as defined by: “in grade 1 there are softening and swelling of the cartilage; in grade 2 there are fragmentation and fissuring in an area half an inch or less in diameter; grade 3 is the same as grade 2 but an area more than half an inch in diameter is involved; in grade 4 there is erosion of cartilage down to bone” (Outerbridge 1961). Recently the grading method from the International Cartilage Repair Society (ICRS) has become popular in assessing the cartilage lesion (Brittberg and Winalski 2003). The ICRS method grades the cartilage lesion mainly based on the surface condition and the lesion depth: grade 0 stands for the macroscopically normal cartilage without notable defects; grade 1 means intact surface but with superficial fibrillation and slight softening; deeper lesion that extends less than 50% of the depth is defined as grade 2; further

lesion into larger than 50% of the cartilage depth but not in the bone is defined as grade 3; finally, when lesion extends into the bone, grade 4 can be given (Brittberg and Winalski 2003). Spahn et al. have demonstrated that the inter-observer reliability of arthroscopic grading of cartilage lesion is poor (Spahn et al. 2011). A related survey conducted by the same authors on orthopaedic surgeons shows that arthroscopists do not regard the arthroscopy as a “gold standard” for the assessment of cartilage lesion and feel unsure of the results in general, or at least in some cases (Spahn et al. 2009). The poor reliability and uncertain feeling of the diagnosis for the arthroscopic assessment of cartilage lesion mainly originates from the subjective description of the lesion which is very dependent on personal experience of the observer. A thorough review of the usefulness of arthroscopy for assessment of cartilage lesion shows that it is still necessary to develop quantitative methods associated with corresponding devices for the purpose of cartilage assessment. In the following part, recent research in this direction is briefly introduced.

1.3. Potential methods for detecting early cartilage lesions

Several methods that are potential for quantitatively assessing the cartilage lesions are reviewed in the following part. Target markers for assessing the lesion of cartilage generally include the morphological properties, mechanical properties, acoustical properties and optical properties of the cartilage. Accordingly, the methods being investigated include the conventional mechanical tests which directly measure the mechanical properties; the medical imaging methods including the MRI and CT-based techniques and spectroscopic methods; and the ultrasound-based methods that are specifically introduced in detail as it is the main method adopted in this study.

1.3.1. Conventional mechanical tests

Articular cartilage is functioning as a mechanical support tissue so the mechanical properties of this tissue are very important for the joint activities. It is generally recognized that the tensile strength of articular cartilage is mainly determined by the collagen network while the compressive stiffness is mainly related to the proteoglycan concentrations (Herzog 2006). As the concentration of collagen and proteoglycans varies in different layers, the mechanical properties of cartilage change

along the depth direction. This has been demonstrated by that the compressive stiffness increased from the superficial zone to the deep zone (Chen et al. 2001; Schinagl et al. 1997) while the tensile strength decreased along this direction (Kempson et al. 1968). These properties were also found to decrease with the aging process (Armstrong and Mow 1982; Kempson 1982).

Mechanical behavior of the articular cartilage is very complicated due to a complex structure of the tissue considering the collagen network, fluid and osmotic swelling induced by proteoglycans. Models to simulate the mechanical behavior of the articular cartilage have also been developed from the single phase (time-independent) to multiple-phase analysis (Hasler et al. 1999). The single phase model assumes that the articular cartilage is a homogeneous and isotropic layer bonded to the subchondral bone and the mechanical properties are time-independent. Young's modulus together with Poisson's ratio is enough to represent the mechanical properties of the cartilage (Hayes et al. 1972). This model is appropriate to represent the instantaneous or equilibrium response of the cartilage under testing when no fluid flow exists. However, this model is not enough for interpreting the viscoelastic behavior of the cartilage in the stress relaxation or creep test. In these tests, the tissue is observed to have strong time-dependent phenomenon which comes from the viscoelastic properties of the cartilage. Then a biphasic model including the porous solid phase (the extracellular matrix) and the incompressible fluid phase was proposed to achieve a better description of the mechanical properties of the cartilage (Mak et al. 1987; Mow et al. 1989). In this model two pairs of material properties, one for the porous solid phase and the other for the fluid phase can be extracted from the experimental data. These parameters are the aggregate modulus H_A and Poisson's ratio ν_s for the solid phase and the permeability coefficient k for the fluid phase. The biphasic model will coincide with the single phase model at the infinite time of the stress-relaxation or creep tests where equilibrium status of the tissue has been reached. Furthermore, a triphasic model was also proposed for the articular cartilage in order to account for the mechanical effect from the third phase – ions. As the proteoglycans are existing in the main form of glycosaminoglycans (GAG) with negative charges and they will repel each other during the chemical or physical loading test, the third phase is very useful for analyzing the swelling behavior and extraction of mechanical properties of the tissues (Wang et al. 2007). Finite element method (FEM)

incorporating these single, biphasic or triphasic theories has been developed for a better analysis of the mechanical testing of articular cartilage (Blankevoort et al. 1991; Simon et al. 1996; Wu et al. 1998). However, the clinical usefulness of these multiple-phase models still needs to be demonstrated.

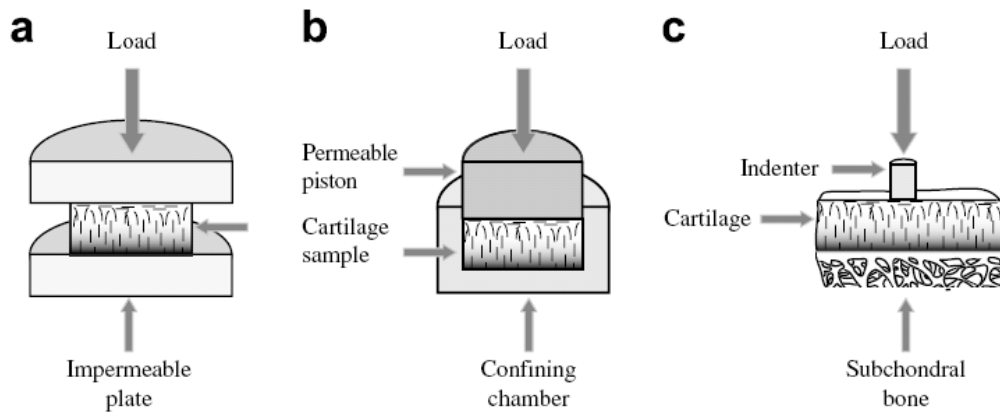


Figure 1-4 Mechanical testing methods for the articular cartilage. (a) Unconfined compression; (b) Confined compression; (c) Indentation (Knecht et al. 2006).

Conventional mechanical testing methods such as compression (both confined and unconfined compression) and indentation as shown in Figure 1-4 have been adopted since long ago as the most frequently used techniques for assessing the mechanical properties of the articular cartilage (Hasler et al. 1999). Through these testing methods, the material properties such as the Young's modulus in the compression test, the aggregate modulus, Poisson's ratio and permeability in the biphasic indentation test (Mow et al. 1989) can be obtained. The unconfined compression is the most simple way to obtain the Young's modulus and Poisson's ratio of the cartilage because it is a standard method for the testing the mechanical properties of material due to its simple boundary conditions. However, unconfined compression is only useful for obtaining the mechanical properties of the solid phase and the bulk modulus/permeability cannot be obtained from the unconfined compression. These properties can be extracted from the confined compression test where the boundary of the cartilage is in contact with the wall of an impermeable cylindrical chamber. Still, careful sample preparation is needed in the two compression tests and the requirement of dissected regular tissue sample prevents the application of these measurement methods on soft tissues in vivo. Among all the testing methods, the indentation test has attracted the most intensive studies for the in

vivo test because it doesn't require special preparation techniques such as microtoming precise strips required for the tensile tests or preparing precise cartilage plugs for compression tests (Mow et al. 2005). A curve-fitting procedure has been proposed in an algorithm to extract three material mechanical properties simultaneously (Mak et al. 1987; Mow et al. 1989).

As discussed in the arthroscopic evaluation methods, the softening is one of the most obvious symptoms for the cartilage degeneration. For example, in the Outerbridge and ICRS cartilage lesion grading methods, the softening has been recognized in both as a symptom to define the low grade degeneration (Brittberg and Winalski 2003; Outerbridge 1961). Using an anterior cruciate ligament (ACL) transection surgery as the canine OA model, Guilak et al. found that the tensile stiffness of the superficial knee cartilage decreased by 44% after 16 weeks post-surgery (Guilak et al. 1994). Setton et al. also demonstrated that after the ACL transection in a canine OA model, the compression, tension and shear modulus of the knee cartilage decreased significantly after 12 weeks post-surgery (Setton et al. 1994). In human cadaveric samples, it has been demonstrated there was significant difference of the indentation stiffness between normal and degenerated cartilages, in both young and old patient groups (Bae et al. 2003). Therefore, the measurement of mechanical properties is a potential method to characterize the degeneration of articular cartilage and the most important issue is how to realize the measurement in a practical way, which will be further discussed in detail in Subsection 1.4.3.

1.3.2. MRI and CT method

MRI is a noninvasive imaging method which is particularly useful for studying the soft tissue in human body. The advantage of using MRI for soft tissue investigation is its ability to scan the tissue all over the human body. Specifically, the MRI can be used mainly for three aspects of studies on articular cartilage, i.e., the morphological study, such as the cartilage volume, thickness, and surface area; the compositional study, such as the proteoglycan contents; and the semi-quantitative scoring of cartilage changes (Eckstein et al. 2006). The cartilage index achieved by the delayed gadolinium-enhanced MRI of cartilage (dGEMRIC) can be used to study the glycosaminoglycan (GAG) content of the cartilage in vivo and has been demonstrated to be related to the physiological and pathological processes of the

tissue (Tiderius et al. 2003; Williams et al. 2004). Therefore, it has the potential to be used for the characterization of early cartilage degeneration. Also, some scoring methods have been proposed to assess the osteoarthritis; for example, the Whole-organ MRI Scoring (WORMS) (Peterfy et al. 2004), the Knee Osteoarthritis Scoring System (KOSS) (Kornaat et al. 2005) and the Boston Leeds Osteoarthritis Knee Score (BLOKS) (Hunter et al. 2008) are three scoring methods which are specifically proposed for assessing the severity of joint osteoarthritis. In WORMS, the articular integrity was assessed as one part of the total scores. Like in arthroscopic assessment of cartilage lesion, the factors in WORMS assessment include the thickness and area of defect and an eight-point score is given for grading the severity (Peterfy et al. 2004). In KOSS, the cartilaginous defect is assessed by three aspects: the depth of cartilaginous defect, the depth of the osteochondral defect and the surface extent of the lesion. A maximal grade of 3 is given for each aspect of lesion and the total score is used to indicate the integrity of the cartilage condition (Kornaat et al. 2005). However, the MRI resolution for cartilage is still not high enough with a high operation price and the quantitative MRI is still in its infancy with respect to its use for cartilage assessment. Further studies are necessary to demonstrate the clinical utility of these techniques in this specific field (Conaghan et al. 2011).

Like radiography, the computed tomography (CT) has also been used to study the articular cartilage pathology. For normal soft tissues, the problem of using CT as an investigation tool comes from the small signal obtained from soft tissues and the small contrast among different soft tissues. Therefore, two specific techniques have been proposed to improve the quality of imaging when CT is used for cartilage study: the first technique is to decalcify the bone to enhance the signal from cartilage and the second is to use contrast agent in the cartilage to improve the quality of imaging (Palmer et al. 2006). Using the contrast-enhanced technique, the X-ray attenuation has been demonstrated to be related to the proteoglycan content (Kallioniemi et al. 2007; Palmer et al. 2006) and then it can be used for the evaluation of cartilage pathology (Piscaer et al. 2008). As the proteoglycan content is related to the compressive stiffness in cartilage, this method can also be used to characterize the mechanical properties of the cartilage (Bansal et al. 2010). In addition, high resolution CT can be used to measure the 3D morphology of the articular cartilage which is also related to the pathological condition of the tissue (Xie et al. 2009).

However, because of the difficulty of contrast agent diffusion in cartilage and the concern of X-ray radiation hazard in the test, further investigation is still needed to apply this technique in real clinical settings.

1.3.3. Optical methods

The optical imaging is also widely used in biomedical field. Some optical methods such as the infrared spectroscopy and optical coherence tomography (OCT) have also been adopted for the characterization of articular cartilage (Herrmann et al. 1999; Spahn et al. 2004). OCT is an optical imaging modality that utilizes the interference of the backscattered infrared light with the reference light beam reflected from the same distance as the basic principle of imaging. It has a relatively high resolution in the scale of microns, which can be used to identify the surface fibrillation, fibrosis, cartilage thickness and new bone growth of the osteochondral tissue microstructure (Herrmann et al. 1999; Rogowska et al. 2003). It has also been implemented in an arthroscopic channel for the endoscopic observation of the articular cartilage cross-sectional images and comparison with the histology showed good consistency for the microstructure (Chu et al. 2004). OCT can be used for not only qualitative study, but also quantitative study, such as the detection of cell death caused by impact (Bear et al. 2010), change of the surface roughness and optical reflection induced by enzymatic digestion (Saarakkala et al. 2009), and change of refractive index after the degeneration (Wang et al. 2010b). However, further studies are still necessary to solve the problems caused by limitations of this technique, such as the angle dependence of measurement (Huang et al. 2011) and small penetration of the OCT signal in opaque tissue, before it can be widely used for clinical applications.

Another big group of studies focuses on the infrared spectroscopy for cartilage study. The general principle is to impinge the tissue using a pulse infrared light with a broad spectral bandwidth, receive the backscattered or transmitted light and then see how the intensity and peaks show in the absorption spectral curve (Brown et al. 2009; Brown et al. 2011; Camacho et al. 2001; West et al. 2004). Using this technique, the change of components such as collagen and proteoglycans has been demonstrated in degenerated cartilage (West et al. 2004) or repaired cartilage (Bi et al. 2006). Spahn et al. have designed an arthroscopy-based probe for the detection of early degeneration of articular cartilage (Figure 1-5) (Spahn et al. 2007). The probe was

designed like a clinically routine one used in conventional arthroscopy and has been demonstrated to be capable of differentiating the severity of cartilage degeneration using a spectral ratio factor (Spahn et al. 2007; Spahn et al. 2008). The characteristic parameter by near infrared spectroscopy was found to be significantly correlated with the visual macroscopic cartilage grade (ICRS grade) and biomechanical properties (Young's modulus) (Marticke et al. 2010) and this parameter was demonstrated to be reliable as a quantitative parameter through a blinded inter-observer study (Spahn et al. 2010). However, this method is not mature yet and further study is still necessary to implement this measurement in clinical situations.

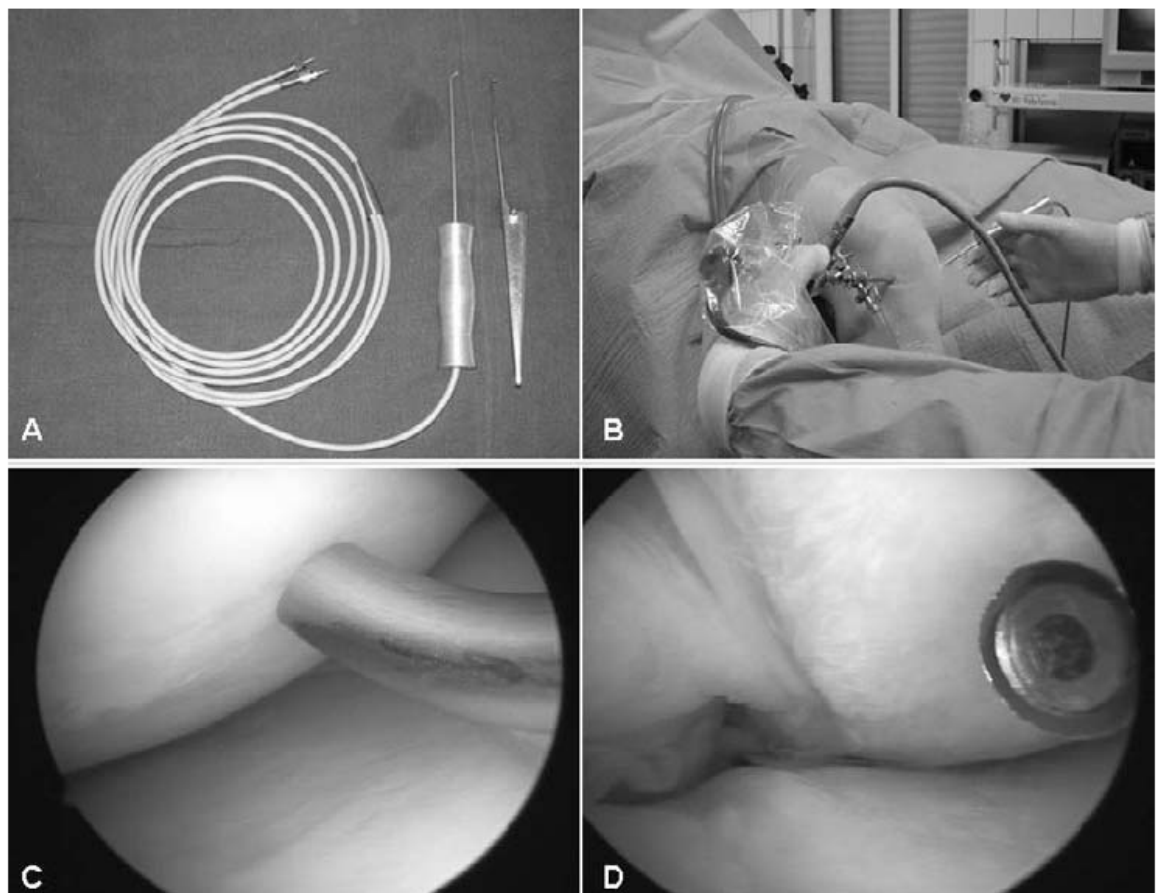


Figure 1-5 (a) The near infrared reflection spectroscopy (NIRS) system with a conventional arthroscopic hook; (b) The operation of the probe with the arthroscopic observation; (c) Probe under the arthroscopic view; (d) The front view of the probe with light source fibers from the surroundings and the center fiber which can collect the optical signal (Spahn et al. 2007).

1.4. Potential method: ultrasound-based techniques

Ultrasound is a low-cost and widely accessible imaging modality which can provide both qualitative and quantitative information of the detected tissues. As for cartilage, the 2D ultrasound images can tell the morphological information of the tissue, such as the smoothness of the cartilage surface and the depth of lesion with respect to its surrounding normal tissue; quantitatively, the quantitative ultrasound (QUS) has been applied for the cartilage characterization and detection of cartilaginous change in pathology; furthermore, the incorporation of ultrasound in the mechanical testing facilitates the measurement of mechanical properties of the cartilage. Those specific applications of ultrasound for the study of cartilage are introduced as follows.

1.4.1. Sonographic examination

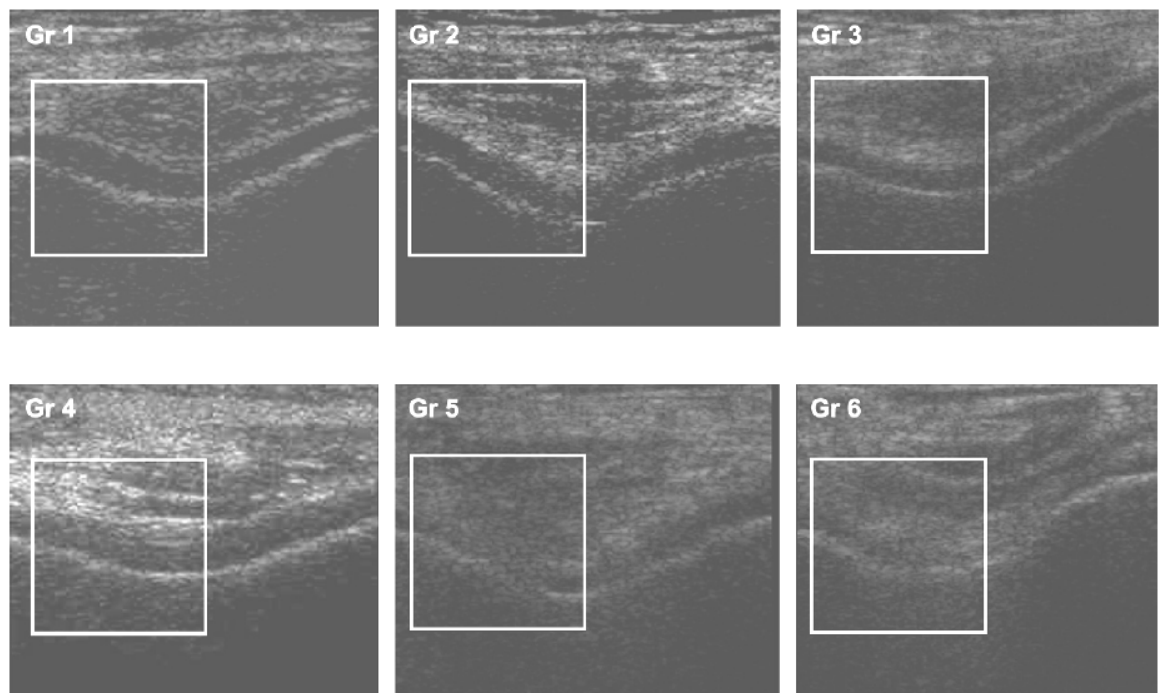


Figure 1-6 Sonographic grading of cartilage degeneration (from grade 1 to grade 6) using the B-mode images obtained through transcutaneous ultrasound. The grading is made by descriptions of surface sharpness, layer clarity, thickness and uniformity of the thickness and etc (Lee et al. 2008).

Ultrasound imaging is a noninvasive and easily accessible modality in the study of the musculoskeletal system (Jacobson 2008). Application of ultrasound for the *in vivo* assessment of joint arthritis also began as early as in the late 1970s' (Cooperberg et al. 1978) and this method has been reviewed in the literature for its development, current status and future directions (Moller et al. 2008; Wakefield et al. 1999). Advantages of percutaneous ultrasonography of the knee include the detection of multiple pathologies coming from various tissues of the joint including articular cartilage, bone and joint cavity. Power Doppler is also useful for detecting the synovial tissue vascularity (Walther et al. 2001). Similar to X-ray radiography, ultrasound could be used to detect the joint space narrowing due to cartilage thinning with more reliable measurement of the cartilage thickness (Castriota-Scanderbeg et al. 1996; Disler et al. 2000; Martino et al. 1993). Compared to X-ray radiography, ultrasound directly measures the thickness of the cartilage rather than uses the joint space as an indirect reflection of the cartilage thickness. Other features observed in the external ultrasonography include the loss of sharpness of the synovia-cartilage interface, cartilage layer clarity and increased intensity of the posterior bone-cartilage interface (Aisen et al. 1984; Grassi et al. 1999; McCune et al. 1990). *In vivo* grading of cartilage degeneration using ultrasonography has been proposed based on the appearance of cartilage in the B-mode ultrasound images and compared with the *in vitro* and histologic grading (Figure 1-6) (Lee et al. 2008; Tsai et al. 2007). High frequency ultrasound imaging was also used for the grading of cartilage degeneration with some improvement compared to the conventional one such as the higher resolution (Spriet et al. 2005; Wang et al. 2011). Although significant correlations were observed in the comparisons with the histological grading, the correlation was moderate which indicated some discrepancy between the two methods. Although clear guidelines were presented in the study to grade the level of cartilage degeneration, the guidelines are essentially quite descriptive based on visual observation and it is quite subjective to make those diagnoses.

Furthermore, as cartilage is a thin tissue of generally 1~3 mm in thickness, it brings an inherent constraint between the imaging resolution and the penetration depth to the conventional ultrasound assessment performed externally from the knee surface. Due to the existence of superficial layers that the ultrasound needs to penetrate before the cartilage, too high frequency cannot be chosen, thus limiting the

accuracy of measurement. Difficulties in performing external ultrasound check also include the restrictions in testing postures, probe positions and orientations, considering that some of the postures such as full knee flexion may not be possible for osteoarthritic patients with knee pain during activities (Friedman et al. 2001; Jacobson 2008; Lee et al. 2008). These limitations have prevented the external ultrasonography from becoming a clinically routine tool for rheumatologists. Clinical investigation is still necessary to establish standard steps in using external ultrasonography for the quantitative or semi-quantitative assessment of articular cartilage, or the whole joint (Chao and Kalunian 2008; Grassi 2003; Grassi et al. 2005; Kane et al. 2004a; Kane et al. 2004b; Meenagh et al. 2007; Moller et al. 2008). The applicability of this method for the early detection of cartilage degeneration is not clear yet or at least this will be difficult to be achieved due to the limited resolution of the conventional ultrasound imaging system. This also stimulates the pursuit of more quantitative method for the evaluation of articular cartilage degeneration associated with OA. At the current stage of investigation, we still cannot say that the externally performed ultrasonography of the articular cartilage is a quantitative method.

1.4.2. Quantitative ultrasound

In the last two decades, ultrasound with frequency > 15 MHz, which is higher than that normally used in routine clinical situation, has been adopted as a new approach to study the articular cartilage. Because of higher frequency, the penetration depth of ultrasound has been compromised and therefore it is usually appropriate for direct study of the cartilage. At current status, most of the high frequency ultrasound was conducted for the in-vitro or in-situ study of articular cartilage with very few studies conducted in vivo. In general, ultrasound has been involved in the study of articular cartilage mainly in the following two aspects.

1.4.2.1. Morphological properties

Morphological properties are related to the physical characteristics of the tissue, such as the volume, thickness, surface area and surface roughness. Quantitative ultrasound can be used to study the morphological properties of the articular cartilage. According to the pervious literature, the morphological properties studied mainly include the cartilage thickness and surface roughness.

To measure the thickness of cartilage, there should be a precise estimation of the speed of sound (SOS) in tissue. How to obtain a precise value of SOS will be discussed in the next section with measurement of acoustical properties of the tissue. A general way to obtain the thickness of articular cartilage is to assume a constant SOS in the tissue and then estimate the thickness by the propagation time, i.e., time of flight. Before measuring the thickness, it should be noted that the two ultrasonic interface reflections normally seen in the ultrasound signals are from the solution-cartilage and tidemark interface (Modest et al. 1989). By assuming a constant SOS, Jurvelin et al. demonstrated that there was a high correlation among the values of thickness measured from needle probe, optical and ultrasonic methods (Jurvelin et al. 1995), although the precision could still be improved by using a higher frequency and more collimated ultrasonic beam to reduce the effect of geometrical heterogeneity. Special attention should be paid to the experimental setup for the extraction of SOS, otherwise incorrect conclusion might be drawn for the use of ultrasound for the measurement of cartilage thickness (Mann 2001; Yao and Seedhom 1999). The affecting factors might include the perpendicularity of the ultrasound beam into the tissue, localization of the testing point (thickness heterogeneity) and precision of the data collection system (Mann 2001). The high frequency ultrasound is useful to study the site dependence of the cartilage thickness (Adam et al. 1998) or other pathological conditions such as the swelling in the early stage of OA and the thinning of the cartilage at late stage of OA (Calvo et al. 2001; Cherin et al. 1998; Karvonen et al. 1994; Myers et al. 1995; Watson et al. 1996). Thickness is also a key parameter for the mechanical testing such as the indentation test (Hayes et al. 1972; Jurvelin et al. 1995; Laasanen et al. 2002; Zheng and Mak 1996). As another related application of the high frequency ultrasound, it could be applied to monitor the digestion of cartilage induced by the enzyme treatments (Wang et al. 2008). In this process, the digestion speed could be observed with real-time imaging and this was useful for us to know how the enzymes would digest the cartilage progressively. Furthermore, 3D ultrasonic imaging and related signal processing has been applied in the morphological study of OA, partially because of its flexibility in image slicing at different cross-sections (Ju et al. 2008; Landes et al. 2006). With the advantages of high frequency ultrasound imaging, this technique could potentially be applied for the quantitative assessment of cartilage morphology involved in pathologies such as OA (Lefebvre et al. 1998).

Ultrasound could be also used to detect the surface roughness of the cartilage. Surface fibrillation is one of the symptoms in the early stage of degeneration of cartilage and the fibrillation will cause the exposure of fibrils on the cartilage surface leading to an increase of the surface roughness. Therefore, methods that can quantitatively detect this change would be useful for the early diagnosis of OA. Traditionally, these changes could be only demonstrated by microscopic methods with enough magnification when viewing the tissue (Gardner et al. 1997). However, some investigators have made efforts in using the high frequency ultrasound to quantify the tissue roughness (Adler et al. 1992; Saarakkala et al. 2006; Saarakkala et al. 2004). Two methods were developed for this purpose. Alder et al. (1992) utilized an indirect method to measure the angle dependence of the reflected ultrasound intensity with respect to the surface roughness. Assuming the reflected ultrasound intensity could be fit using a Gaussian profile, the width of the Gaussian curve was a relative reflection of the surface roughness. The capability of this method was demonstrated in emery papers with different grit size as well as cartilages with different visional levels of roughness. When a curvature of the specimen exists, the sensitivity of detection could be improved by using a focused transducer (Chiang et al. 1994). This detection technique was also validated by the confocal microscopy (Chiang et al. 1997). The second approach to measure the surface roughness was a more direct method for which the roughness was defined as ultrasound roughness index (URI) (Saarakkala et al. 2006; Saarakkala et al. 2004). This method first uses ultrasound transducer to have a lateral scanning along the tissue surface and then the tissue surface line profile was extracted from the ultrasound signal. After a high-pass filtering of the signal to remove the tissue curvature effect with a low frequency change, the parameter URI is extracted by calculating the variation of the surface profile, which is used similarly in the definition of “roughness” (Ateshian and Mow 2005). This method was firstly demonstrated with sandpaper abraded cartilage samples in vitro (Saarakkala et al. 2004). Then subsequently in cartilages with enzyme digestions, only the group with collagenase treatment had a significant increase of the surface roughness, indicating that collagen fibrils might act as the main factor in affecting the surface roughness. The URI was then applied in normal bovine and repaired porcine cartilages to demonstrate the spatial variability of the surface roughness and the defect of the repaired cartilages compared to the intact normal ones (Laasanen et al. 2005; Laasanen et al. 2006). Interestingly, it was found

the surface reflection had a significantly negative correlation with the URI (Laasanen et al. 2005). This was actually understandable that a rougher surface would cause a more random scattering of the ultrasound energy so the backscattered part would be significantly reduced. Study on spontaneously degenerated bovine cartilages using URI associated with other quantitative ultrasound parameters showed that the surface URI was sensitive to the cartilage degeneration (Saarakkala et al. 2006). In summary, the first method of indirect measurement of the surface roughness, where a precise control of the rotation of the probe is necessary, is not appropriate for clinical arthroscopic situations where space is limited, while the second method is more practical if 1-D or 2-D array high frequency ultrasound imaging transducers with small profiles can be provided and applied in this situation.

1.4.2.2. Acoustical properties

The second type of properties that can be measured from quantitative ultrasound for characterizing the articular cartilage is the acoustical properties. As ultrasound is a specific kind of mechanical wave induced by the vibration of the propagation medium, those properties that are characteristic of the sound can also be used to characterize the status of the tissues. Generally speaking, conventional B-mode ultrasound images are also reflections of the acoustical properties of the detected object as the image is constructed from the magnitude of reflected ultrasound waves, which represents the capabilities of the tissue to backscatter the incident ultrasound energy. The acoustical properties that have been adopted for the study of OA in articular cartilage mainly include the speed of sound (SOS), acoustical reflection amplitude (cartilage surface reflection, cartilage-bone interface reflection), frequency-dependent backscattering and attenuation of the internal layer of the cartilage.

One of the most important parameters in acoustical properties is the speed of sound (SOS). It can be used not only to characterize the change of the tissue status, but also to gain another intrinsic parameter: the tissue thickness (through the calculation of propagation distance). The thickness can be measured from SOS based on the time of flight technique. This technique has already been used broadly for the non-destructive detection of material flaws in industries and material science (Mouritz et al. 2000). As long as we have an accurate SOS, the thickness of the tissue can be measured. In the literature mainly three methods were proposed to measure the

SOS in articular cartilage: reference thickness measurement method (Ling et al. 2007; Toyras et al. 2003; Toyras et al. 1999), partial compression method (Suh et al. 2001) and the specimen insertion method (Hsu and Hughes 1992; Patil et al. 2004). The reference thickness method means that a reference value of the thickness is measured from another approach, for example the optical method or needle probe penetration technique. Then this referenced thickness will be used as one of the two known parameters in the propagation equation $d = v * t$ to extract the SOS. This method is relatively straightforward but usually suffers from the invasive nature during the process to get the true tissue thickness. For example, the histological method for measuring the thickness needs tissue dissection and the needle probe penetration for this purpose needs to insert a needle in the cartilage. The second method uses an indentation method to calibrate the SOS in articular cartilage (Suh et al. 2001). Specifically, a known indentation of tissue would cause the reduction of the propagation time. The extent of indentation is registered by micrometer or a displacement measurement sensor such as linear variable differential transformer (LVDT). The decreased time of flight plus the known indentation depth will be used together to calculate the SOS. This method is thought to be an improvement from the first method because no direct measurement of the initial cartilage thickness is necessary. However, the compression during the indentation of the tissue may itself induce some change to the SOS in articular cartilage because it has been demonstrated that the SOS was strain-dependent (Ling et al. 2007; Nieminen et al. 2007). Then the a-prior assumption of a constant speed will be violated which makes the measurement results not so accurate. The third method can simultaneously measure the speed and thickness of the cartilage without a change of the tissue status. The propagation time between an ultrasound transducer and a reflection plate is measured before and after the insertion of the tested tissue. In this situation, change of the propagation time is assumed to be caused by the difference between the SOS of the solution and that of the cartilage specimen. As SOS in solution can be measured and known before the experiment, the SOS of cartilage can be measured in relation to that of the immersing solution. This method has been applied to measure the depth-dependence and anisotropy of the SOS in cartilage (Patil et al. 2004). The limitation of this method is that the specimen inserted between the transducer and the reflection plate should be a pure cartilage without the subchondral bone; otherwise, the difference of the propagation time would be attributed to two different tissues

(cartilage and bone) and no separate SOS of the cartilaginous layer can be extracted. From the methodological point of view, all the three aforementioned methods are not appropriate to be applied for the in vivo measurement: a reference thickness cannot be measured noninvasively during an in vivo test; it is difficult to have a precise control of the small indentation without the motion of the diarthrodial tissues in vivo; and in the third case, pure cartilage layer cannot be obtained separately in vivo for the simultaneous measurement of SOS and thickness of cartilage. Therefore, it is still a quite challenging problem to get an accurate measure of SOS in vivo in clinical operations and therefore, most of the time, a constant value of SOS needs to be assumed for calculating the thickness of cartilage (Adam et al. 1998). A simultaneous measurement of SOS and thickness on one side of the tissue was proposed using two laterally displaced ultrasound transducers (Kim et al. 2003), which may be useful in the future applications where two or more elements can be laterally displaced in array transducers for in vivo measurement.

According to the literature study, normal cartilage has a speed of 1520~1750 m/s (Nieminen et al. 2009). Based Jurvelin's study (1995) with a 10 MHz transducer, the accuracy is about 0.127 mm for thickness measurement. Toyra et al. (2003) reported that using a constant velocity of 1627 m/s for speed of sound in articular cartilage, it induced an error of 2.9 ± 3.8 % for cartilage thickness, and 0.9 ± 1.3 % for dynamic modulus. Therefore, generally a constant SOS can be used to measure the cartilage thickness and further used to calculate the mechanical properties where needed. As SOS of articular cartilage was demonstrated to be dependent on a lot of tissue components such as water, uronic acid and hydroxyproline contents and these components are all involved in the osteoarthritic process, SOS could be potentially used as an indicator of the cartilage degenerations.

Another parameter that has been used frequently is the acoustical reflection from the cartilage surface. Consistent with early investigation of the B-mode ultrasonography of articular cartilage, the surface reflection showed a significant change after enzyme digestions, especially for the collagenase treatment (Nieminen et al. 2002; Toyra et al. 1999). Therefore, the surface reflection is a good indicator of the surface collagen network integrity. Recent study showed that the surface reflection was more affected by the surface roughness and the content of collagen might play a less important role in contributing to the surface reflection amplitude

(Laasanen et al. 2005). Smoother surface, just like a mirror, will produce a larger reflection of the ultrasound as energy is more uniformly reflected back to its incident direction. However, it should be noted that the ultrasound surface reflection is a parameter that depends heavily on the system settings such as the transducer, distance between probe and cartilage, pulser/receiver settings and a partial correction of the effects through calibration will be preferred for its use in clinical situations. Other reflection parameters such as the cartilage-bone interface reflection and also the frequency domain reflection coefficient have also been proposed and used by some investigators (Cherin et al. 1998; Laasanen et al. 2005), but the extra information provided by these additional parameters is quite limited, due to a complicated situation where more factors are involved in affecting the measured parameters such as the cartilage thickness.

Another two parameters that have been used for the characterization of acoustical properties of articular cartilage are the attenuation and backscatter coefficients (Cherin et al. 1998; Nieminen et al. 2004). Attenuation represents the extent of signal reduction in a unit length of tissue due to absorption and scattering. Backscattering is a measurement of the capability of the tissue to scatter the ultrasound energy back to its incident direction. Both the two parameters can be measured in the time domain and frequency domain. Cherin et al. (1998) used apparently integrated backscatter (AIB) to quantify the aging and osteoarthritic changes associated with the rat articular cartilage. Nieminen et al. (2004) studied the relationship between attenuation and histological, histochemical, and biomechanical properties of the cartilage and found the attenuation was sensitive to the degenerations. There were also authors trying to analyze the frequency profile of the reflected ultrasound signals (Brown et al. 2007) but the validity and utility of this method needs further investigation.

In summary, the acoustical properties provide an indirect way to reflect the change of tissue compositions and microstructure and special attention should be paid to explain those quantitative results, although some parameters such as the surface reflection has been broadly used in the literature (Saarakkala et al. 2007). Intrinsically physical properties should be preferred as long as they are possible in the measurement (Zheng and Huang 2008).

1.4.3. Ultrasound indentation and water-jet ultrasound indentation

As mentioned in Subsection 1.3.1, indentation is nowadays one of the most frequently used methods for the mechanical testing of biological soft tissues due to its less restricted requirement for tissue preparation therefore making it possible for measurement in living tissues (Gefen et al. 2001; Kim et al. 2008; Klaesner et al. 2002; Lu et al. 2004; Pailler-Mattei et al. 2008; Samani and Plewes 2004; Vannah and Childress 1996). The indentation test has been successfully applied to a lot of tissues including skin (Pailler-Mattei et al. 2008), liver (Kerdok et al. 2006), muscle (Vannah and Childress 1996), breast (Samani and Plewes 2004), lower limb (Silver-Thorn 1999) and heel pad (Hsu et al. 1998; Rome et al. 2001). Most of the studies adopted a stiffness index directly obtained from the force/deformation relationship or extracted essential material properties such as Young's modulus based on a theoretical analysis of the indentation (Hayes et al. 1972) or through the inversion solution with the finite element (FE) method. Linear elasticity was usually assumed in the studies and there were also a small number of investigations on studying the nonlinear aspect of the mechanical properties using indentation (Huang et al. 2005; Rome et al. 2001; Tonuk and Silver-Thorn 2003; Vannah and Childress 1996).

Ultrasound has been proposed as an alternative method to measure the deformation during the indentation test, being so called “ultrasound indentation” in the last two decades (Han et al. 2003; Hsu et al. 1998; Kawchuk and Elliott 1998; Zheng and Mak 1996). As discussed in the above section, ultrasound has the capability of measuring the tissue thickness as well as quantifying the dynamic change of the thickness (deformation) without causing damage to the tissue, which are the advantages of using this modality. Therefore, it is very appropriate for the testing of biological soft tissues in vivo. A tissue ultrasound palpation system (TUPS) was developed for the indentation of soft tissues to extract their mechanical properties (Figure 1-7) (Zheng and Mak 1996). In this method, the ultrasound transducer serves both as the displacement sensor and as the indenter. A load cell is connected in series with the ultrasound transducer for recording the force response of the indentation. The ultrasound signals as well as the indentation force will be recorded during the indentation process for offline processing. This system has several advantages including, for example, a thickness measurement, a small profile and insensitivity to the subject motion during test. As long as an obvious reflection from bony interface

can be obtained, this system can be used for the mechanical testing of the targeted soft tissue. Up to now, quite a lot of soft tissues have been successfully tested by using this portable ultrasound indentation system. It has been used for the assessment of the stiffness of the neck soft tissues after radiotherapy (Leung et al. 2002; Zheng et al. 2000b), for the differentiation of the mechanical properties of normal and diabetic plantar tissues (Zheng et al. 2000a; Zheng et al. 2012) and for the effect of chronic spinal cord injury on soft tissue stiffness (Makhsous et al. 2008). Trials have also been conducted for other tissue pathologies such as healing scars and carpal tunnel syndrome (Lau et al. 2005; Zheng et al. 2006).

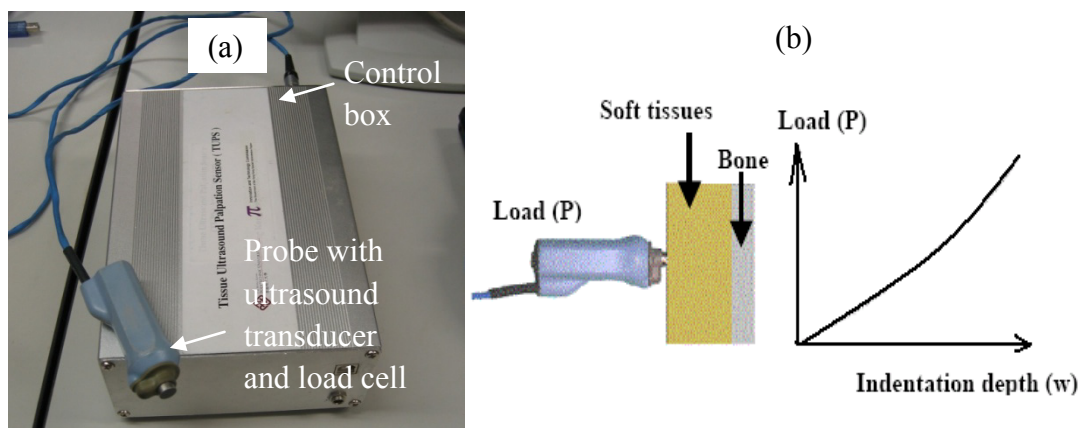


Figure 1-7 (a) The compact tissue ultrasound palpation system with a probe and the main control box; (b) A typical indentation process and the load/indentation, i.e., force/deformation, curve for calculating the tissue stiffness.

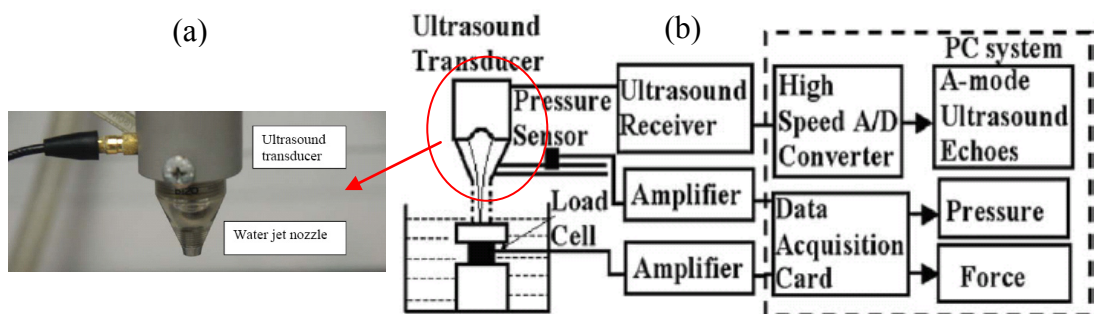


Figure 1-8 The water-jet ultrasound indentation system developed for measuring the mechanical properties of soft tissues. (a) The probe for water-jet indentation and (b) the data collection schematics of the system (Lu et al. 2005).

In situations where the acoustical properties are to be measured, the rigid ultrasound transducer in contact with the tissue surface is unable to collect the reflection from the surface. A certain distance between the tissue and ultrasound

transducer will be a better choice in this situation. This is also true for the focused transducer where tissue should be put in the focus point for a better signal-to-noise ratio (SNR). Furthermore, for focused transducers, the concave surface will be troublesome for the conduct of indentation. Targeting at these shortcomings of the rigid indentation method, a water-jet ultrasound indentation system has been developed for measurement and fast scanning of the mechanical properties of soft tissues (Figure 1-8) (Lu et al. 2005). Water-jet technology has been among the choices of armamentarium in medical applications such as lavage and surgery (Byrick et al. 1989; Honl et al. 2000; Loehne 2007). Low pressure pulsatile water-jet can be used to remove the debris and bacteria from the trauma site and help improve the healing of the wound (Bhandari et al. 1998; Caprise et al. 2002). Very high pressure water-jet can even be applied as a surgery tool in operation. In order to cut the tissue in surgical operations, water-jet with pressure as large as hundreds of bars has been applied with a small nozzle of $\sim 100\ \mu\text{m}$ (Honl et al. 2000). Within the water-jet ultrasound indentation technique, small pressure water-jet is used as a method to compress/indent rather than destroy the soft tissue.

Briefly, this system incorporates a nozzle to produce a water-jet and then makes an indentation on the specimen which is just placed under the nozzle. The water-jet serves both as the indentation tool and as the coupling media for the ultrasound propagation. The ultrasound signal will be used as a method to measure the initial thickness before indentation and also the tissue deformation during indentation. However, as a difference from the contact indentation, the water-jet indentation force will be calculated from the pressure of the water-jet. Corresponding relationship between the pressure of the water-jet and its force on the tissue is established by a calibration process. Preliminary tests on phantoms showed that the system was able to measure the elastic properties of soft tissues and had the capability for an elasticity mapping of the tissue in a C-scan test (Lu et al. 2005; Lu et al. 2007). The system has also been demonstrated to be capable of detecting the articular cartilage degeneration induced by trypsin digestions in vitro (Lu et al. 2009). However, no experiment has been conducted in animal model of osteoarthritis with the natural degeneration of cartilage for this system. Further development for this water-jet ultrasound indentation system includes its miniaturization and adopting it for arthroscopic operation, which is discussed subsequently.

1.5. Arthroscopic instrumentation

A minimally invasive operation is preferred nowadays in comparison with traditional open surgeries because of its reduced surgical trauma and shorter hospitalization time for the patient (Fuchs 2002). Arthroscopic operation has become popular for the surgeries of various joints for various purposes, which mainly include, for example in knee, the partial meniscectomy, chondroplasty/arthroplasty, ACL and PCL reconstruction, loose body removal, synovectomy and etc (Treuting 2000). On the other hand, diagnostic exam through arthroscopy is also a very good approach to examine the condition of the joint situation for making follow-up decisions (Treuting 2000). Therefore, it is very useful to develop arthroscopy-based diagnostic procedures if a new technique is considered to be appropriate for test on intra-articular tissues such as articular cartilage.

In the last two decades, quantitative arthroscopic evaluation of the articular cartilage has attracted a lot of attention from the research societies due to an acceptable balance between the invasiveness of the arthroscopic operation and the advantage of an in-situ and direct inspection of the intact cartilage (Oakley and Lassere 2003). In addition to the mechanical testing, a lot of related techniques were proposed for the diagnostic purpose. Optical coherence tomography (OCT), as briefly introduced in Subsection 1.3.3, has been proposed as a new imaging facility for the arthroscopic evaluation of cartilage and handheld probe has been developed for this purpose (Herrmann et al. 1999; Pan et al. 2003). Berkenblit et al. proposed the electromechanical surface spectroscopy to detect the compositional and chemical changes of the cartilage and this technique could be designed with arthroscopy (Berkenblit et al. 1994; Sachs and Grodzinsky 1995). They used a sinusoidal current to excite the cartilage and then observed the response of stress of the tissue to quantify the change or vice versa, using the periodical mechanical stimulation as the source of excitation and observing the electric current response. Ishihara et al. (2006) incorporated a photoacoustic method to measure the change of mechanical properties of the cartilage by measuring the relaxation time of the optical intensity change which was related to the ratio of viscosity and elasticity of the tissue (Ishihara et al. 2006). In this system, the acoustic wave was produced by an optical irradiation pulse and the whole system was easy to be incorporated in an arthroscopic system. Spahn et al.

(2007, 2008) proposed the near-infrared (NIR) spectroscopy for the evaluation of low grade degenerated cartilage lesions and found the measured parameter was sensitive to early degeneration due to the correlation of the measured parameter (two band absorption ratio) to the water content of the tissue (Spahn et al. 2007; Spahn et al. 2008). This system is also potential to be incorporated in arthroscopic device due to an optic fiber operation of the measurement. All these measurements are still quite preliminary and have not been used and practiced routinely in clinics. A Japanese group incorporated the ultrasound sensor into an arthroscopic probe and then detected the change of the acoustic properties of the cartilage surface. However, the acoustic properties alone were not intrinsic properties of the cartilage and more parameters were necessary to characterize the intrinsic properties for the quantitative assessment of cartilage degeneration (Hattori et al. 2004; Zheng and Huang 2008).

Indentation is the only mechanical testing method that can be applied to the intact articular cartilage in situ or in vivo as described in Subsection 1.3.1. Since the possibility of being incorporated in arthroscopic applications for in vivo test, efforts have been made to develop miniaturized probe in this direction. Dashefsky (1987) developed probably the first arthroscopic indentation probe to detect the softening of the articular cartilage in chondromalacia (Dashefsky 1987). They produced a constant amplitude of indentation by a silastic tip and then measured the responsive pressure with an in-series pressure sensor. It should be noted the reading was just an indicator of the stiffness but not intrinsic elastic material properties of the articular cartilage (Dashefsky 1987). This system was improved by adopting the strain gauge to measure the force response with a constant indentation of the cartilage (Figure 1-9a) (Lyyra et al. 1995). The device has been developed to a CE-marked commercial product ArtScan (<http://luotain.uku.fi/bbc/equipment/biomechanics/>, successfully accessed on Sep 12, 2012) (Figure 1-9b). The constant indentation was produced by the cylindrical or spherical indentation tip and the corresponding force was picked up by a pair of strain gauges attached in series with the probe tip (Figure 1-9a). The constant indentation was ascertained by the use of a larger plate surrounding the indentation tip. Indentation force of the external socket and the internal indenter was recorded by two pairs of strain gauges for the ease of applying the constant indentation. Although the resulting parameter – the reaction force of the tissue is still

not intrinsic, but it can be used to obtain elastic properties such as the Young's modulus based on theoretical indentation models (Hayes et al. 1972).

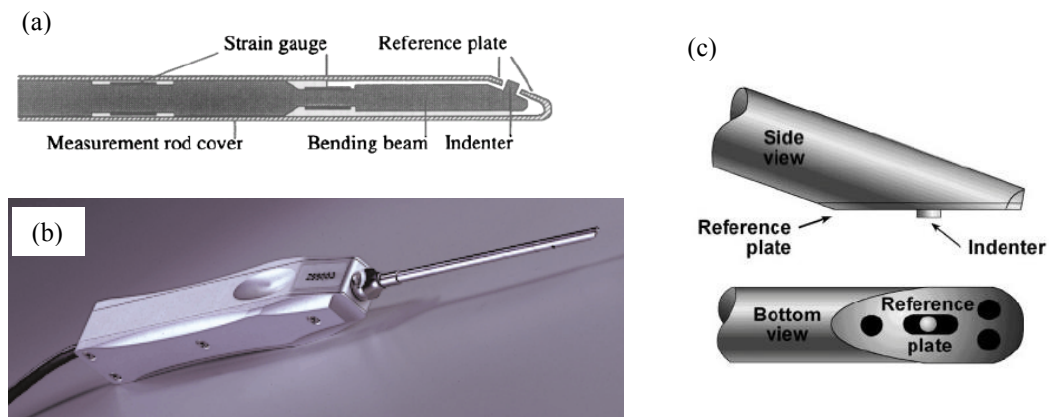


Figure 1-9 (a) A schematics showing the principle of an arthroscopic indentation device for the testing of articular cartilage stiffness; (b) The ArtScan probe; (c) A side view and bottom view of the head of the indentation probe (Lyyra et al. 1995).

Quite a variety of investigations have been conducted since the introduction of this arthroscopic indentation system. These included the improvement of the design of the indentation tip from a cylindrical to a spherical shape (Korhonen et al. 2003b; Lyyra-Laitinen et al. 1999) and the coating of the reference plate for a better operation on the cartilage surface (Toyras et al. 2005). Finite element analysis as well as experiment was used to demonstrate the advantages from the new design (Korhonen et al. 2003b; Lyyra-Laitinen et al. 1999; Lyyra et al. 1999a; Toyras et al. 2005). Among the techniques of improvement, the use of the ultrasound transducer for performing the ultrasound indentation has led to a lot of new research with the mechano-acoustical measurement of the cartilage (Figure 1-10) (Laasanen et al. 2002). This system can not only perform mechanical testing, but also measure the acoustic properties of the cartilage thus demonstrating its functional versatility. A lot of parameters can be measured from the system, for example, the instantaneous and equilibrium modulus, the creep rate, the surface reflection, and the tissue thickness. With the capability of performing arthroscopic operations, the system has been applied to study the site dependence of the mechanical properties within the joint cartilage (Laasanen et al. 2003a; Lyyra et al. 1999b), the correlation of mechanical properties and tissue compositions (Kiviranta et al. 2008; Lyyra et al. 1999a), the

change of mechanical properties in repaired cartilage (Laasanen et al. 2003b), and the effect of spontaneous OA on cartilage properties (Saarakkala et al. 2003).

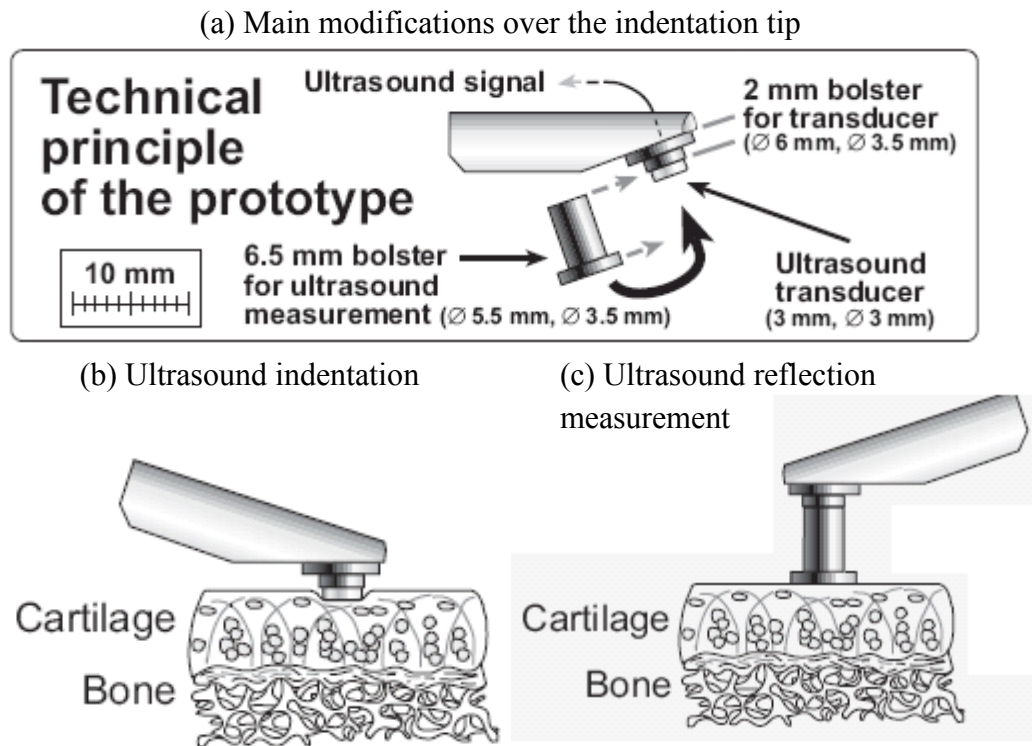


Figure 1-10 Improved arthroscopic indentation system for mechano-acoustical measurement of articular cartilage. (a) Principle (b) Indentation operation and (c) acoustical reflection measurement (Laasanen et al. 2002).

However, it should be noted that this system needs a special mechanism (insertion of bolster, Figure 1-10b) to switch between two modes: the mechanical testing and surface acoustical reflection measurement, which is quite inconvenient especially in clinical operations. Furthermore, the problems with the concave surface of a high frequency transducer are also present when the rigid ultrasound indentation is performed.

A water-jet indentation system utilizing an optical method to detect the cartilage deformation has also been proposed by a German group (Figure 1-11) (Duda et al. 2004). A pulses water-jet was used to compress the targeted tissue and the pressure of the water jet was registered by a pressure sensor. A simple photoacoustic intensity detection approach was adopted in this system to detect the surface displacement of the cartilage during water pulsation. To simplify the detection of deformation, it was assumed the optical intensity was proportional to the distance between the detected

surface and the probe tip in a certain range of deformation. By combining the deformation detected from the displacement of the tissue surface and the water pressure, the hardness of the tissue could be quantified. One limitation of the system is the assumption of linear relationship between the optical intensity and cartilage deformation, which may be easily affected by the real situations such as the color of the cartilage surface.

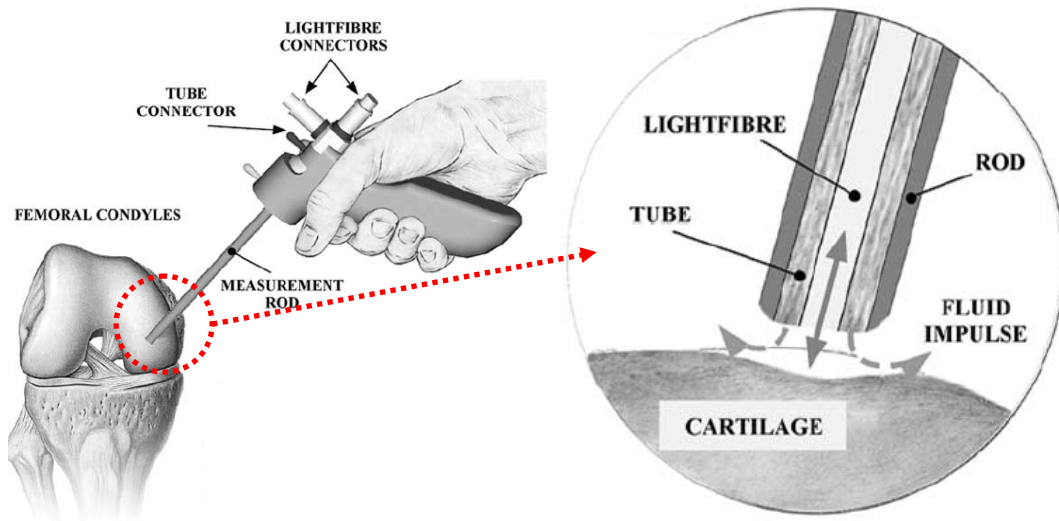


Figure 1-11 A water-jet indentation system incorporating an optical measurement for the measurement of mechanical properties of cartilage (Duda et al. 2004).

1.6. Objectives of the current study

We have reviewed the state-of-the-art new approaches using various modalities including optical, MRI, CT, ultrasound and arthroscopy-based indentation tests that may be potential for the mechano-acoustic assessment of articular cartilage degeneration at the early stage. The shortcomings of these approaches are briefly summarized as follows: for the radiographic diagnosis of OA and cartilage degeneration, it is still not sensitive enough for the early detection and usually too late for a preventive treatment when significant joint space narrowing is found in radiographic images; for the MRI technique, clinical routine use for articular cartilage diagnosis is still not so feasible as its resolution is not so high, the results are indirectly related to intrinsic properties and the cost is too high; for the optical methods, the investigation is still at its infancy stage and more research is necessary before these methods can become clinical tools. Therefore, high frequency ultrasound,

as an easily accessible modality with acceptable cost, is quite a preferable tool warranting much more future research for the quantitative assessment of articular cartilage.

Traditional ultrasonography of cartilage performed on the joint surface requires good posture of the subject, correct orientation of the probe and does not have high enough resolution for studying the articular cartilage. Direct observation through pure arthroscopy is not sensitive enough to detect the changes undertaken within the cartilage when low-grade degeneration happens. The arthroscopy-based indentation system Artscan (Figure 1-9) was developed to characterize the change of mechanical properties in articular cartilage. However, for this probe with a rigid indenter, it cannot measure the initial thickness of the cartilage, which is a very important parameter for calculating the stiffness of the cartilage in the indentation test, especially when the indenter diameter is comparable to the thickness of the tissue (Hayes et al. 1972). Furthermore, it is not so easy to reliably define the preset loading level on the reference plate without inducing significant deformation on the part of the cartilage under the reference plate. A constant loading on the reference plate induces a second level of indentation on the cartilage, which makes the test become more complicated and renders the analysis of the standard indentation model void. To introduce an ultrasound transducer at the tip of this probe was a good idea to solve the problem of measuring the initial thickness. However, for situations where higher frequency is a better choice, the concave shape at the tip of the focused transducer might hinder its use as a rigid contact indenter. In this situation, the water-jet ultrasound indentation is a better solution as a type of non-contact indentation. The use of a non-contact water-jet indentation will ensure the measurement of surface acoustic reflections without the necessity to add a bolster in the ultrasound indentation as developed by Laasasnen et al. (2002). On the other hand, the capability of the water-jet indentation system developed by Duda et al. (2004) is limited by the use of light intensity photo-detector for the measurement of the indentation depth, because it is based on the principle that the light intensity received by the photo detector is proportional to the distance between the probe and the cartilage surface in a certain range. However, the relationship between received light intensity and the distance is essentially nonlinear, and it may also depend on the color of the cartilage surface, which may change with the condition of the cartilage. Therefore, this method

may be difficult to be generalized as a reliable and systematic approach to measure the tissue deformation. Because no signal is present in the intensity photodetector for the cartilage-bone interface, the deformation can only be extracted from the surface displacement, i.e., the distance between the cartilage surface and the probe tip. Therefore, this method is also incapable of measuring the initial thickness of the tissue, which is an important parameter for calculating the Young's modulus of the cartilage in an indentation model (Hayes et al. 1972).

For the water-jet ultrasound indentation system (Lu et al. 2005; Lu et al. 2007; Lu et al. 2009), it has several advantages compared to previous systems: the first one is that it can provide a non-contact indentation, which is not limited by the concave shape of the ultrasound transducer or too small transducer as in the intravascular ultrasound (IVUS) system with catheter transducer; the second is that the indentation force induced can be measured from the water pressure, which is easy to be quantified by a pressure sensor not necessarily installed at the water-jet tip, where the space may be quite limited in arthroscopic applications; the third is the easier sterilization and disinfection because the indentation is induced by a fluid-jet but not rigid contact indenter, which may induce negative reactions of the tissue such as inflammation or even damage the tissue. The water-jet can be produced by a commercial medical pump and the coupling medium can be replaced by the physiological saline solution when used in clinical applications. Therefore, it is recognized very meaningful to further develop the water-jet ultrasound indentation system into a miniaturized one for the arthroscopic use which may lead to a lot of further research through using the developed probe for the quantitative assessment of articular cartilage. Furthermore, most previous work on study of articular cartilage degeneration used the enzymatic digestion as a model to induce the degeneration of cartilage. No study was conducted on cartilage sample with natural degeneration such as that in the animal model of osteoarthritis. In this study, the ultrasound-based measurement (Please be noted that the measurement based on the water-jet ultrasound indentation probe is also called “ultrasound-based measurement” in this study as ultrasound is the uniquely essential element in this technique) was also applied to the naturally degenerated cartilage samples to evaluate its usefulness. In summary, the objectives of the current study can be described as follows:

1. To develop an arthroscopy-based water-jet ultrasound indentation system, mainly the probe, which is potential for the intra-articular ultrasound-based measurement of cartilage degeneration;
2. To demonstrate the feasibility of using the developed system for the morphological, acoustic and mechanical assessment of early cartilage degeneration induced by enzymatic digestion or surgery in an animal model of osteoarthritis.

The ultimate goal of this project is to provide the related society a clinically potential tool for quantifying the changes in the early degeneration of the articular cartilage for the diagnosis of osteoarthritis and assessment of the treatment efficacies.

2. Methodology

2.1. Development of arthroscopy-based water-jet indentation probe

A two-step scheme was arranged for the development of the arthroscopy-based water-jet ultrasound indentation probe. The first step of miniaturization was realized by incorporation of a small metal rod (12 mm in diameter) and a small profile single element ultrasound transducer, which significantly reduced the size of the probe compared to the prototype; at the second step, a real arthroscopic version of the water-jet ultrasound indentation system was designed based on a realistic arthroscopic channel (5.5 mm in diameter) which adopted an intra-articular ultrasound (IAUS) catheter. Details of the probe design are presented as follows.

2.1.1. Miniaturized probe with a single-element ultrasound transducer

The miniaturized probe in Step-1 was constructed as shown in Figure 2-1, which also shows the comparison with the prototype probe (Lu et al. 2005). In the previous design, the prototype probe used a focused high frequency ultrasound transducer (Model V316B, Olympus Panametrics, Olympus NDT Inc., Waltham, MA, USA) which was about the size of 20 mm in diameter (bubbler included). Thanks to the incorporation of a small ultrasound transducer, the current miniaturization of probe was obvious compared to the prototype. The current probe was mainly consisted of a pen-sized aluminum rod with a diameter (Φ) of 12 mm. The length of aluminum rod was arbitrarily set as 11 cm for a convenient operation. A central channel with a diameter of $\Phi_1 = 3$ mm was excavated in the rod and a 10 MHz unfocused ultrasound transducer (XMS-310-B, Olympus Panametrics, Olympus NDT Inc., Waltham, MA, USA) with a diameter of 3 mm was installed at the tip of this probe. A smaller channel with a diameter of $\Phi_2 = 2$ mm was drilled on one side of the transducer as the exit of water-jet, which also served as the passage of ultrasound signal propagation. A water pipe was connected at the other side of the aluminum rod for input of the water-jet. During test, the water-jet is input from the pipeline at the left of the rod and then exits before the ultrasound transducer at the right side of the

rod. The water-jet serves both as the indenter and the coupling media for ultrasound propagation.

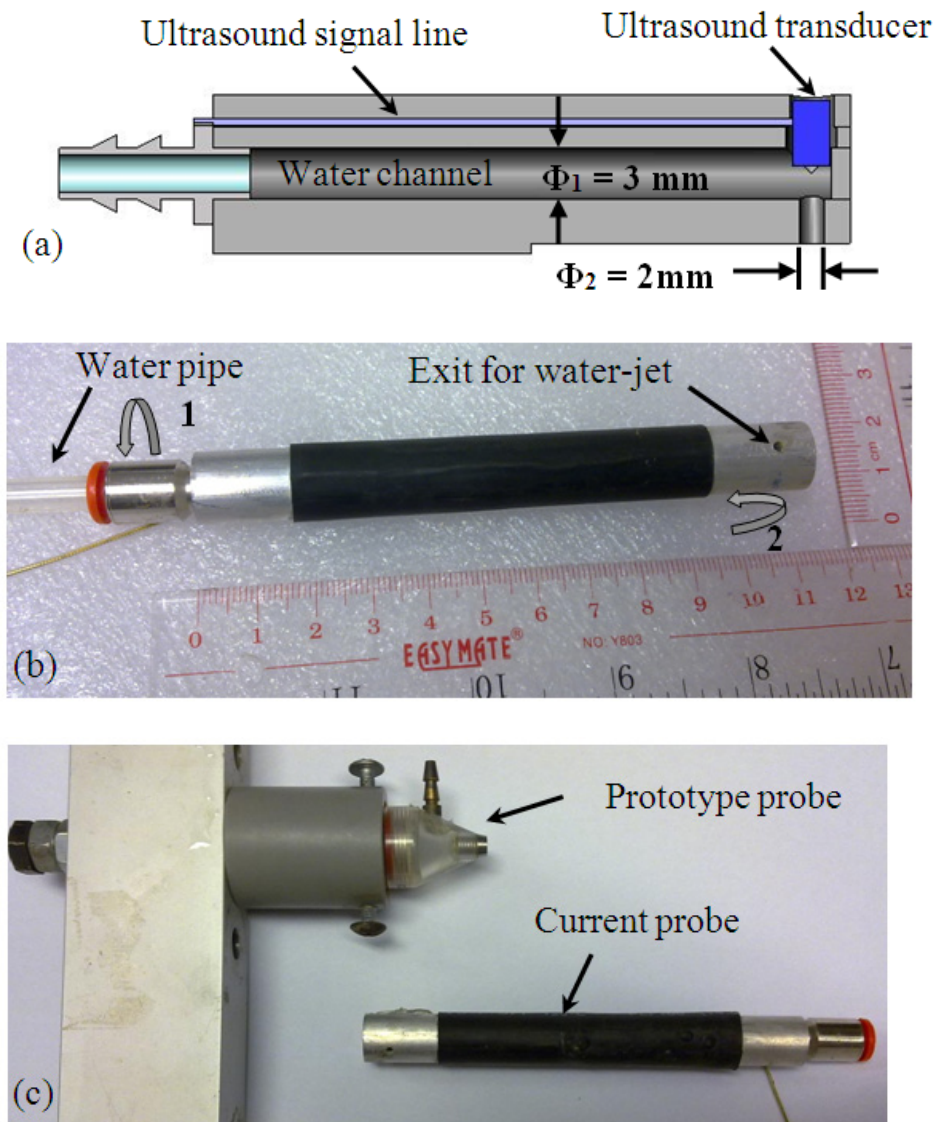


Figure 2-1 (a) A schematic diagram of the probe in Step-1 design; (b) A real picture of the probe. “1” and “2” indicate rotation or orientation of the probe for an optimal reception of the ultrasound signal during operation; (c) A comparison with the previous prototype of the water-jet ultrasound indentation probe.

In addition to the schematics of the miniaturized probe as shown in Figure 2-1, the schematics of the data collection system is shown in Figure 2-2. It mainly consisted of a control part and a data collection part. For the control part, the power of the water-jet was adjusted by an electronic proportional hydraulic valve (2835-A-04, Christian Burkert GmbH & Co. KG, Ingelfingen, Germany). A signal generator was

used to generate a cyclic sawtooth voltage signal in the range of 0~10 V to control the orifice size of the hydraulic valve in order to adjust the water pressure provided by normal tap water. For the data collection part, two signals, i.e. A-mode ultrasound signal and water pressure signal were recorded in the test. The ultrasound transducer was excited by an ultrasound pulser/receiver (Panametrics 5601A, Olympus NDT Inc., Waltham, MA, USA), which also received the ultrasound signal before it was transferred to personal computer for digitization by a 500 MHz sampling frequency 8-bit A/D converter (CS8500, Gage Applied Technologies Inc., Lockport, IL, USA). Ultrasound signals were sampled in the form of A-mode line with a fixed number of 4096 points, corresponding to a distance of about 6.3 mm using a 1540 m/s speed of sound assumed in soft tissues. The water pressure was recorded by a pressure sensor (PMP 1400, GE Druck Ltd., Leicester, UK) outside the probe and the signal was digitized by a 12-bit DAQ card (PCI 6024E, National Instruments Co., Austin, TX, USA). The ultrasound A-line signal and the pressure signal were synchronically sampled with a frame rate of 10 Hz and saved during a test for later offline analysis. A software program written in Microsoft C++ was used for the data collection and the offline processing (Figure 2-3). The initial thickness of the cartilage was measured by the time of flight from the two interfaces of the cartilage (surface and subchondral bone). The deformation during indentation was calculated by tracking the movement of the interface reflections from the upper surface of the tested specimen using a cross-correlation algorithm. In order to track the displacement, a small window was

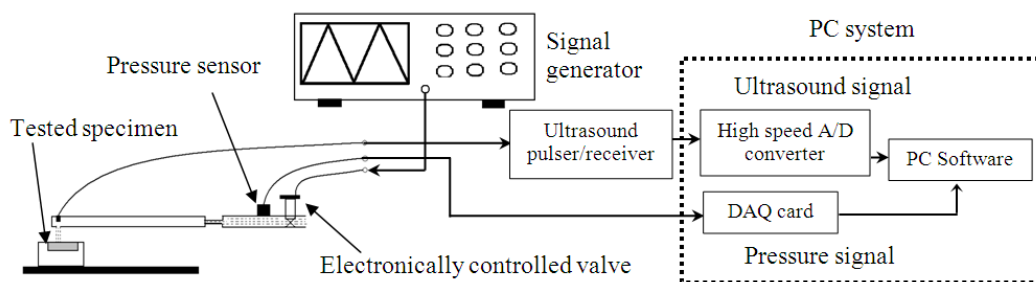


Figure 2-2 A schematics of the data collection system for the miniaturized water-jet ultrasound indentation probe.

chosen at the first frame and then it was used as a reference signal to search the interface movement during the indentation. As a linear relationship was established for the water pressure and the water-jet indentation force (Lu et al. 2005), the force of indentation was obtained from the water pressure through a calibration process and a

linear coefficient was used to convert the water pressure into the indentation force used for parameter calculation.

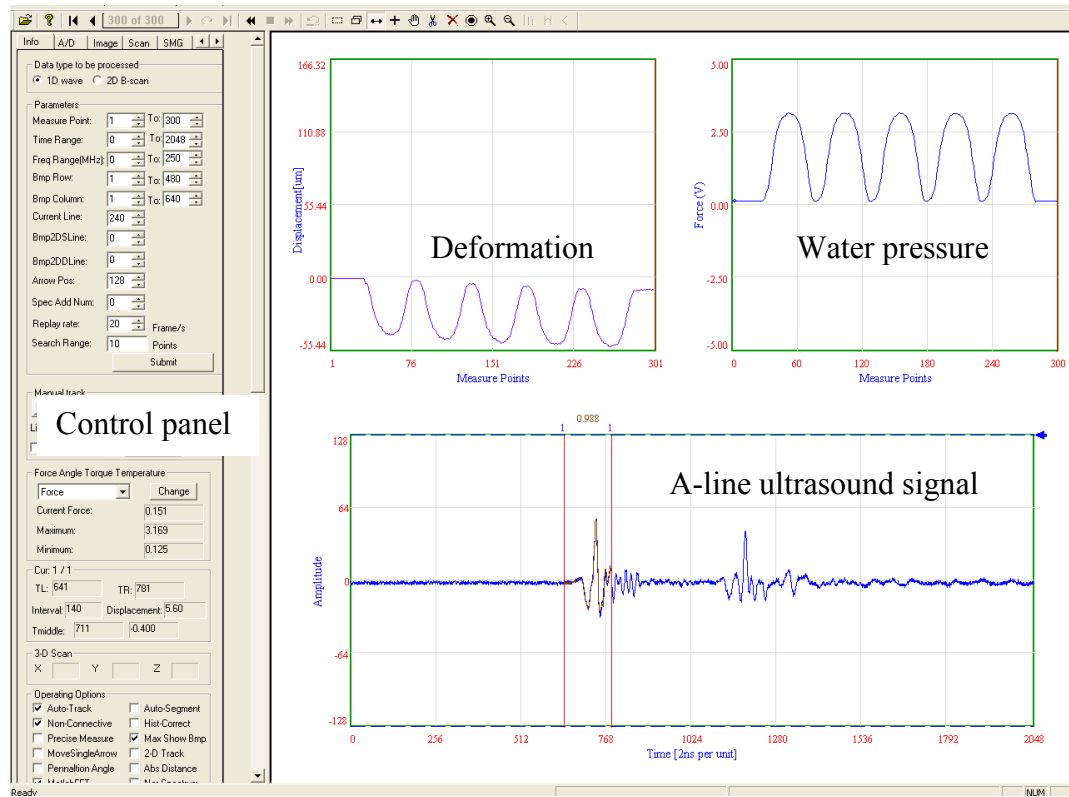


Figure 2-3 Software interface for the data collection of the water-jet ultrasound indentation system. The main two parameters acquired in the software are ultrasound A-line signal from the tissue and the water pressure signal. A-line signals were further processed to obtain the deformation.

2.1.2. Arthroscopy-based probe with IAUS catheter

Although the miniaturization was achieved using the single element ultrasound design as described in Subsection 2.1.1, the size of the probe was yet not small enough for an arthroscopic operation. Therefore, further miniaturization was still necessary for making a real arthroscopic measurement of the cartilage within an intact joint. The intravascular ultrasound (IVUS) transducer is a potential intra-articular ultrasound (IAUS) imaging device that can be directly adopted for the design. In the following sections, IAUS was generally used to indicate the use of IVUS catheter for the imaging of cartilage in the current study. Firstly, in order to verify the usefulness of IAUS, experiment was conducted to demonstrate that IAUS could be used to detect

the early degeneration of articular cartilage as described later in Subsection 2.2.4.1. Then after the verification experiment, the IAUS was adopted in the arthroscopic design (Step-2) to realize a real endoscopic version of the water-jet ultrasound indentation system. Details of the design are described as follows.

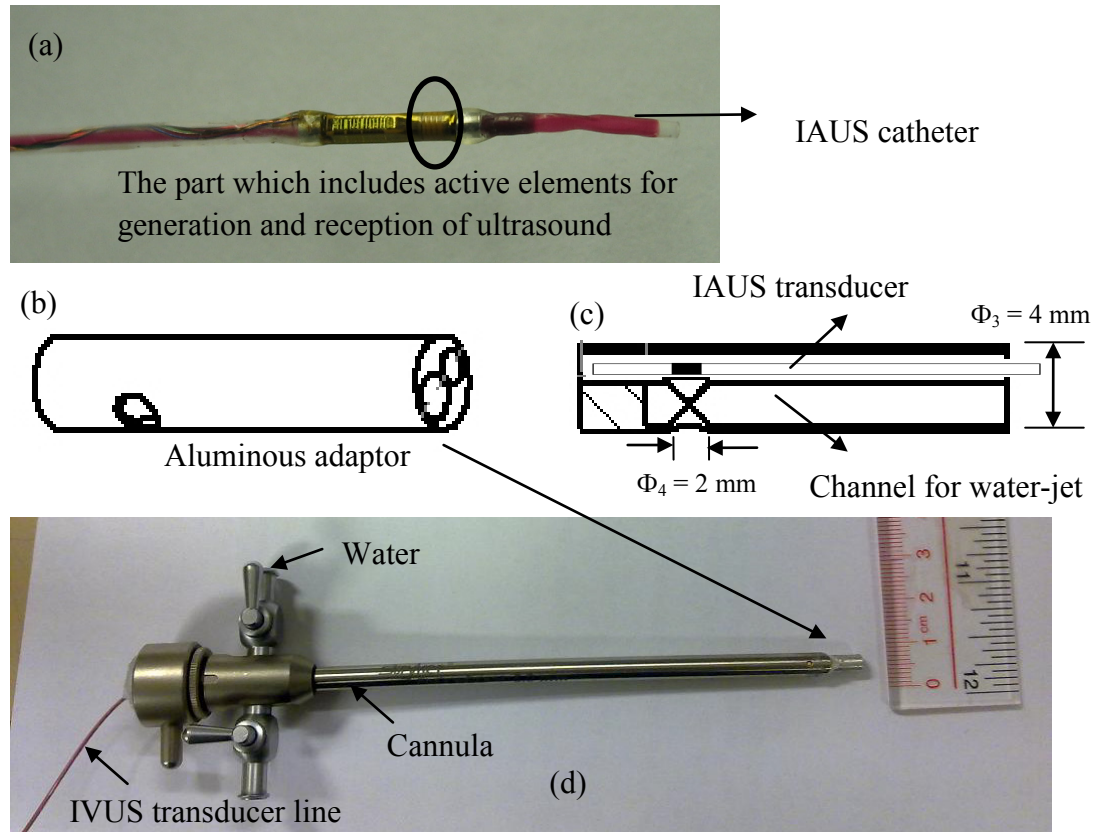


Figure 2-4 (a) A real picture of the IAUS probe; (b) An overall view of the aluminous adaptor for incorporation of the IAUS transducer used in arthroscopic channel; (c) A sectioned view of the internal structure of the adaptor. The black part of the IAUS transducer indicates the active elements which transmit and receive ultrasound signals; (d) A real picture of the arthroscopy channel-based water-jet ultrasound indentation probe.

In order to include the IAUS transducer in the probe, a small adaptor was fabricated. The schematics of the adaptor is shown in Figure 2-4 (b) and (c). It is made of aluminum with a diameter of $\Phi_3 = 4 \text{ mm}$ and a length of 20 mm. Two channels were excavated in the aluminous adaptor. One with a diameter of 1.5 mm was used for the installation of the IAUS catheter and the other with a diameter of 2 mm was used for the passage of the water-jet. An opening orifice of $\Phi_4 = 2 \text{ mm}$ was designed at one side of the adaptor for producing the water-jet. A real-time

intravascular ultrasound imaging system (In-Vision Gold, Volcano Inc., San Diego, CA, USA) with a catheter of 3.5 F (~1.2 mm) (Ref 85900, Eagle Eye Gold, Volcano Inc., San Diego, CA, USA) and frequency of 20 MHz was used for the system setup. A real picture of the small catheter of the IAUS system is shown in Figure 2-4 (a). In order not to block the reception of IAUS signal from the detected object, the part of the IAUS catheter which included the active elements for transmitting and receiving acoustic wave was just installed on top of the open orifice as shown in Figure 2-4 (c). After the IAUS transducer was fixed inside the adaptor, it was further installed at the tip of the working channel of an arthroscopic cannula with an internal diameter of 4.7

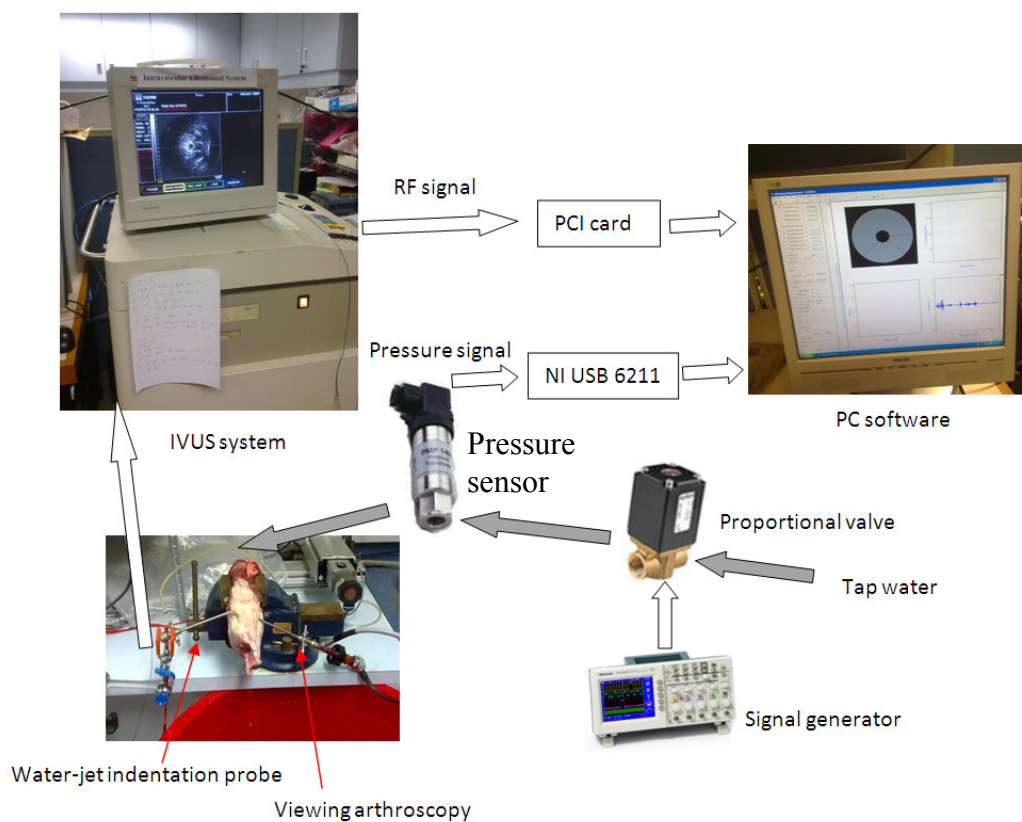


Figure 2-5 A schematics showing the main components of the arthroscopy-based water-jet ultrasound indentation system.

mm and an external diameter of 5.5 mm (Stryker arthroscopy, Stryker Inc., Kalamazoo, MI, USA) as shown in Figure 2-4 (d). The IAUS catheter passed through the channel and then left at the back of the cannula before it was connected to the main unit of the IAUS imaging system. The back of the cannula where the IAUS catheter went out was then sealed by adhesive tape to prevent the leakage of water. The prevention was effective with the current design but it should be carefully

reconsidered if this probe will be marketed as a commercial device later. The water was input from the two side inlets of the cannula as shown in Figure 2-4 (d). When one inlet was used for input of water-jet, the other one was closed for preventing water leakage during water-jet indentation.

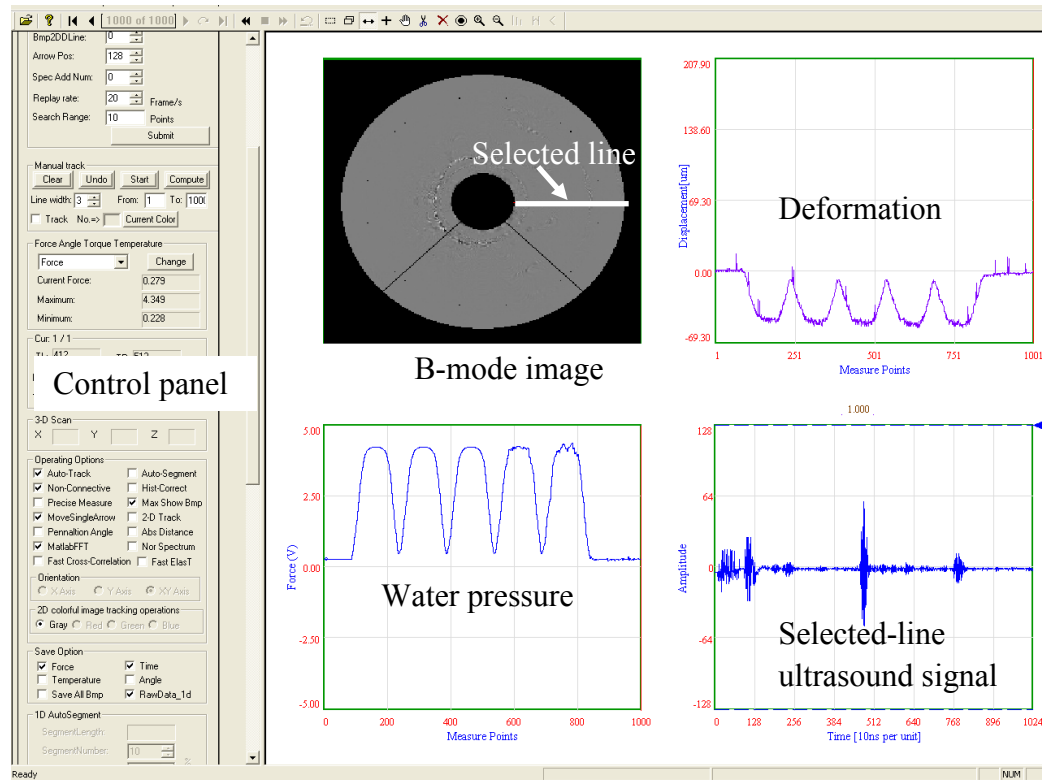


Figure 2-6 Software interface for the data collection of the arthroscopy-based water-jet ultrasound indentation system. The two parameters acquired in the software are ultrasound A-line signal from the cartilage tissue and the water pressure signal. Compared to the software version of the single element transducer-based miniaturized probe, a B-mode image is shown in this software interface and a target line is selected for the signal display and data storage.

Figure 2-5 shows the main components of the arthroscopic water-jet ultrasound indentation system. The IAUS system basically provided a high frequency ultrasound imaging for the cartilage and the radiofrequency (RF) signal could be separately output in real time for the custom use. A custom-designed PCI card was used to input the ultrasound RF signal into a personal computer for display and storage. For the RF signals, it was sampled at 100 MHz at a frame rate of ~30 Hz. In each frame, it included 512 A-lines forming a 360° view of the object surrounding the catheter.

Each A-line consisted of 1024 points for analysis. Custom-designed software programmed using C++ was used to control the data collection and processing as shown in Figure 2-6. For simplicity, a single A-line passing the center of the water-jet channel was selected for the data storage and analysis. The specific angle could be adjusted in the range of 0~360° in the software. For the water-jet production and water pressure data collection, it was similar to that part as described in Subsection 2.1.1. In brief, a sawtooth voltage was generated by a signal generator to control the orifice size of the proportional valve and consequently control the power of the water-jet. The water pressure was sampled by a pressure sensor and was connected to the personal computer using a DAQ card (NI USB-6211, National Instruments Co., Austin, TX, USA). The RF A-line ultrasound signal and pressure signal were synchronically collected by the software and then saved for off-line analysis. When the probe was applied to the intra-articular measurement of intact joint, the view arthroscopy can be incorporated to guide its operation.

2.2. Experimental validation studies

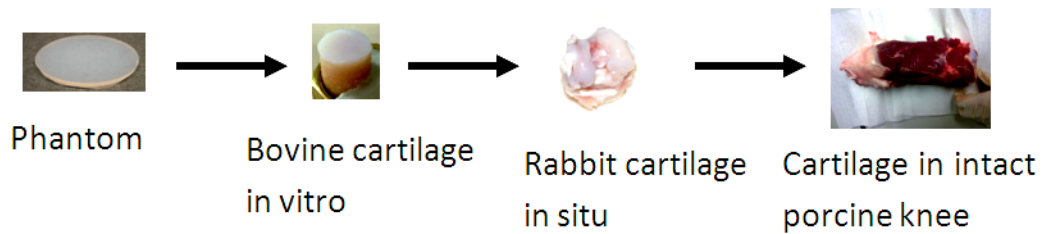


Figure 2-7 A flowchart of the experimental validation studies for the developed arthroscopy-based water-jet ultrasound indentation system.

The experimental studies were divided into four parts as shown in Figure 2-7. The first part validated the performance of the miniaturized probe using silicone phantoms. The second part validated the developed system on in-vitro bovine cartilage samples using the enzymatic digestion as a model to induce cartilage degeneration. The third part validated the ultrasound-based measurement on the in-situ rabbit knee cartilages in an animal study of OA. As the previous studies were all based on the degeneration model using the enzymatic digestion, this was the first time

that the ultrasound-based measurement technique was applied to naturally degenerated articular cartilage. In the fourth part, preliminary pre-clinical experiment was performed to demonstrate the potential of the developed arthroscopy-based probe for practical assessment of cartilage located in intact unopened porcine knee joints. For all the experimental studies, the details were all presented in the order of specimen preparation, experimental test, extraction of parameters and statistical analysis. It should be noted that when similar parameters were used in different experimental studies, the details for extraction of these parameters were given when they first appeared and only brief description was given subsequently.

2.2.1. Experiments on silicone phantoms

2.2.1.1. Phantoms preparation

Totally 28 silicone phantoms with a diameter of 4 cm were fabricated to test the feasibility of the Step-1 miniaturized water-jet ultrasound indentation probe for the measurement of soft tissue elasticity. The phantoms were made of mixture of silicone and softening oil and the stiffness was controlled by mixing different proportions of the two components, with increased proportion of oil rendering a decreased stiffness of the phantom. The speed of sound (SOS) and the thickness of these phantoms were simultaneously measured using an object insertion method. This method was described in detail in a previous publication for the simultaneous measurement of SOS and thickness for articular cartilage (Patil et al. 2004). In brief, the ultrasound signals reflected from the interval between the ultrasound transducer and an underlying metal plate were recorded with and without the insertion of the phantom to be measured. The change of propagation time before and after the insertion of object was used to calculate the SOS and then the thickness of phantom based on a constant SOS of the immersing solution.

2.2.1.2. Phantom tests

The indentation was performed on the phantoms with a manual operation using the miniaturized water-jet indentation probe (Figure 2-8a). The silicone phantom was fixed on a steel plate. A cyclic indentation was conducted with the whole probe immersed in water. A typical cyclic indentation included two cycles of loading and unloading processes which were completed in approximately 10 s. A maximum

pressure of 200 kPa was used for the water-jet which was supplied directly from the tap water system. The phantoms were also tested using a rigid indentation in order to validate the results of the water-jet indentation. The rigid indentation system was a custom-designed testing machine used for convenient mechanical test on small specimens (Figure 2-8b). Briefly, an LVDT displacement sensor (stroke: ± 15 mm) and a force sensor with a capacity of 10 N were installed at the tip of a stepper motor with a maximum travel range of 8 mm and a minimum motion step of 0.03 mm. A custom-designed program in LabWindows/CVI (National Instruments Co., Austin, TX, USA) with a graphic user interface (GUI) was employed to control and collect data from the system. An indentation process with similar maximal indentation force and indentation speed to that conducted by the water-jet probe was performed on the phantoms with a metal cylindrical indenter of $\Phi = 2$ mm. Three repeated tests were conducted for each phantom under the two types of indentation test.

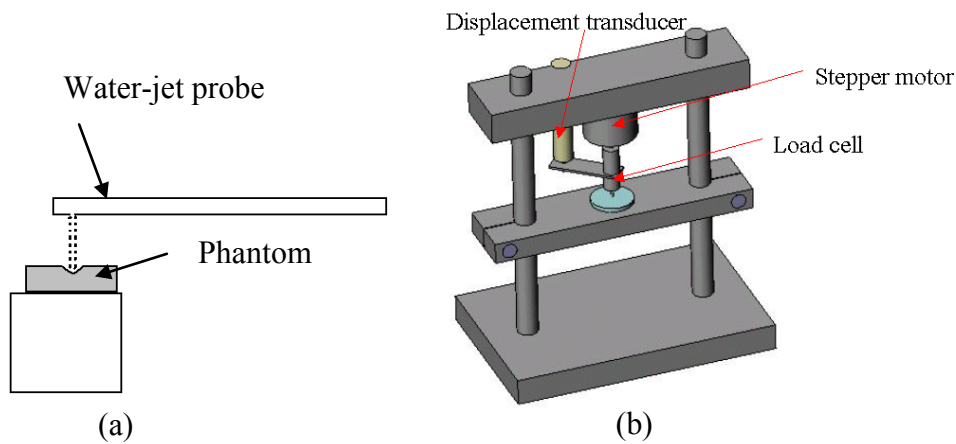


Figure 2-8 The test of phantom under (a) the miniaturized water-jet indentation probe and (b) a custom-designed indentation device.

2.2.1.3. Extraction of parameters

An f/d coefficient indicating the force/deformation was extracted from the water-jet indentation test to demonstrate the effectiveness of mechanical properties measurement using the newly developed probe on silicone phantoms. The averaged SOS measured from the abovementioned object insertion experiment was used for calculating the deformation of the phantom. For the data processing, a pre-load force of 0.05 N was applied for calculating the f/d coefficient:

$$k = f/d \quad \text{E 2.1}$$

where f is the indentation force and d is the deformation. When the tissue thickness becomes large enough compared to the radius of the indenter, the defined f/d coefficient is a good indicator of the Young's modulus of the tested samples (Huang et al. 2009). The f/d coefficient was calculated within a 10% deformation of the initial thickness. Only the loading phase was adopted for the data extraction. The averaged value of the three repeated tests was used for each phantom for final comparison between the water-jet and contact indentation.

2.2.1.4. Statistical analysis

For the phantom test, the two f/d coefficients obtained from the water-jet indentation test and contact indentation test were correlated to see whether they were high-correlated as a parameter to indicate the stiffness of the silicone phantom. The Pearson correlation coefficient was used to indicate the level of correlation with $p < 0.05$ used as the level for judging the significance of correlation.

2.2.2. Experiments on bovine cartilage in vitro

2.2.2.1. Cartilage specimen preparation and histology

For the cartilage test, mature fresh bovine patellae with a normal color without surface disruption, trauma or erosion were obtained from a local market within six hour of sacrifice. A total of 50 osteochondral disks (16 mm in diameter and ~15 mm in height) were prepared from the upper lateral quadrant of the patella (Figure 2-9a). Among them, 10 were used for measurement reliability study and the remained 40 were used for enzymatic digestion study. These osteochondral disks were made by drilling from the patellar surface using a hole-saw and then prying using a screw driver. During the preparation process, physiological saline solution was added occasionally in order to keep a good hydration of the specimens. The osteochondral disks were then embedded in a sample holder using epoxy putty (Figure 2-9b). Then the specimen was steadily fixed in the sample holder during the experiment for a reliable test. After preparation, the specimens were stored at -20°C in a refrigerator. On the experimental day, the disk was thawed in physiological saline for at least two hours under a room temperature of $24 \pm 1^\circ\text{C}$ before the test. Two enzymes, i.e.,

collagenase and trypsin were used to digest the cartilage samples to introduce a simulated degeneration of the cartilage, typically inducing the breakdown of its collagen network and depletion of PGs, respectively. Collagenase is used to mainly digest the collagen network (Shingleton et al. 1996), and trypsin has the most significant effect on PG depletion with some minor effect on the collagen network (Harris et al. 1972). The disks for testing ($n = 40$) were divided equally into two groups: collagenase ($n = 20$) and trypsin ($n = 20$) treatment groups. For the collagenase treatment group, disks were immersed in 30 U/ml collagenase (GIBCO, Invitrogen Corporation, Carlsbad, CA, USA) solutions and kept in an incubator (Incucell-V111; MMM Medcenter Einrichtungen GmbH, Munich, Germany) at 37 °C for 24 h (Wang et al. 2010a). For the trypsin treatment group, disks were placed in 0.25% trypsin-ethylenediaminetetraacetic acid (EDTA) solution (GIBCO, Invitrogen Corporation, Carlsbad, CA, USA) and kept in the incubator at 37 °C for 4 h (Wang et al. 2010a). After the digestion, the disks were rinsed and submerged in the physiological saline solution for one hour before retest.

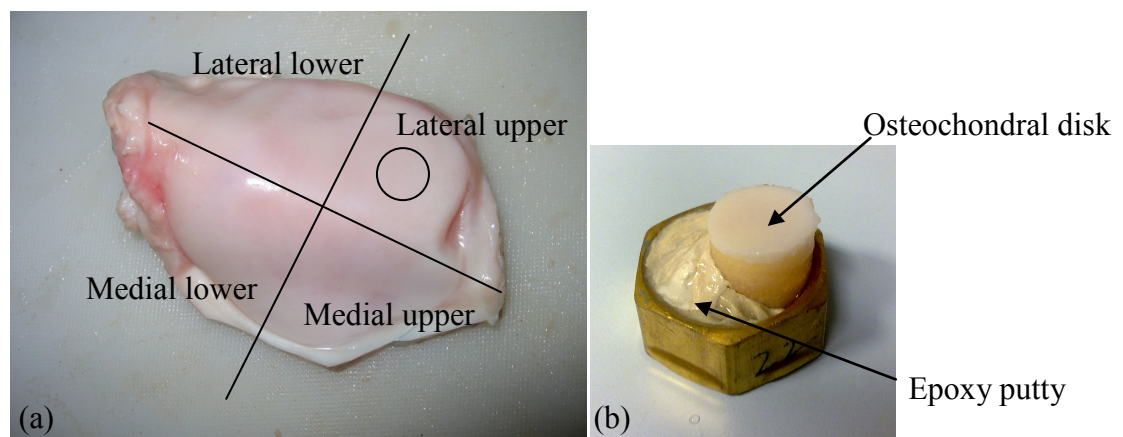


Figure 2-9 (a) A typical picture of a bovine patella; (b) Embedding of an osteochondral disk in a sample holder.

After all the tests were conducted, six normal cartilage samples from the reproducibility study, six samples from the trypsin-digested group, and six samples from the collagenase-digested group were randomly selected from each group for histological evaluation of proteoglycan content according to the protocol used in an earlier study (Wang et al. 2010a). In brief, the cartilage samples went through the procedures of fixation, decalcification, dehydration and sectioning, before the 6- μ m

tissue sections were stained and contra-stained by the Safranin O red and fast green, respectively, to observe the change of PG contents in cartilage samples. After staining, the region stained with Safranin O red showed where PG existed while that with green color indicated the depletion of PG in the histological image (Leung et al. 1999).

2.2.2.2. Cartilage tests

The cartilage specimens were also tested to study the feasibility of using the currently developed miniaturized probe to detect the early degeneration of articular cartilage. During the test, the probe was installed horizontally with a maneuverable arm which could be translated in a vertical direction using a manual micrometer-driven linear stage (Figure 2-10). The probe could also be rotated along its long axis to adjust the acoustic beam direction so that a maximum signal could be obtained from the cartilage surface to ensure a perpendicularity of the incident ultrasound into the cartilage. The sample holder with the osteochondral disk was installed in a heavy base stage for a steady fixation of the cartilage during test. The probe was just placed over the center of the osteochondral disk and in the experiment the distance between the cartilage surface and the probe was set to be fixed at 1 mm. Both the probe and the base stage were immersed in a water tank during the measurement (Figure 2-10a). Acoustic signal and indentation test data were collected during the experiment. The experiment procedure is described as follows: firstly, the cartilage was measured for the thickness and the acoustic parameter, i.e. the surface reflection. In detail, the ultrasound A-line signals reflected from the center of the disk were measured for three repeated times. Between two consequent tests, the specimen was taken away and then relocated, and the orientation of the probe would be readjusted to get the maximal reflected signal for each measurement. Secondly, after data collection for the morphological and acoustic parameters, a cyclic water-jet ultrasound indentation test was then conducted on the osteochondral disk. Cyclic indentation was performed on the cartilage. Totally 4 cycles of loading and unloading with a period of 10 s were conducted in the indentation test. During the indentation, the maximum pressure of the water-jet was set to be 330 kPa, which equaled to a maximal indentation force of 0.5 N on the cartilage surface. A typical indentation curve along with time is shown in Figure 2-10 (b). A typical indentation test was completed in less than three minutes. The water-jet indentation test was also repeated for three times for one specimen.

Between two indentation tests, the sample was placed back into physiological saline solution for full recovery for at least half an hour (Bae et al. 2006; Wang et al. 2010a).

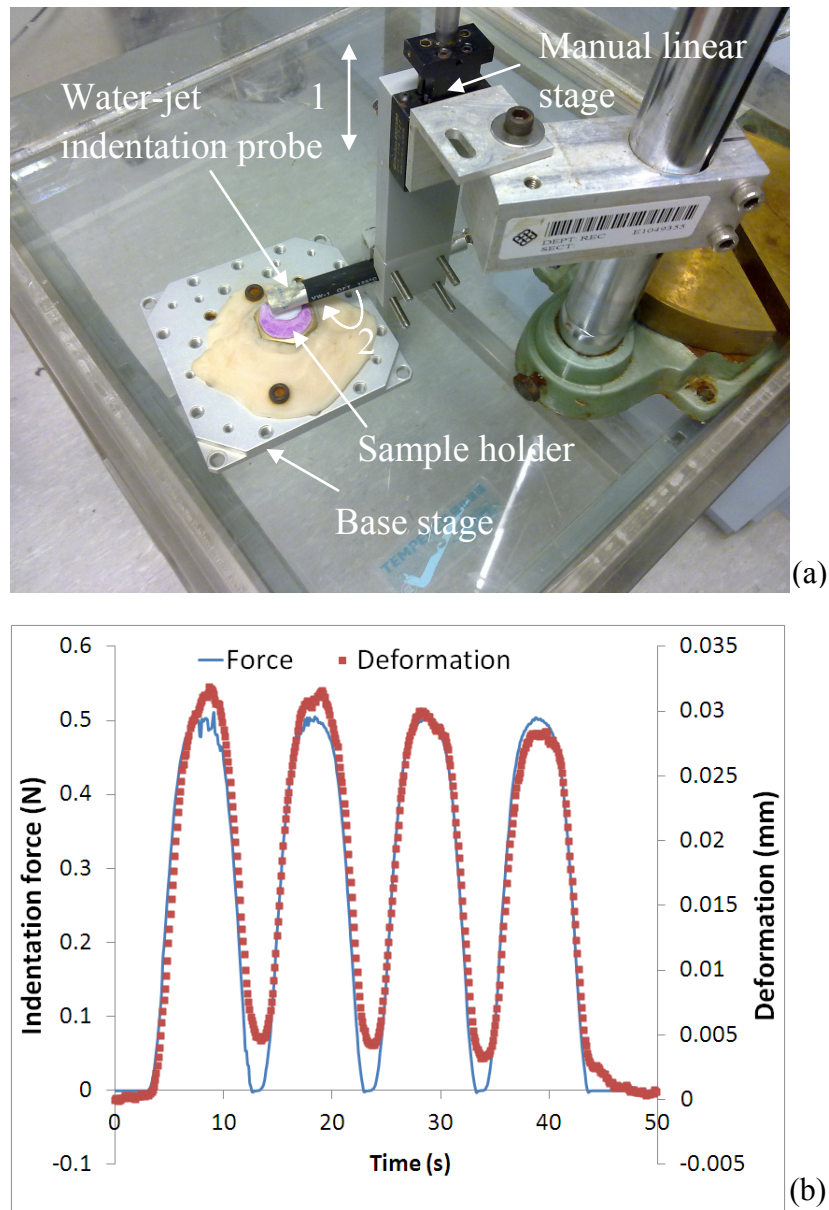


Figure 2-10 (a) The experimental setup for the miniaturized water-jet indentation probe. “1” indicates the flexible adjustment for the distance between probe and sample, and “2” indicates adjustment of orientation of the probe; (b) A typical loading profile as shown by the force and deformation curves along with time

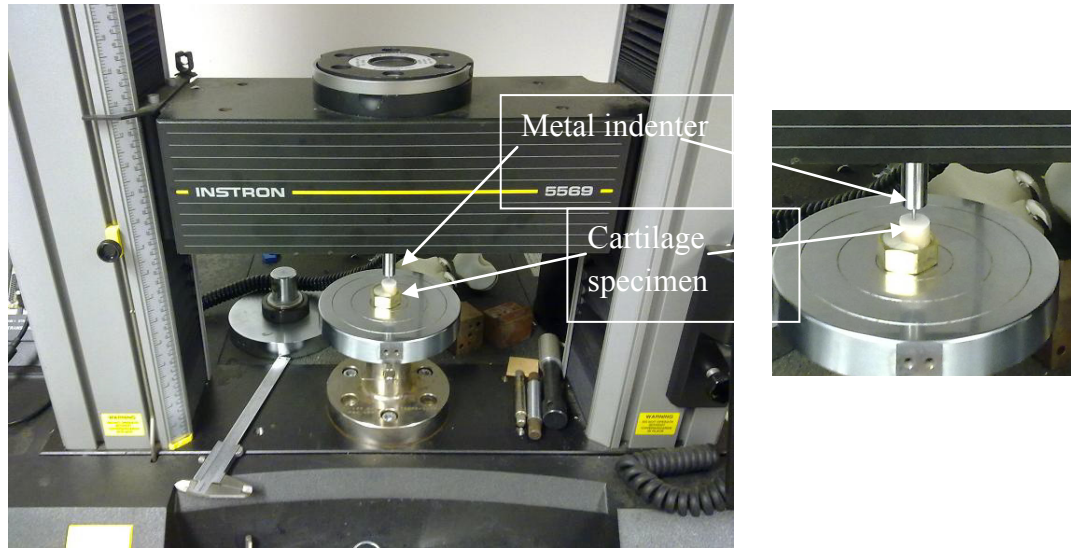


Figure 2-11 Mechanical indentation test for the articular cartilage. Details of the indenter on the specimen are enlarged as shown on the right side.

As reference, the osteochondral disk was also tested using a traditional rigid indentation under a standard mechanical testing machine (Instron 5569, Instron Co., Norwood, MA, USA) after the water-jet indentation (Figure 2-11). A stainless steel cylindrical indenter with a plane surface of 2 mm in diameter was used and similar indentation protocols were adopted in this test: a maximum indentation force of 0.6 N (slightly larger than that of water-jet indentation, but was truncated in data processing), an indentation speed of 1 mm/min and a total of 4 indentation cycles for each test. Between two indentation tests, the cartilage specimen was immersed in physiological saline solution for half an hour for full recovery. The averaged value of those three repeated tests was used to represent the properties of each disk. For the reproducibility test, six tests were conducted for each disk and the value of each of the 6 tests was used to analyze the measurement reproducibility, as described in Subsection 2.2.2.4.

2.2.2.3. Extraction of parameters

In this part, three types of parameters were used to demonstrate the capability of the current developed probe to detect the degeneration of articular cartilage. These parameters included the morphological (thickness), acoustic (integrated reflection coefficient, IRC) and mechanical properties (stiffness and energy dissipation ratio -

EDR) of the cartilage. The methods to extract these parameters are described as follows.

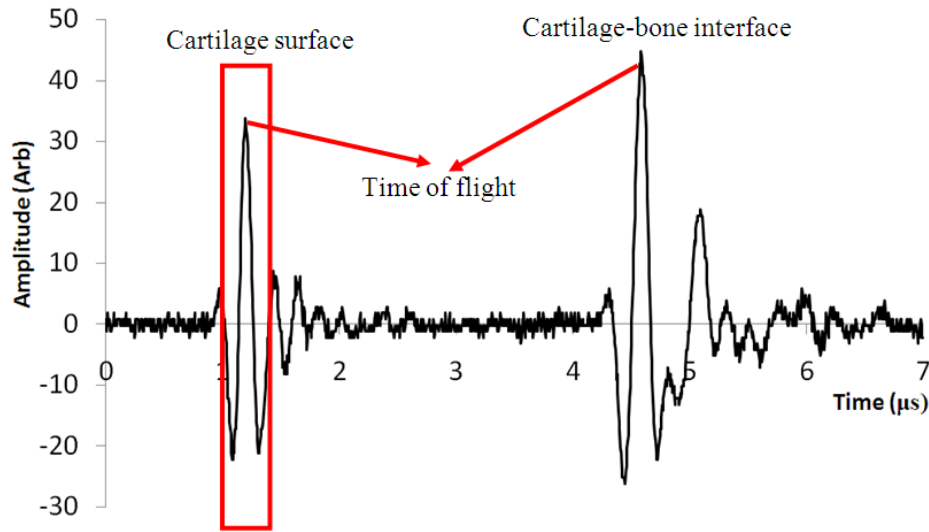


Figure 2-12 The measurement of cartilage thickness by the time of flight calculated from the two reflections indicating the cartilage surface and cartilage-bone interface. The red rectangular window indicates where to apply the Hamming windowing in order to calculate the integrated reflection coefficient (IRC) of the cartilage surface.

The thickness of cartilage was calculated by the time of flight from the cartilage surface to the subchondral bone multiplied by the speed of sound. The time of flight was measured from the distance of the peaks of two echoes observed in the ultrasound A-line, representing the reflections from the water-cartilage interface and cartilage-bone interface, respectively (Figure 2-12). A speed of sound value of 1610, 1595 and 1580 m/s was used in calculating the cartilage thickness in normal, trypsin-digested and collagenase-digested situations (Laasanen et al. 2002; Wang et al. 2010a).

The integrated reflection coefficient (IRC) was used to represent the strength of ultrasound reflection from the cartilage surface, showing the difference of acoustic impedance between the superficial layer of the cartilage and the water. The IRC was calculated after calibration based on the reference signal received from a stainless steel plate immersed in physiological saline solution placed at the same distance between transducer and target (Cherin et al. 1998; Saarakkala et al. 2004; Wang et al.

2010a). In details, the surface reflection signal was obtained by applying a Hamming window of 140 points in length which was centered at the peak value (Figure 2-12). The windowed signal was then zero-padded to 1024 points and FFT-transform was used to get its frequency spectrum $S_c(f, d)$ (f is frequency and d is the distance between transducer and cartilage surface). The frequency dependent reflection coefficient was then obtained by:

$$R_c(f) = \frac{S_c(f, d)}{S_r(f, d)} \quad \text{E 2.2}$$

where $S_r(f, d)$ is the reference spectrum from a steel plate placed at the same distance with respect to the cartilage surface. The distance d was neglected in $R_c(f)$ because the distance effect was eliminated after this calibration for the system-dependent effect. The reflection coefficient was then translated into a decibel unit and the integrated reflection coefficient (IRC) was calculated as:

$$IRC = \frac{1}{\Delta f_1} \int_{\Delta f_1} R_c^{dB}(f) df \quad \text{E 2.3}$$

where $R_c^{dB}(f)$ is the frequency-dependent reflection coefficient in unit of dB and Δf_1 is the -6 dB bandwidth of the ultrasound transducer, which was 4 to 18 MHz as measured in the current study.

The mechanical parameters of the cartilage were obtained from the indentation curve, which is typically shown in Figure 2-13 for a specimen before and after trypsin digestion. For the elasticity, a stiffness coefficient (SC) was obtained using the following equation:

$$SC = \frac{f/A}{d/L_0} = \frac{f}{d} \cdot \frac{L_0}{A} = k \cdot \frac{L_0}{A} \quad \text{E 2.4}$$

where $k = f/d$ in a unit of N/mm is the curve slope from a regression of the indentation force and deformation, L_0 is the initial thickness of the cartilage as measured by ultrasound and $A = \pi D^2/4$ is the indentation area, which is assumed to be circular having the same size with the water-jet beam, i.e. $D = 2$ mm as a diameter. The loading phase of the three indentation cycles from two to four was used to calculate the stiffness, regarding the first cycle as a preconditioning for the indentation test, as it was observed the preconditioning effect was most significant for

the first cycle. During the calculation, a minimal indentation force of 0.05 N was used and the deformation was controlled to be within 3% of initial thickness to assure a good linear relationship of stress and strain (Nitta and Shiina 2002), macroscopically, force and deformation. Cartilage is a viscoelastic, inhomogeneous and anisotropic tissue and the stiffness in the current study was obtained under specific experimental conditions, i.e. selected indentation speed at certain deformation range and a specific water-jet diameter, and reflecting the mechanical properties of the whole cartilage layer. Therefore, the stiffness should be called as “apparent stiffness”. For simplicity, “stiffness” was still used throughout this thesis. For the contact indentation test, a Young’s modulus E was calculated to represent the stiffness of the cartilage based on previous studies (Hayes et al. 1972; Lu et al. 2009):

$$E = \frac{1 - \nu^2}{2a \kappa(a/h, \nu)} \cdot \frac{f}{d} \quad \text{E 2.5}$$

where $a = 1$ mm is the radius of the indenter, ν is the Poisson’s ratio of the cartilage, f/d is defined as force/deformation ratio which has the same meaning with that of E 2.4, and κ is a scaling factor which is related to the aspect ratio a/h and the Poisson’s ratio ν . A constant Poisson’s ratio of 0.45 was used in the current study, assuming a large incompressibility of the cartilage (Lu et al. 2009). The κ value can be obtained from a table disclosed in a previous study (Hayes et al. 1972). To reduce the effect of cycle-dependence such as preconditioning typically shown in the degenerated cartilage, the stiffness or E was calculated for each indentation cycle separately and then averaged among cycles. The same protocols (preload of 0.05 N and 3% maximal deformation of the initial thickness) were used to calculate f/d for the contact indentation method as to the water-jet ultrasound indentation. For the viscous parameter, an energy dissipation ratio (EDR) was used by calculating the percentage of energy dissipated in each indentation cycle. Energy dissipation is a general phenomenon induced by hysteresis which can be typically observed in a mechanical test of soft tissues (Han et al. 2003; Hsu et al. 2005), which also exists for articular cartilage (Varga et al. 2007). The loading and unloading curves in an indentation cycle form a closed area which represents the dissipated energy. If the closed area is X and the area under the unloading curve is Y (see the symbolic illustration in Figure 2-13), then EDR is defined as:

$$EDR = \frac{X}{X + Y}$$

E 2.6

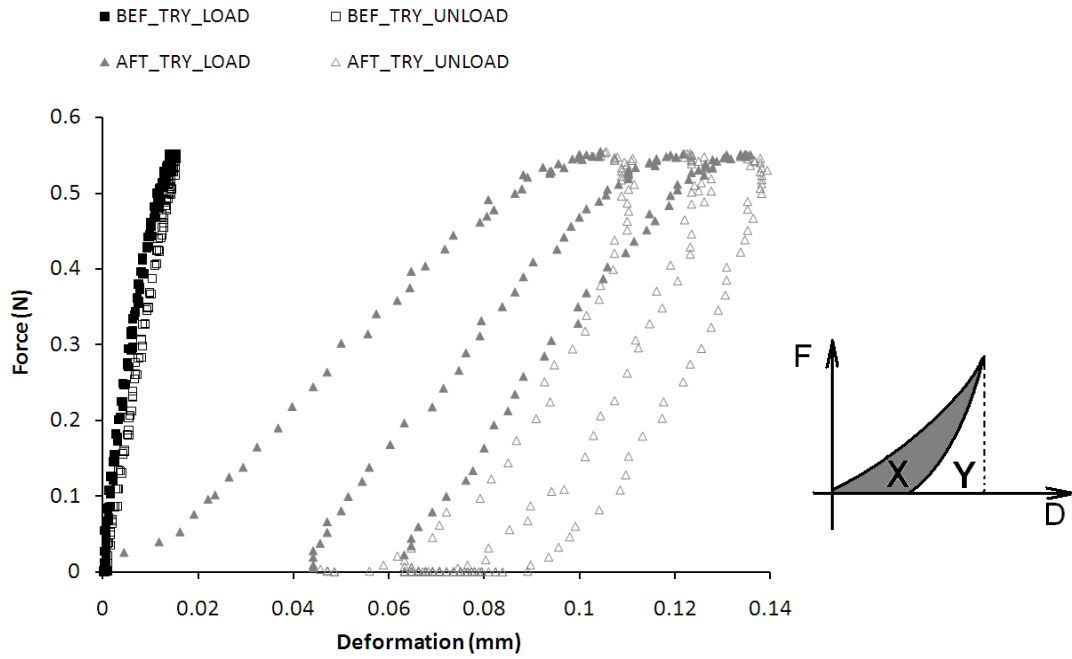


Figure 2-13 Typical force/deformation curves for the cartilage specimen before and after the trypsin digestion. A symbolic curve is also shown on the right to indicate how to calculate the energy dissipation ratio (EDR) from one cycle of loading and unloading.

EDR is a percentage value calculated by a numerical integration based on the trapezoid rule. All the data points were used in each indentation cycle for calculating EDR. All the extractions of acoustic and mechanical parameters were conducted using graphic user interface (GUI) scripts of Matlab (Mathworks Inc., Natick, MA, USA) using data files saved from the water-jet ultrasound indentation system.

2.2.2.4. Statistical analysis

For reproducibility study, a standardized coefficient of variation (SCV) was used. In detail, the measurement coefficient of variation (CV) is:

$$CV_j = \frac{SD_j}{\mu_j}$$

E 2.7

where μ_j is the mean and SD_j is the standard deviation of the six measurements on specimen j . For all the samples, the global measurement CV is calculated as (Gluer et al. 1995):

$$CV = \frac{\sqrt{\sum_{j=1}^m SD_j^2 / m}}{\sum_{j=1}^m \mu_j / m} \quad \text{E 2.8}$$

where $m = 10$, representing the total number of cartilage specimens. To compare the variation induced by measurement with that induced among samples without the effect of mean, SCV is defined as (Fournier et al. 2001):

$$SCV = \frac{CV \cdot \mu_{1st}}{4SD_{1st}} \quad \text{E 2.9}$$

where μ_{1st} and SD_{1st} represent the mean and standard deviation of the specimens when only the first measurement of each specimen was used for the calculation.

For the degeneration study, other statistical tests were performed to evaluate the change of tissue properties induced by the enzyme digestions. The parameters before and after each enzyme treatment were compared using the paired- t test and comparison between effects of trypsin and collagenase was conducted using the unpaired t -test. For comparison between the effects of trypsin and collagenase, a percentage value is calculated for the treatment effect using the following equation:

$$V_R = \frac{V_{post} - V_{pre}}{|V_{pre}|} \cdot 100\% \quad \text{E 2.10}$$

where V_R is the percentage change for each parameter V and the subscript indicates whether it is pre- or post-digestion value. The percentage change was calculated for the parameters of thickness, IRC and stiffness. For EDR, a direct difference between post-digestion and pre-digestion was adopted as it was already a percentage value. To compare the results of viscoelastic parameters with the reference indentation method, the Pearson correlation coefficient was calculated. A level of $p < 0.05$ was used to indicate a significant difference or the existence of a significant correlation. All the statistical tests were performed using the SPSS software (SPSS Inc., Chicago, IL, USA).

2.2.3. Experiments on rabbit cartilage in situ

2.2.3.1. Animal model and specimen preparation

Forty normal adult New Zealand White female rabbits weighing from 2.5 to 3.8 kg (mean, 3.2 ± 0.3 kg) were used in this study. These animals breeding and surgeries were conducted in the Beijing 301 Hospital through collaboration and specimens were the measured in Hong Kong. Surgical transection of the anterior cruciate ligament in the right femorotibial joint was performed in 30 rabbits under general anesthesia to induce osteoarthritis (OA). Medial arthrotomy was performed on the right femoropatellar joint to permit the transection of the anterior cruciate ligament. A routine procedure for skin incision closure was performed after the surgery. Antibiotics (penicillin 20,000 IU) were injected intramuscularly twice a day preoperatively and for 2 days postoperatively in the operated rabbits. Following surgery, free movement was allowed in separate cages for the duration of the experimental period. The control group consisted of 10 unoperated rabbits. Experiments on the rabbits were approved by the institutional animal care and use committee of the Beijing 301 Hospital and performed under the guidelines of the National Institutes of Health for the care of laboratory animals.

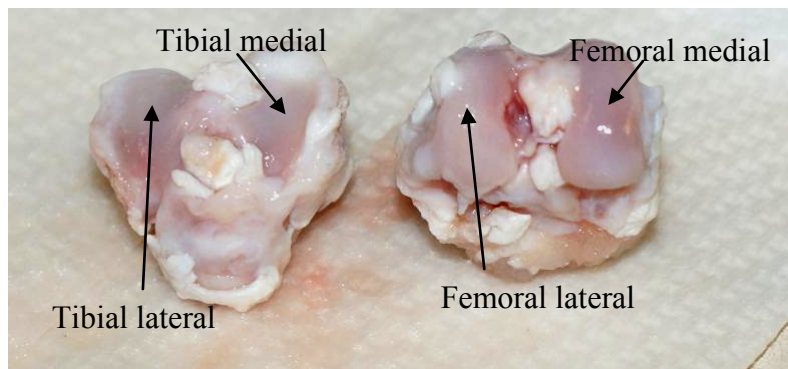


Figure 2-14 Preparation of the rabbit knee samples for the test of cartilage. Left: the tibial side; Right: the femoral side. Typical positions for the assessment are indicated by arrows.

At 3, 6, and 9 weeks after surgery, every 10 experimental animals were euthanized, respectively. The 10 animals in control group were euthanized after 1 week of breeding in the animal experimental center. Each of the right knees was dissected and sectioned with a band saw to expose the four surfaces: medial and

lateral femoral condyle and medial and lateral tibial plateau. A total of 80 cartilage samples, with size of about 10 mm × 10 mm × 15 mm in terms of width × length × height, including 40 from the femoral side and 40 from the tibial side (Figure 2-14), were obtained, wrapped with saline solution gauze and frozen at -20° C in a refrigerator before the test. The test positions included two sites from the femoral side and another two from the tibial side as shown in Figure 2-14.

2.2.3.2. Experimental tests

Samples were taken out from the refrigerator and then thawed in physiological saline solution for at least 2 hours before the test under a room temperature of $24 \pm 1^{\circ}\text{C}$. The assessment mainly included two parts: the high frequency ultrasound assessment for acquiring the morphological and acoustic properties and the tests of water-jet indentation and contact indentation for extracting the mechanical properties of the cartilage. The assessment points were selected as the center of the lateral and medial plateau and the apex of the lateral and medial condyles. After ultrasound and mechanical test, the samples were then sectioned for the histology study. The details of the procedure for the assessment were described as follows.

2.2.3.2.1. High frequency ultrasound measurement

A high frequency ultrasound imaging system (Vevo 770, VisualSonics Inc., Toronto, Canada) and a high frequency ultrasound transducer (Scanhead RMV708, VisualSonics Inc., Toronto, Canada) with a diameter of 4.5 mm and a central frequency of 40 MHz (Figure 2-15), were adopted for the imaging of rabbit articular cartilage. The 2D ultrasound imaging was achieved by a mechanical linear scanning of the ultrasound transducer. The -6 dB bandwidth of the transducer was 18 MHz to 55 MHz, which was experimentally determined for the reflected ultrasound pulse from a polished steel plate positioned at the focal point and immersed in saline solution. The lateral resolution of this transducer was approximately 70 μm . The focus length of the transducer was 4.5 mm in saline solution, counting from the surface of the transducer.

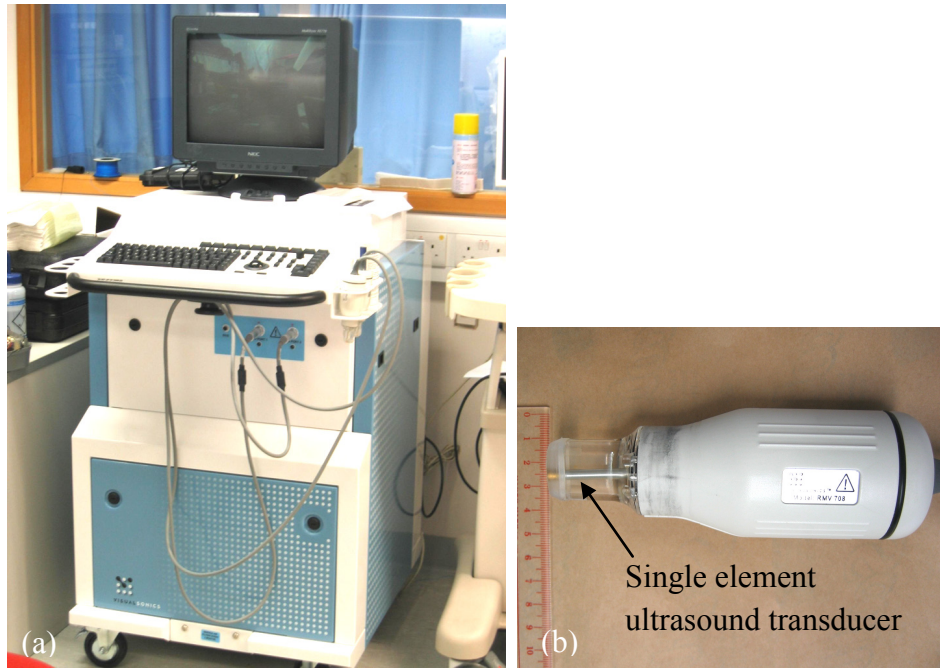


Figure 2-15 (a) The high frequency ultrasound imaging system (Vevo 770); (b) The RMV708 ultrasound probe.

The measurement setup is shown in Figure 2-16 (a). The sample was fixed on the bottom of a container in physiological saline solution using the Blu-Tack (Bostik, Thomastown, Australia). The ultrasound probe was fixed in by a cantilever of a frame and it could be moved in the vertical direction to set a proper distance between transducer and the cartilage surface. The container can be rotated during the measurement to scan the targeted region in different directions as shown in Figure 2-16 (b). A four-direction scan with an interval of 45° was arranged for each sample. The focus of the ultrasound transducer was placed at the surface of the articular cartilage during the measurement. The ultrasound scan included the measurement of B-mode images for the measurement of cartilage thickness and the collection of radiofrequency (RF) signals for the quantitative analysis as described in the following section. Typical pictures of the software interface for B-mode image and RF data collection are shown in Figure 2-17. The RF signals were obtained by entering the RF signal collection mode of the ultrasound imaging system. In this mode, a region of interest (ROI) with the size of $1.4 \text{ mm} \times 3.9 \text{ mm}$ was selected on the guided B-mode image. 100 lines were sampled in an A/D sampling frequency of 420 MHz and these RF signals were used for the data analysis (Figure 2-17b).

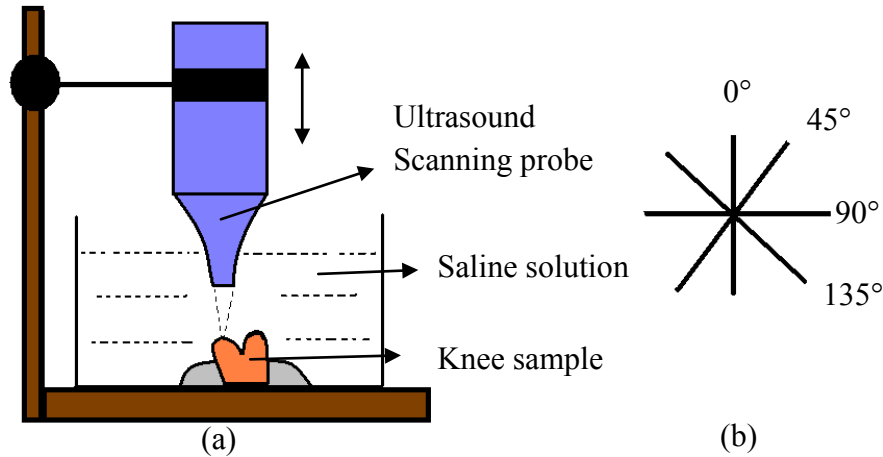


Figure 2-16 (a) The scanning of the rabbit cartilage using the high frequency ultrasound; (b) The pattern of the scanning directions for the ultrasound measurement at one point. The scanning width is ~ 1.5 mm for each direction.

For the data collection process, the cartilage sample was firstly fixed, and then the ultrasound transducer was placed at a proper position on top of the sample. Then B-mode images and RF signals were collected at one scanning direction before the container was rotated to scan the next direction following the pattern as shown in Figure 2-16 (b). For each rabbit knee, ultrasound scanning was conducted consequently at the femoral lateral, femoral medial, tibial lateral and tibial medial sites as shown in Figure 2-14. The position of the sample was finely adjusted before the test to assure that the right region of cartilage surface was scanned by the ultrasound imaging system. During the scanning, the cartilage surface was adjusted to be perpendicular to the ultrasound transducer in order to obtain maximal signal from the cartilage surface (Kaleva et al. 2009).

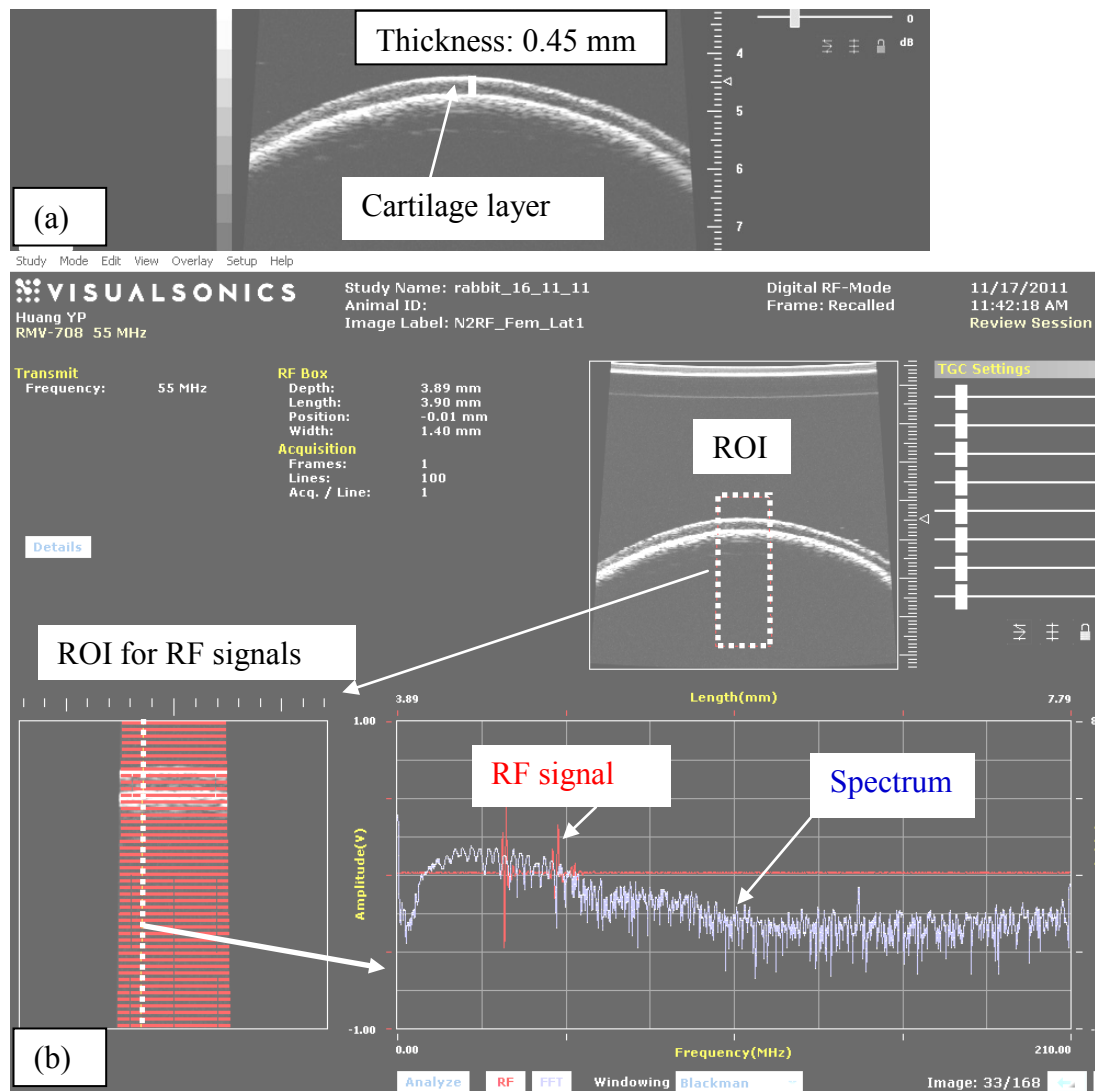


Figure 2-17 (a) A typical software interface showing the B-mode image for the knee rabbit cartilage at the femoral lateral condyle. The cartilage layer can be seen where two bright lines indicate the cartilage surface and the cartilage-bone interface; (b) A typical software interface showing the collection of RF signals. A region of interest (ROI) was selected at the B-mode images where 100 RF lines were collected without saturation of the amplitude. The single line RF signal and its spectrum coming from the dotted line are shown on the right lower corner of the image.

2.2.3.2.2. Water-jet indentation and contact indentation test

A water-jet ultrasound indentation was conducted on the cartilage to measure their mechanical properties. Firstly, the sample was fixed in a custom-designed sample holder as shown in Figure 2-18. Then it was placed under the water-jet ultrasound indentation probe. Fine adjustment of the sample holder was also

conducted to assure the right region of the cartilage was tested. When optimal signal was obtained from the cartilage surface, the indentation test was conducted. Similar indentation parameters as set in the previous Subsection 2.2.1.2 were used in the rabbit indentation test. In brief, a cyclic indentation with 4 cycles of loading and unloading was conducted on the cartilage. The period of one indentation cycle was 10 s and the maximum loading pressure was 330 kPa in each cycle.

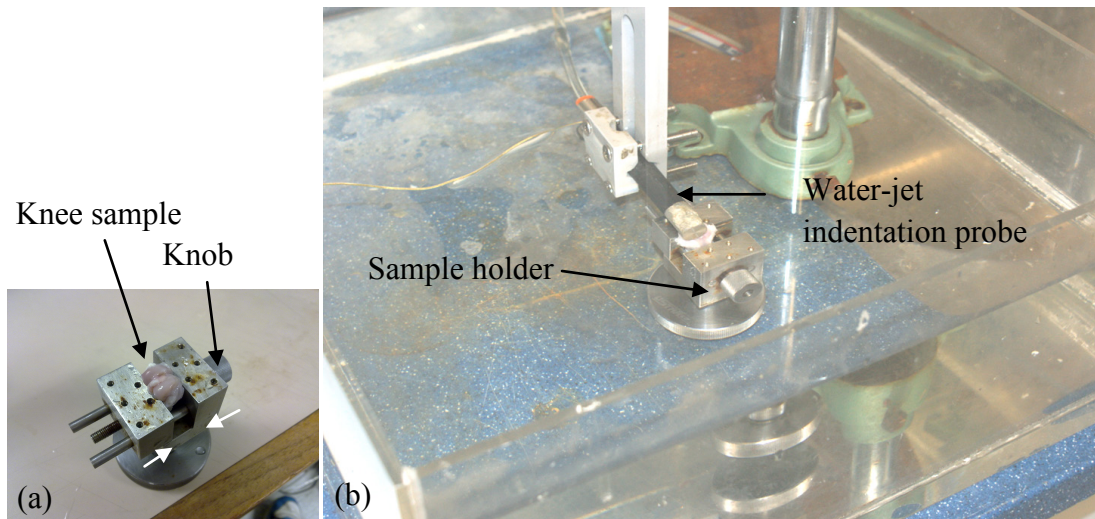


Figure 2-18 (a) The fixation of the knee sample for an indentation test in a sample holder. The two white arrows indicate the two arms can be adjusted by the knob to clamp the sample for a firm fixation; (b) The indentation test of cartilage sample with the water-jet ultrasound indentation probe.

As reference, the sample was also tested by the Instron mechanical testing machine as shown in Figure 2-19. A similar indentation protocol was adopted as described in Subsection 2.2.2.2. In brief, a maximum indentation force of 0.6 N was set for the cyclic indentation with a speed of 1 mm/min. Four cycles of indentation were performed for each test site and the average of the 4 tests was used to represent the mechanical properties of the tested tissue.

2.2.3.2.3. Histology and grading

After the acoustic and mechanical measurement, the femoral and tibial articular cartilage samples were fixed in 10% neutral buffered formalin. Tissue blocks were decalcified with 14% ethylenediaminetetraacetic acid (EDTA), dehydrated through graded alcohols, cleared with toluene, and embedded in paraffin. Six-micrometer (6-

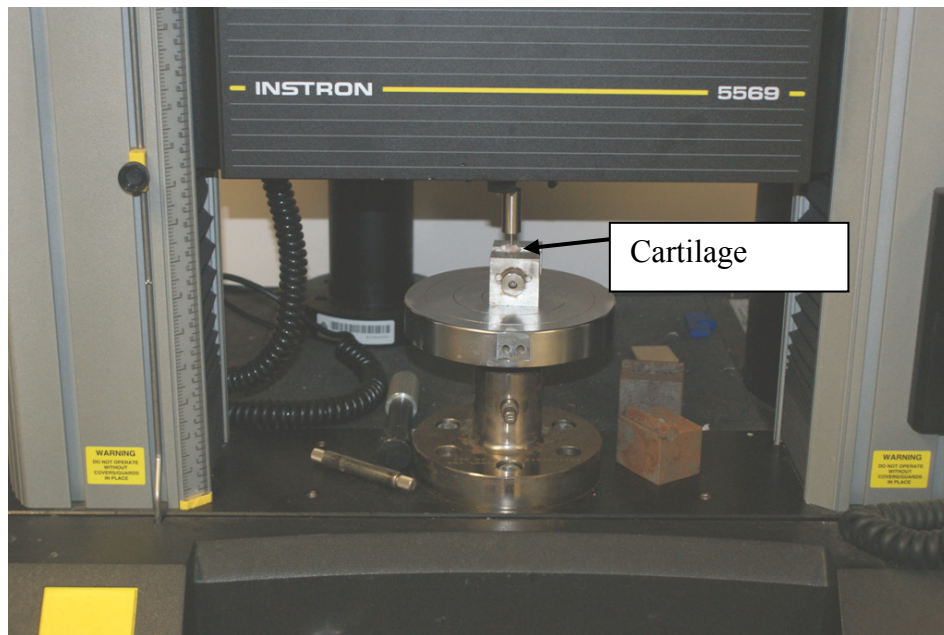


Figure 2-19 The fixation of the rabbit knee sample for an indentation test using the Instron mechanical testing machine.

μm) thickness sections were cut at the selected site centrally in the articular cartilage where acoustic and mechanical measurement was conducted. The sections were then stained with Safranin O, fast green and toluidine blue. Two histological sections from each site were evaluated by one certified pathologist blinded with regard to the surfaces studied. According to Osteoarthritis Research Society International (OARSI) grading, all the lesions of the samples were divided into five grades (Pritzker et al. 2006; Wang et al. 2011): Grade-0: normal; Grade-1 = uneven surface that can demonstrate superficial fibrillation; Grade-2 = surface discontinuity that may be accompanied by cell proliferation, increased or decreased matrix staining in the middle zone; Grade-3 = vertical fissures extending into the mid zone or erosion; and Grade-4 = denudation (the unmineralized hyaline cartilage is completely eroded); and Grade-5 = deformation. Samples were also further divided into three stages: normal (OARSI Grade-0), early OA (OARSI Grade-1 and Grade-2), and advanced OA (OARSI Grade-3 to Grade-5), for comparison of different stages.

2.2.3.3. Extraction of parameters

The parameters used here were similar to those described the Subsection 2.2.2.3, except an ultrasound roughness index (URI) was used here for representing the surface condition of the cartilage. In brief, the morphological, acoustic and

mechanical parameters were obtained to compare the difference among cartilage samples from different time points after surgery or among groups with different histological grades.

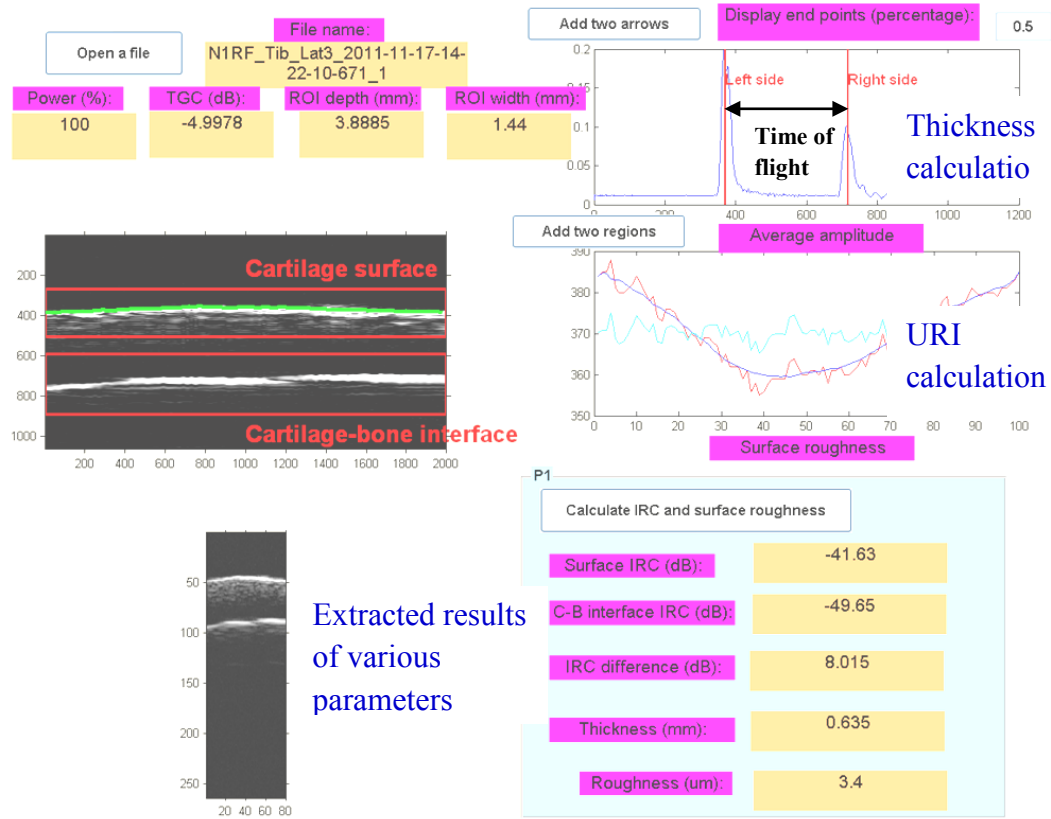


Figure 2-20 Matlab GUI interface for processing the data from the acoustic measurement. Thickness, roughness index and acoustic parameters were calculated in this GUI. For thickness, two cursors were used to indicate the two interfaces of the cartilage layer; For URI, a cartilage surface region was selected to indicate where to extract the surface profile and then the roughness index; for integrated reflection coefficient, the cartilage surface region was also used.

The morphological parameters included the thickness and surface roughness index of the cartilage (Wang et al. 2010a). The thickness could be measured from three different sources: Vevo 770 B-mode image, Vevo 770 RF signal and the water-jet probe ultrasound signal. For the first measurement from the B-mode image, measurement tool in the software was used as shown in Figure 2-17 (a). A line of which the two ends indicated the cartilage surface and cartilage-bone interface, respectively, was manually added in the image and then the thickness easily showed

up in the software. The second method utilized the high frequency RF signals for the measurement of cartilage thickness. A custom-designed graphic user interface (GUI) was programmed to calculate the cartilage thickness as shown in Figure 2-20. An amplitude signal which was an overall average of the signals in ROI was displayed in the GUI and two cursors were added in the peaks of the two interface signals to obtain the average time of flight for the ultrasound to propagate through the cartilage layer. Then based on constant speed of sound, the cartilage thickness was calculated according to the measured time of flight. The third method to measure the thickness of the cartilage was based on the ultrasound signal from the water-jet probe. This method was similar to that reported in previous Subsection 2.2.2.3 and thus not repeated here. The results from the three methods were all obtained and from the comparison, it was found that they were very similar. The result from the second method was used in this report. However, when the cartilage thickness was used for the calculation of mechanical parameters, the result from the third method was adopted because the thickness was directly obtained under the mechanical test.

For the surface roughness, a small region was selected in the image to indicate where the surface was located. Then for each line, the exact position of the surface was detected where 80% of the maximum amplitude of the surface region was met, counting in the direction from the surface to the bone. In order to exclude the effect of nature fluctuation of the surface profile on calculating URI, a nature surface profile was also calculated by a smoothing technique. The root-mean-square of the surface profile was defined as the ultrasound roughness index (URI) of the cartilage which is calculated according to the following equation:

$$URI = \sqrt{\frac{\sum_{k=1}^{100} (s_k - \bar{s}_k)^2}{100}} \quad \text{E 2.11}$$

where s_k is the originally extracted surface profile and \bar{s}_k is the smoothed surface profile at line k between 1 and 100. URI was defined in the unit of μm in this study and it was potential to reflect the change of cartilage surface due to the fibrillation at the early stage of degeneration (Saarakkala et al. 2004).

For the acoustic parameters, the integrated reflection coefficient (IRC) was also adopted in this part of study. The basic steps to calculate IRC were similar to that reported in Subsection 2.2.2.3. In brief, frequency-dependent reflection coefficients

$R_c(f)$ were obtained after the spectrum calibration process and then IRC was calculated by:

$$IRC = \frac{1}{\Delta f_2} \int_{\Delta f_2} R_c^{dB}(f) df \quad \text{E 2.12}$$

where in this case, Δf_2 is the -6dB bandwidth of the ultrasound transducer RMV708, and it was 18~55 MHz based on experimental measurement.

For the mechanical parameters, the stiffness coefficient (SC) and Young's modulus were calculated in a similar way as reported in Subsection 2.2.2.3. In brief, water pressure and deformation with cartilage initial thickness were obtained from the original software interface as shown in Figure 2-3. Then custom-programmed Matlab GUI was used to extract SC and YM using Equations E 2.4 and E 2.5, respectively. The similar protocols were applied in calculating the mechanical parameters.

2.2.3.4. Statistical analysis

Three types of comparisons were conducted for the results of this part of study. Firstly, different groups were formed according to the time after the ACL transection surgery (Week-0, Week-3, Week-6, and Week-9). The parameters were then compared among different groups to see the longitudinal effect of the surgery. Secondly, the cartilage samples were divided into different groups according to their histological grades and then the various parameters were compared according to different groups (from Grade-0 to Grade-5). Comparisons were conducted separately at the femoral side and the tibial side because significant differences such as the thickness and stiffness existed for the two sides. For comparison among groups, one-way ANOVA was used firstly to detect the existence of significant differences and then unpaired t-test was employed for further comparison of two groups if significant difference was found in the first step. Finally, the inter-correlations of the parameters obtained from the rabbit knee cartilage were analyzed to see whether some correlation relationship existed for these parameters. The Pearson correlation coefficient was adopted for the correlation analysis. In all the statistical analyses, SPSS (SPSS Inc., Chicago, IL, USA) was used and $p < 0.05$ was set as a level to indicate the existence of significant correlation or significant difference.

2.2.4. Experiments on cartilage in intact porcine knees

The intravascular ultrasound (IVUS) transducer is with a small profile which can be used for the intra-articular ultrasound (IAUS) measurement of cartilage. Therefore, in this part of study, the IAUS catheter was adopted for the design of a real arthroscopic channel-based water-jet ultrasound indentation transducer. Firstly, the feasibility of using IAUS for the detection of cartilage degeneration was tested using the enzymatic digestion as a model. Then the arthroscopic water-jet ultrasound indentation probe developed based in the IAUS was applied to the in-situ cartilage in intact porcine knees to demonstrate the utility of the developed probe.

2.2.4.1. Feasibility of IAUS for detection of cartilage degeneration

2.2.4.1.1. Measurement system

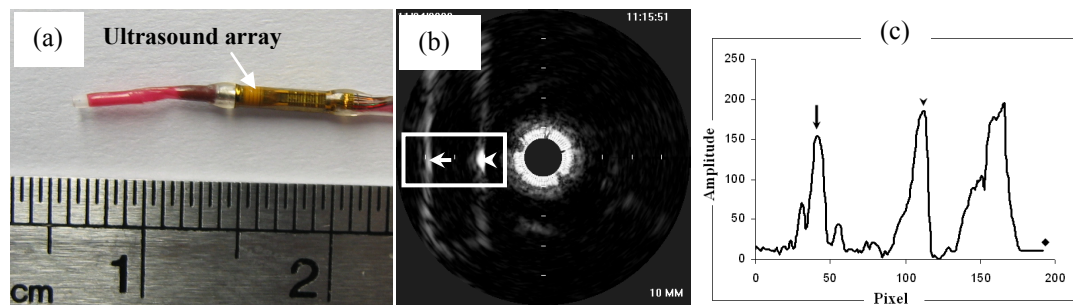


Figure 2-21 (a) The catheter tip which included the ultrasound array elements in the IAUS system. The diameter of the catheter is about 1.2 mm. The core part of the ultrasound transducer is shown as the yellow part of the catheter tip; (b) A typical IAUS B-mode image of articular cartilage. The two interfaces of the cartilage are shown. Arrowhead: the cartilage-saline solution interface; arrow: the cartilage-subchondral bone interface. The rectangular window shows where the average was taken (~ 1 mm in width) for obtaining the parameters of the articular cartilage; (c) Typical interface echoes after spatial averaging in the selected rectangular region. Arrowhead: the cartilage-saline solution interface; arrow: the cartilage-subchondral bone interface; diamond: the center of the image.

As described in Subsection 2.1.2, an IVUS real-time imaging system (In-Vision Gold, Volcano, San Diego, CA, USA) with a catheter of 3.5F (~ 1.2 mm, Figure 2-21a) (REF 85900, Eagle Eye Gold, Volcano) was used as a method of IAUS in the current study. A multi-element (64) solid-state cylindrical array transducer was installed at

the tip of the catheter providing a 360° view of the surrounding tissue (Figure 2-21). The central frequency of the ultrasound transducer was 20 MHz with a spatial peak temporal average (SPTA) derated intensity of 0.354 mW/cm². Usable length of the catheter was 150 cm, which was far enough for the current study. A surrounding circular area could be imaged by the catheter and the diameter was adjustable between 8 mm and 16 mm. A viewing diameter of 10 mm was used in the current study because it optimized the spatial resolution in the B-mode image while capable of imaging the whole thickness of the cartilage (Figure 2-21b). Cross-sectional image data with 8-bit storage precision were recorded for off-line analysis of the cartilage. It should be noted that the data used in the current study were the amplitude image data but not the radiofrequency signal as shown in Figure 2-21 (c).

RF signals were also collected by another high frequency ultrasound system - Vevo 770 (VisualSonics, Toronto, Ontario, Canada) using a scanhead RMV708 (VisualSonics, Figure 2-15a), in order to compare with the measurement results from IAUS image. The basic information of the system has been described in Subsection 2.2.3.2.1. In brief, the diameter of the probe was about 45 mm with a cover at the tip where a single element ultrasound transducer was installed (Figure 2-15b). Ultrasound images were acquired by fast lateral mechanical scanning of the ultrasound transducer within the cover. The cover was firmly attached to the probe with a thin film just installed in front of the ultrasound transducer, serving as a window for passing through the ultrasound beam. The cover was injected with deionized water serving as the coupling media for ultrasound. The axial and lateral resolutions of the transducer were about 30 and 70 µm, respectively. The focus of the probe was 4.5 mm in front of the transducer surface. A digital radio-frequency (RF) mode with 12-bit data precision was used in the Vevo system for collecting the raw RF data in order to increase the measurement sensitivity. A rectangular window could be selected in the B-mode ultrasound image for collecting the RF data (Figure 2-17b, Figure 2-22). For this window, the location, size and the number of A-lines could be set before data collection. For the current RF setting, a lateral interval of 110 µm was used for each A-line collection and also for subsequent spatial averaging to measure the thickness and acoustic parameters. The location of the window was selected to include both the reflections from the surface and the bone-cartilage interface.

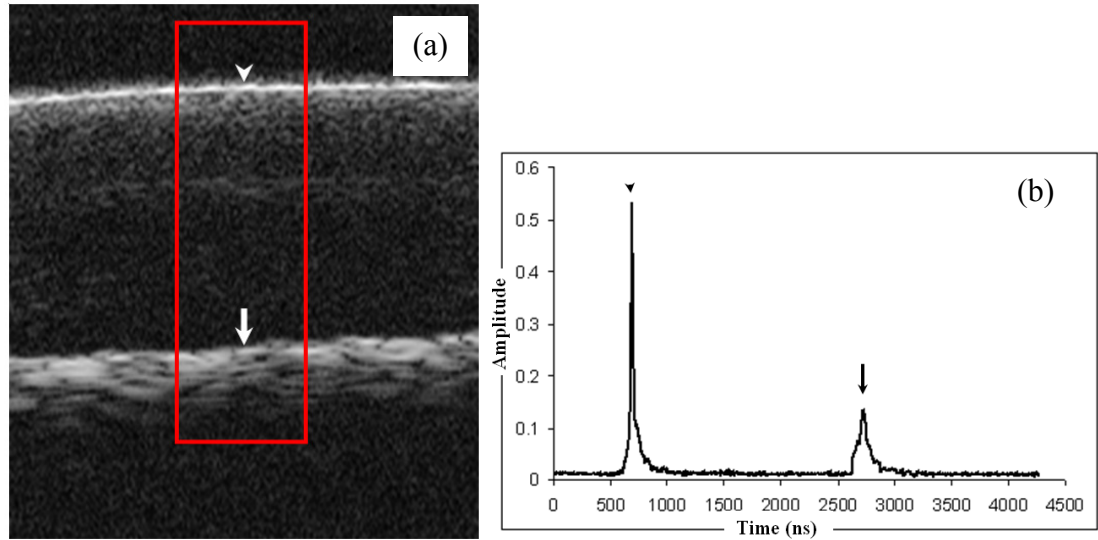


Figure 2-22 (a) A typical B-mode image of articular cartilage obtained from the Vevo ultrasound imaging system. The two interfaces of the cartilage are shown. Arrowhead: the cartilage-saline solution interface; arrow: the cartilage-subchondral bone interface. The rectangular window shows where the average was taken (~ 1 mm in width) for calculating the parameters of the articular cartilage; (b) Typical interface echoes after spatial averaging in the selected region. Arrowhead: the cartilage-saline solution interface; arrow: the cartilage-subchondral bone interface.

2.2.4.1.2. Specimens and experimental tests

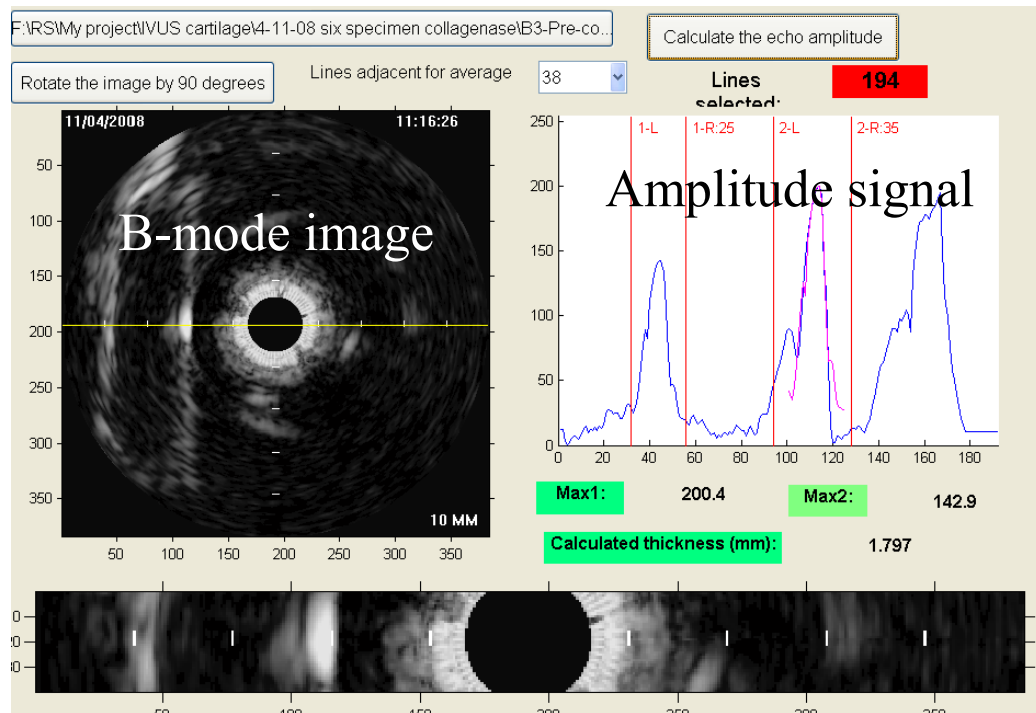
Experiment was conducted on two groups of samples (Group 1 and Group 2), each group containing 8 cartilage specimens. Each specimen was a disk of cylindrical articular cartilage ($\Phi = 6.35$ mm) attached to its subchondral bone excised from various quadrants of 5 bovine patellae (Patil et al. 2004). The patellae were obtained from a local market within 6 hours of sacrifice of the animal and those without obvious visual lesions were selected for preparing the disk samples. In brief, osteochondral slabs were prepared from the patella and an osteochondral disk of about 5 mm in thickness was cored out from the flat area of the slabs for experiment. After preparation, the specimens were wrapped in gauze soaked with physiological saline solution (0.15 M/L in concentration) and stored at -20°C before testing. On the day of testing, the specimens were first thawed in physiological saline solution for 1.5 hour before the ultrasound experiments. Each specimen was fixed using plasticine (Blu-Tack) in a container to ensure a horizontal surface for performing the scanning.

During the scanning process, the sample was also immersed in physiological saline solution to minimize the effect of shrinking and swelling of the cartilage and the IAUS catheter tip was placed manually over the center of the sample for the imaging. For each sample, three repeated tests were conducted and the averaged value was used to represent the tissue properties of the tested specimen. For the test using the Vevo system, similar procedures were performed except that the probe was fixed vertically by a clamp which could be adjusted in the vertical and lateral directions for the ease of the scanning operation (Figure 2-16a). Special attention was paid to get the maximum signal reflected from the cartilage surface in all the scans as this would affect the amplitude of the reflection measurement. After the scanning using IAUS and Vevo, samples in Group 1 were digested with 0.25% trypsin-EDTA solution (GIBCO, Invitrogen, Carlsbad, CA, USA) to mainly deplete the proteoglycan (PG) (Harris et al. 1972) for 5 h at room temperature ($25 \pm 1^\circ\text{C}$), while those in Group 2 were treated with 30 U/ml collagenase solution (GIBCO, Invitrogen, Carlsbad, CA, USA) at 37°C to mainly digest the collagen network (Shingleton et al. 1996) for the same period of 5 h. After the enzyme digestions, the samples were then immersed in physiological solution for 1 h in order to allow the digestion process to be stabilized. Then the scanning process was repeated again using IAUS and Vevo. For each scan, the distance between the ultrasound probes and the cartilage surface was kept roughly the same by observing the location of the cartilage surface from B-mode images and all other configurations such as gain and display settings of the device were set to be all the same to facilitate the intra-specimen comparisons.

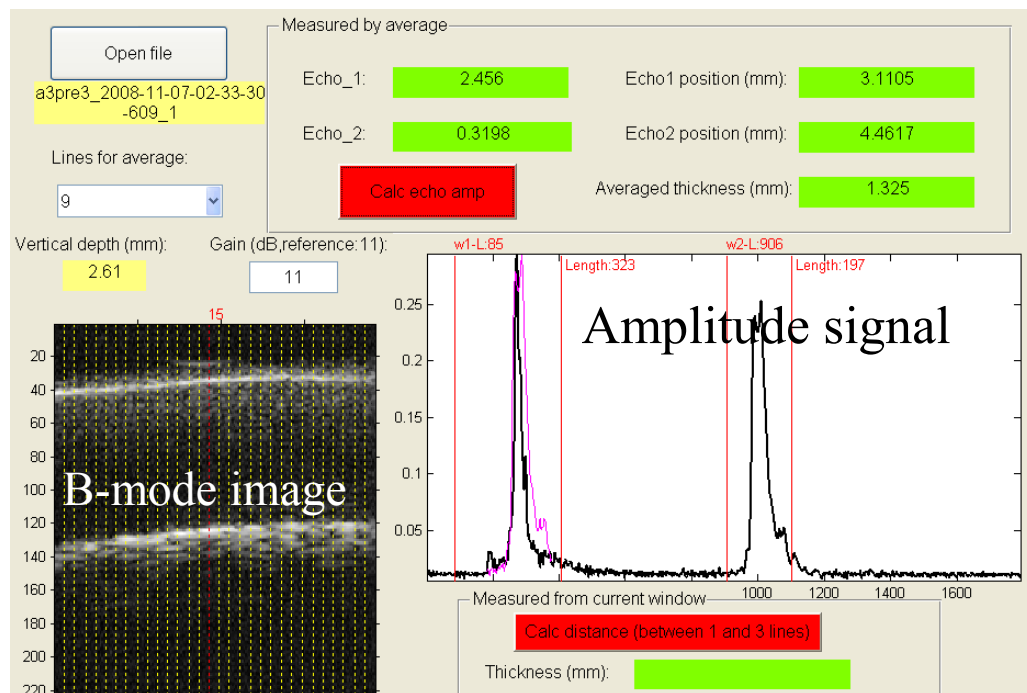
2.2.4.1.3. Data processing method

A program with graphic user interface (GUI) written in Matlab (MathWorks, Natick, MA, USA) was used to extract the two parameters: the thickness of cartilage and surface reflection amplitude of the ultrasound signals. The locations of the cartilage surface and cartilage-bone interface could be selected from the GUI by adding two windows to include the two interface reflections (Figure 2-23a). The surface reflection was calculated as the maximum amplitude of the echo from the cartilage-saline interface after averaging in the horizontal direction. The thickness was calculated by on the interval between the two interface reflections after spatial averaging and the speed of sound. A region with a width of 1 mm was used for the spatial averaging to get the averaged amplitude of the interface for calculating the two

parameters (Figure 2-21b). In this study, the speed of sound was assumed to be 1610 m/s in normal articular cartilage and be 0.988 and 0.984 of this value after trypsin and



(a)



(b)

Figure 2-23 The processing of (a) the image data from IAUS system and (b) the RF signals from Vevo 770 imaging system using custom-designed GUI in Matlab.

collagenase treatment, respectively (Laasanen et al. 2002). For the IAUS measurement, there were 384 pixels for the width and length, which equaled to a real width and length of 10 mm for the image. Therefore, in the B-mode image each pixel represented a length of approximately 0.027 mm in each direction for the articular cartilage, which determined the resolution of the measurement using IAUS images. A-mode lines were extracted from each row data of the B-mode images. During the experiment, the cartilage surface was also deliberately aligned to be parallel with the vertical direction of the image so a row signal of the image would represent an A-line signal of ultrasound waves penetrating in the depth direction of the cartilage (Figure 2-23a).

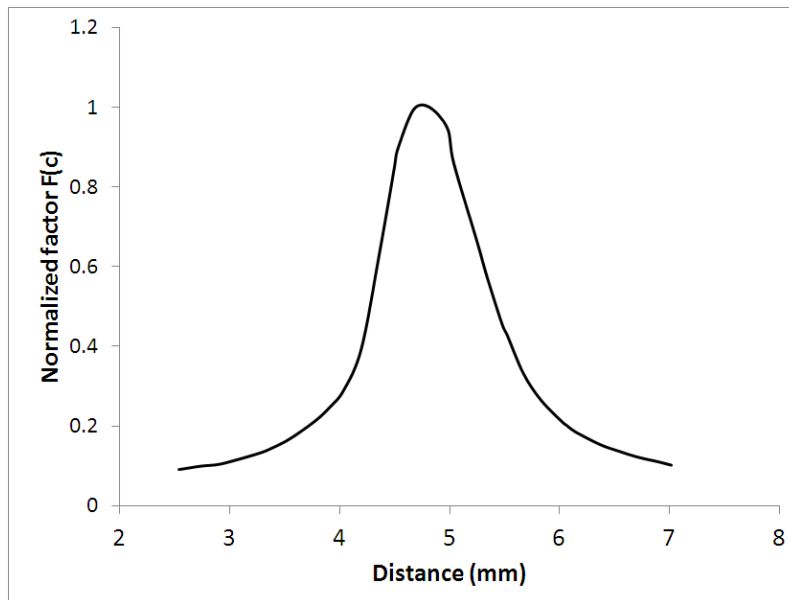


Figure 2-24 The change of normalized factor F_c according to distance to the transducer surface.

For the measurement using Vevo, similar procedures were applied to calculate the surface reflection coefficient and thickness with caution that the ultrasonic signals were without saturation which could be indicated in the software in another color. Using a sampling frequency of 420 MHz and a constant speed of sound of 1610 m/s, each point in the RF digital data represented a length of approximately 0.0019 mm, which was much smaller than that of IAUS. A Hilbert transform was performed to obtain the amplitude signal for each A-line before averaging for the selected region. In order to compensate for the effect of focusing of the focused transducer used in the

Vevo system, the surface reflection amplitude was corrected using a normalized factor obtained by a perfect reflector at the same distance (Laasanen et al. 2002):

$$A_{cor} = \frac{A}{F_c} \quad \text{E 2.13}$$

For this correction method, the normalized factor $F_c = 1$ at the focus and at other distance, it was the proportion of the amplitude compared to that at the focus. The normalized factor according its distance to the transducer surface is plotted as follows in Figure 2-24:

2.2.4.1.4. Statistical analysis

A coefficient of variance (CV) was used to represent the repeatability of measurement. For the thickness measurement, the values of the 16 specimens (Group 1+Group 2) before enzyme treatments measured from IAUS were correlated using Pearson correlation to those measured from Vevo. As the thickness from the two measurements was both calculated based on the principle of the time-of-flight technique, a significant correlation would suggest that the two methods were comparable except a constant difference which might come from the discrepancy in measuring the propagation time. For values of thickness and surface acoustical reflection amplitude, paired *t*-test was used for comparison before and after enzymatic digestion for each cartilage disk. Paired *t*-test was also employed to compare the extent of the change of the surface reflection amplitude induced by trypsin and collagenase treatment, respectively. $P < 0.05$ was used as a significant level for the analysis of correlation or group difference. All the statistical analyses were conducted using SPSS (SPSS Inc., Chicago, IL, USA).

2.2.4.2. Arthroscopic tests on cartilage in intact porcine knees

After demonstrating of the utility of IAUS for cartilage assessment, the next step of study was to validate the feasibility of test the newly developed arthroscopy-based water-jet ultrasound indentation probe to characterize the cartilage degeneration. In this part of the study, porcine knees with intact knee joint were obtained and intra-articular measurement of the mechanical properties of the cartilage using the developed probe was conducted before and after enzymatic digestions. Through this

study, the potential of the developed probe to be applied in an arthroscopic operation would be demonstrated.

2.2.4.2.1. Samples, experimental setup and tests

10 porcine knees with intact normal knee joint were obtained from a local market within 2 hours of sacrifice for the current test. The knee capsule was maintained to be intact by keeping most of the surrounding tissues of the joint such as the ligaments and tendons. Muscles were partially maintained as shown in Figure 2-25 (a). Enzymatic digestion using the 0.25% trypsin-EDTA solution (GIBCO, Invitrogen Corporation, Carlsbad, CA, USA) for 4 hours was adopted to induce the cartilage degeneration in the joint. This was achieved by injecting the trypsin solution into the joint capsule continuously using a small electronic water pump during the whole digestion process. A beaker was used to collect the leaked solution which could be reused and pumped again into the joint. Before and after the enzymatic digestion, measurement was conducted by the water-jet ultrasound indentation probe and the results were compared.

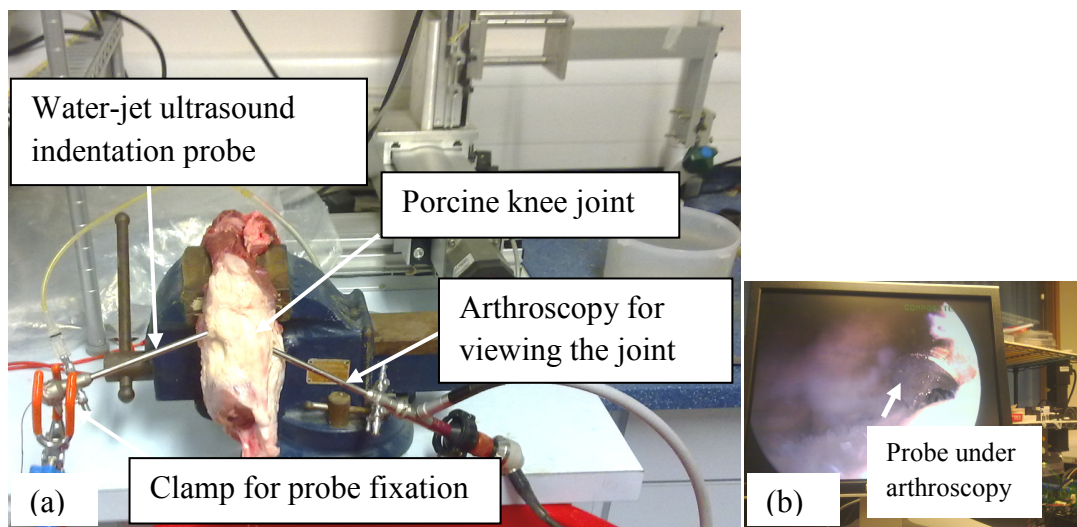


Figure 2-25 (a) The test of intra-articular cartilage using the developed water-jet ultrasound indentation probe with the help of the arthroscopy; (b) A typical view of the water-jet indentation probe under arthroscopy.

The newly developed arthroscopic water-jet ultrasound indentation probe could be inserted into the inner joint by using the tubular trochar like that used with traditional surgery instrument. Furthermore, the operation of the probe such as

localization could be guided by an arthroscopic viewing system (Figure 2-26). The arthroscopic viewing system consisted of a light source system (Quantum 3000, Stryker Endoscopy, Stryker Inc., Kalamazoo, MI, USA) for lightening the inner part of the joint and a video camera system (597T, Stryker Endoscopy, Stryker Inc., Kalamazoo, MI, USA) for viewing the inner joint. Then the water-jet ultrasound indentation probe could be operated under the guidance of the arthroscopic view (Figure 2-25b).

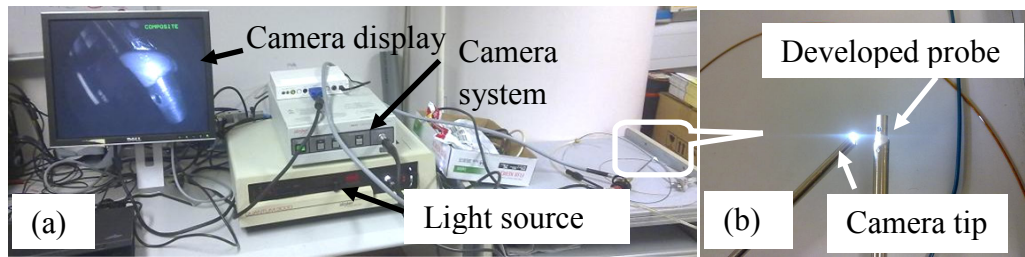


Figure 2-26 (a) The arthroscopic system used for guiding the tested position of the water-jet ultrasound indentation probe; (b) Enlarged view of the camera tip and the developed water-jet indentation probe.

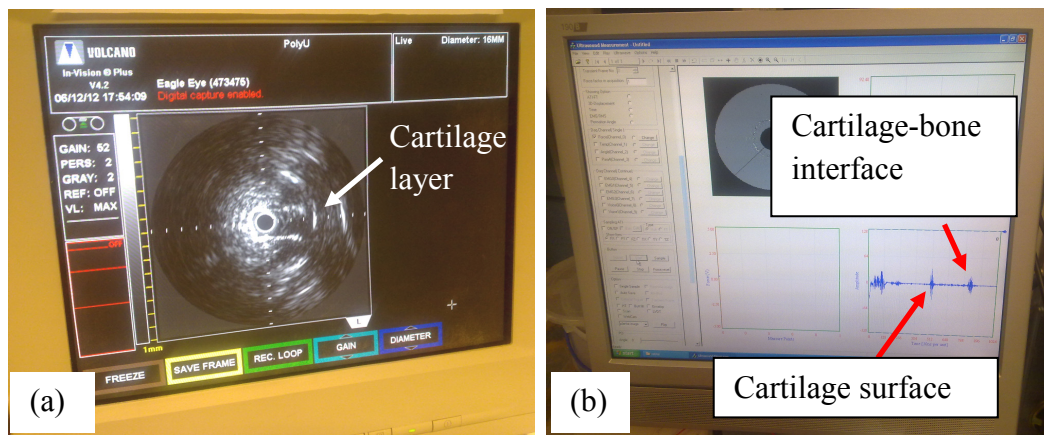


Figure 2-27 (a) An IAUS imaging of the articular cartilage obtained through the water-jet channel of the developed probe; (b) In the custom-designed software, a typical A-line signal of the cartilage layer is shown.

During the test, the water-jet indentation probe was fixed using a mechanical clamp (Figure 2-25a) in order to facilitate the operation. After the water-jet indentation probe was inserted into the joint, the position and orientation of the probe were adjusted to obtain an optimal signal from the articular cartilage. Then the water-jet indentation was performed and data were collected for off-line processing. Similar

protocols for the water-jet indentation test as described previously in Subsection 2.2.2.2 were used during the measurement. Six repeated tests were performed on one site at the femoral groove before and after the enzymatic digestion and results were averaged for characterizing the change of stiffness of the cartilage as described in the following subsection. The typical observation of the cartilage under the IAUS and in the custom-designed software is displayed in Figure 2-27.

2.2.4.2.2. Data processing and statistical analysis

For simplicity, only a stiffness coefficient (SC) was extracted from the water-jet indentation test for the demonstration. The stiffness coefficient was defined very similar to that in the Equation E 2.4. In calculating the SC, the force was obtained from the water pressure after the force calibration process. The initial thickness and deformation of the cartilage were calculated based on the ultrasound signals.

Paired sample *t*-test was used for the comparison of stiffness before and after the enzymatic digestion. The mean percentage decrease of stiffness after the digestion was calculated by calculating the change of stiffness divided by its initial stiffness. $P < 0.05$ was employed as a level to indicate the significance of difference and all the statistical analyses were conducted using SPSS (SPSS Inc., Chicago, IL, USA).

3. Results

3.1. Results of experiments on phantoms

The averaged value for the speed of sound (SOS) of the phantoms was 999 ± 30 m/s, which was obviously smaller than the generally accepted value of SOS for soft tissues (1540 m/s). Due to this large difference, the SOS of phantoms was measured firstly to accurately calculate the thickness and then the deformation of the phantom during indentation test. The mean thickness of all the silicone phantoms was 4.61 ± 1.21 mm ranging from 1.89 to 6.47 mm. The thickness could be used as a basic parameter to extract the Young's modulus (YM) of the phantoms based on some known indentation models (Hayes et al. 1972; Zhang et al. 1997). The f/d coefficient measured from the water jet indentation and the rigid indentation for each phantom was calculated and their relationship is plotted in Figure 3-1. The mean value of the f/d coefficient was 0.63 ± 0.49 N/mm and 0.73 ± 0.63 N/mm for the water-jet and the rigid Instron indentation, respectively. These two values were highly correlated with a Pearson correlation coefficient $r > 0.95$ ($p < 0.001$).

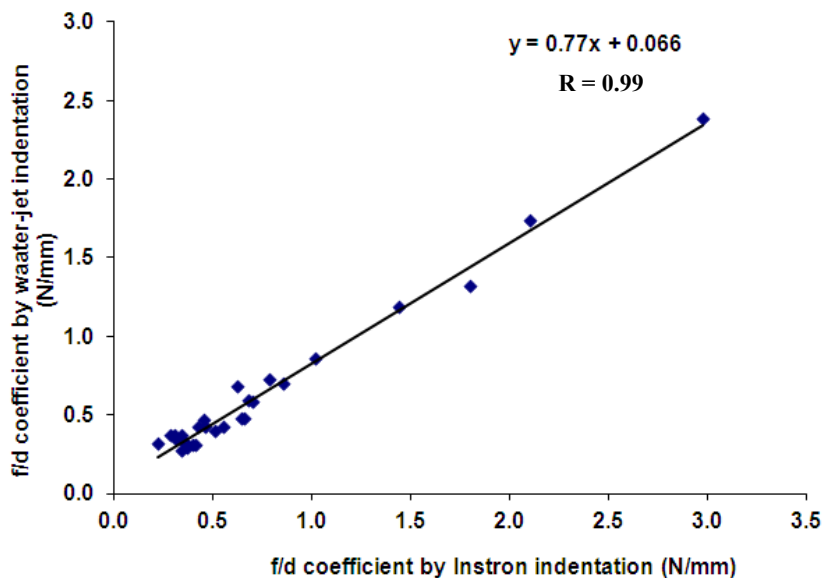


Figure 3-1 The correlation between the two f/d coefficients measured from the water-jet ultrasound indentation and the Instron indentation.

3.2. Results of experiments on bovine cartilage in vitro

3.2.1. Reproducibility study

The measurement SCV of the four parameters obtained by the miniaturized probe was 2.6% for thickness, 10.2% for IRC, 11.5% for SC and 12.8% for EDR. Thickness measurement was the most highly reproducible, while that of IRC, stiffness and EDR was similar (of ~10%). The SCV of measurement from the rigid Instron indentation test was 6.5% and 10.0% for Young's modulus (E) and EDR, respectively. The reproducibility of the water-jet ultrasound indentation test was slightly lower than that of the mechanical testing from the rigid indentation test with respect to the two viscoelastic parameters.

3.2.2. Enzymatic digestion effect

The changes of thickness and IRC before and after enzymatic digestion are shown in Figure 3-2 and Table 3-1. There was no significant change of the thickness after the two enzymatic digestions ($p > 0.05$). For IRC, it significantly decreased after collagenase treatment ($p < 0.001$) while the treatment of trypsin had no significant effect on it ($p > 0.05$), which was consistent with previous results (Laasanen et al. 2002; Wang et al. 2010a). The mean decrease of IRC was $-27.7 \pm 16.5\%$ induced by the collagenase treatment. The change of IRC induced by collagenase was significantly larger than that induced by trypsin ($p < 0.001$, Table 3-1).

The changes of stiffness and EDR induced by the two enzymatic digestions are also listed in Table 3-1. The compressive stiffness of the cartilage (SC) significantly decreased after both the trypsin and collagenase digestions (Figure 3-2, both $p < 0.001$). As shown in Table 3-1, the decrease of SC induced by trypsin treatment was significantly larger than that induced by collagenase treatment (66.4 % vs. 51.8 %, $p < 0.01$). EDR was small in normal cartilage (~20%); however, it significantly increased to ~60% after the trypsin and collagenase digestion (both $p < 0.001$). The increase of EDR was significantly larger for the trypsin treatment than that for the collagenase treatment (40.6% vs. 32.9%, $p < 0.01$). All the results demonstrated

that the current probe could be used to discriminate the degeneration of articular cartilage induced by different enzymes.

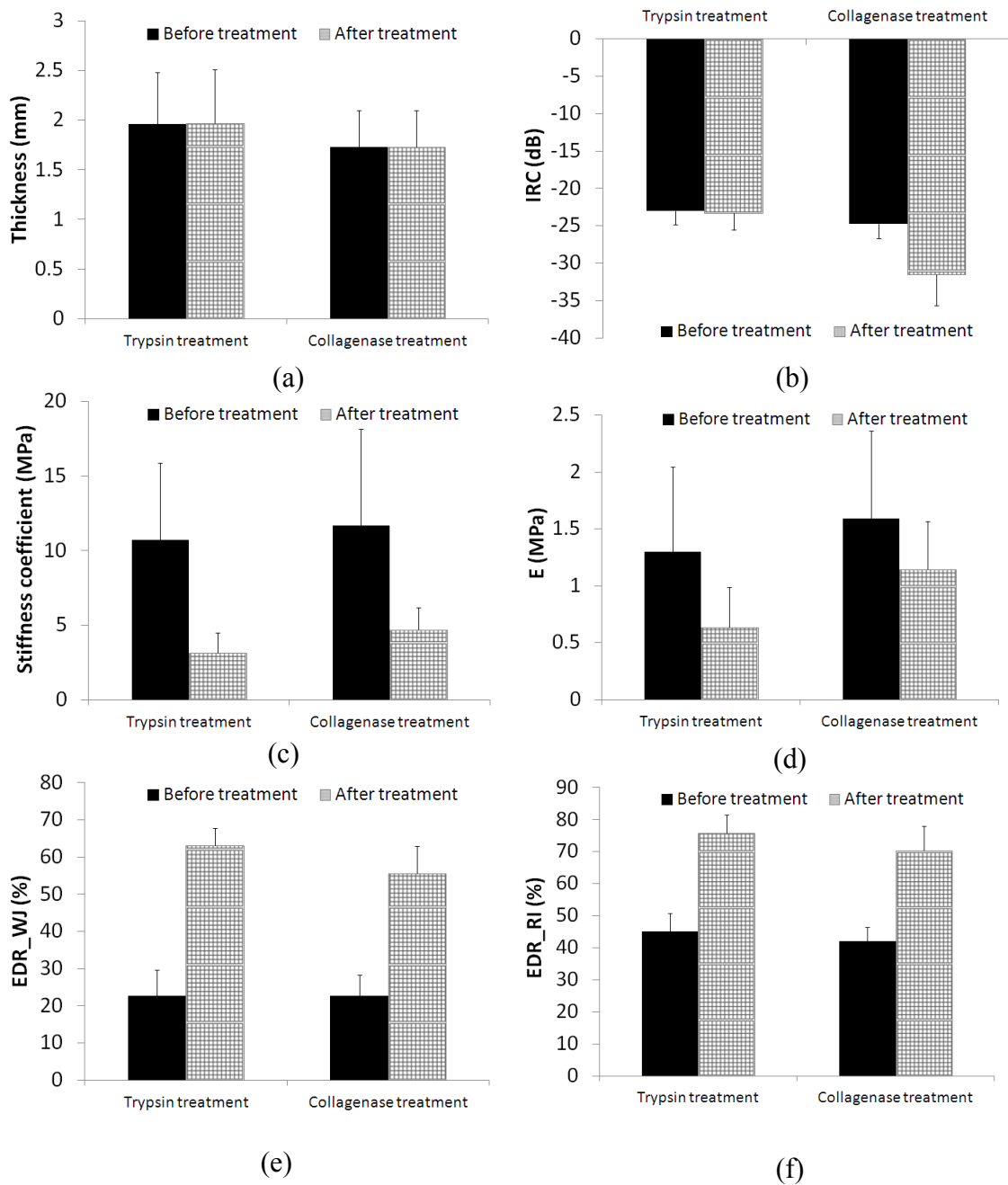


Figure 3-2 The changes of various parameters measured by the water-jet ultrasound indentation system after the trypsin and collagenase digestions: (a) Thickness; (b) IRC; (c) Stiffness coefficient; (d) Young's modulus; (e) EDR obtained from the water-jet indentation; and (f) EDR obtained from the Instron indentation.

Table 3-1 Changes of various parameters after enzymatic digestions.

Parameters	Enzymes	Before treatment	After treatment	Change	
Thickness	Trypsin	1.96 ± 0.52	1.97 ± 0.54	-0.2 ± 4.4%	
(mm)	Collagenase	1.73 ± 0.37	1.73 ± 0.37	0.2 ± 3.6%	
IRC (dB)	Trypsin	-23.05 ± 1.80	-23.34 ± 2.22	-1.6 ± 9.1%]***
	Collagenase	-24.77 ± 1.92	-31.53 ± 4.15	-27.7 ± 16.5% ***	
SC (MPa)	Trypsin	10.732 ± 5.154	3.119 ± 1.367	-66.4 ± 15.4% ***]**
	Collagenase	11.699 ± 6.426	4.679 ± 1.520	-51.8 ± 18.9% ***	
E (MPa)	Trypsin	1.298 ± 0.748	0.636 ± 0.351	-49.7 ± 17.8% ***]***
	Collagenase	1.590 ± 0.768	1.143 ± 0.420	-24.6 ± 13.3% ***	
EDR _{WJ} (%)	Trypsin	22.7 ± 6.9	63.2 ± 4.5	40.6 ± 9.2% ***]**
	Collagenase	22.7 ± 5.5	55.5 ± 7.5	32.9 ± 8.9% ***	
EDR _{RI} (%)	Trypsin	45.0 ± 5.8	75.9 ± 5.6	31.0 ± 3.9% ***	
	Collagenase	42.0 ± 4.5	70.3 ± 7.7	28.3 ± 6.4% ***	

Values are expressed as Mean ± standard deviation (SD). IRC – integrated reflection coefficient, SC – stiffness coefficient, E – Young's modulus, EDR – energy dissipation ratio, WJ – water-jet, RI – Rigid Instron indentation. Level of significance of change compared to pre-treatment or comparison of changes between the two types of enzymatic digestion: ** $p < 0.001$, *** $p < 0.001$.

3.2.3. Comparisons with reference methods

The results from the rigid Instron indentation test are also included in Table 3-1. It was found that the Young's modulus (E) significantly decreased after the two enzymatic digestions (both $p < 0.001$), with the degree of decrease by trypsin treatment being significantly larger than that by the collagenase treatment (49.7% vs. 24.6%, $p < 0.001$). For EDR, it significantly increased after both the enzymatic digestions (both $p < 0.001$). The increase was slightly larger for the trypsin digestion than that for the collagenase treatment but did not reach a significant level (31.0% vs. 28.3%, $p = 0.06$). The correlation of results from the two mechanical testing methods was analyzed. There was a significant positive correlation between the stiffness from the water-jet indentation and E from the rigid indentation ($r = 0.73$, $p < 0.001$, Figure 3-3). EDR measured from the two methods was also significantly correlated ($r = 0.93$, $p < 0.001$, Figure 3-4).

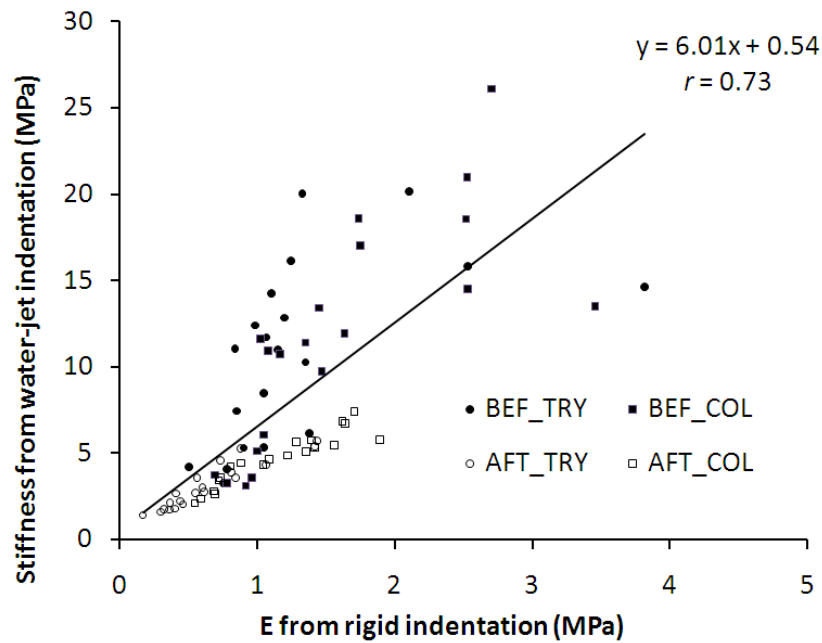


Figure 3-3 The relationship between the stiffness coefficient (SC) from the water-jet indentation and the Young's modulus (E) from the rigid Instron

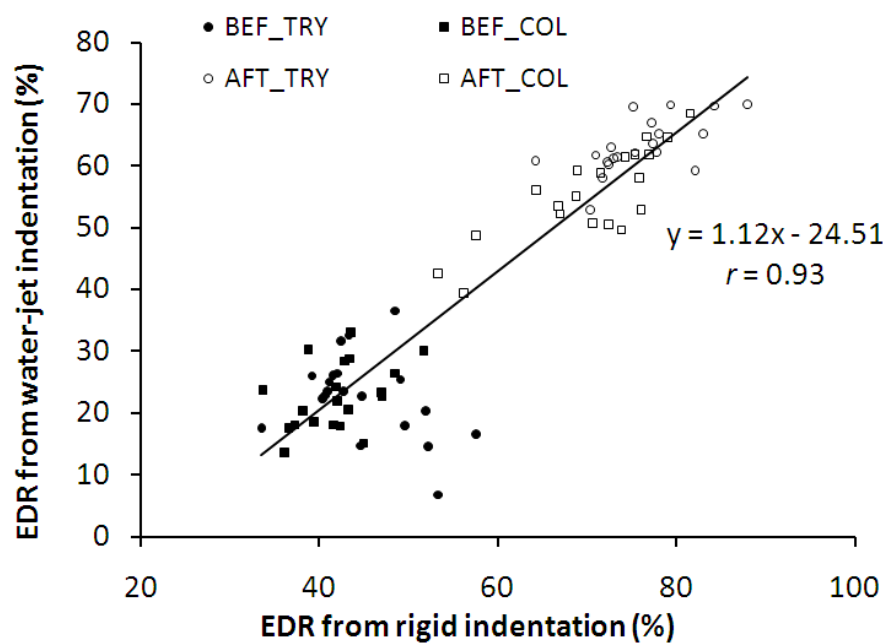


Figure 3-4 The relationship between EDR from the water-jet indentation and that from the rigid Instron indentation.

Typical histological results are shown in Figure 3-5. Based on observation from all the histological images, it was found that PG contents were not affected in the

normal cartilage. For the trypsin treatment, almost all PGs were digested while for the collagenase treatment, there was also partial PG loss, for which the possible reason would be discussed in Subsection 4.2.2 of the Discussion chapter.

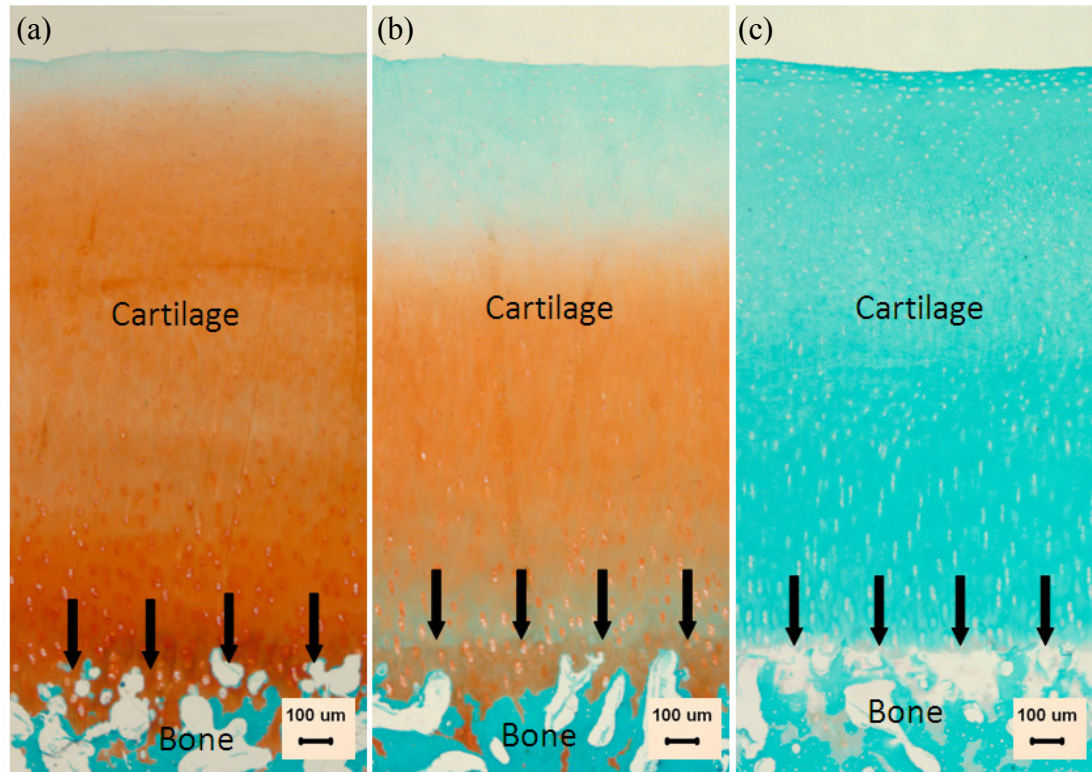


Figure 3-5 Typical histological pictures showing the Safranin O and fast green staining for the (a) normal (b) collagenase-digested and (c) trypsin-digested cartilage. It was typically observed that in collagenase-digested cartilage, there was partial loss of proteoglycans (red color) while they were completely depleted in trypsin-digested samples. Arrows indicate the cartilage-bone interfaces.

3.3. Results of experiments on rabbit cartilage in situ

3.3.1. Histological results

Typical histological images for the rabbit cartilage samples from Grade 0 to Grade 3 are shown in Figure 3-6. The histological observations mainly included the loss of the Safranin O red staining and fibrillation, based on which the OARSI grade was given. The analysis of the semi-quantitative pathological grade obtained from the histology is presented in the following subsection.

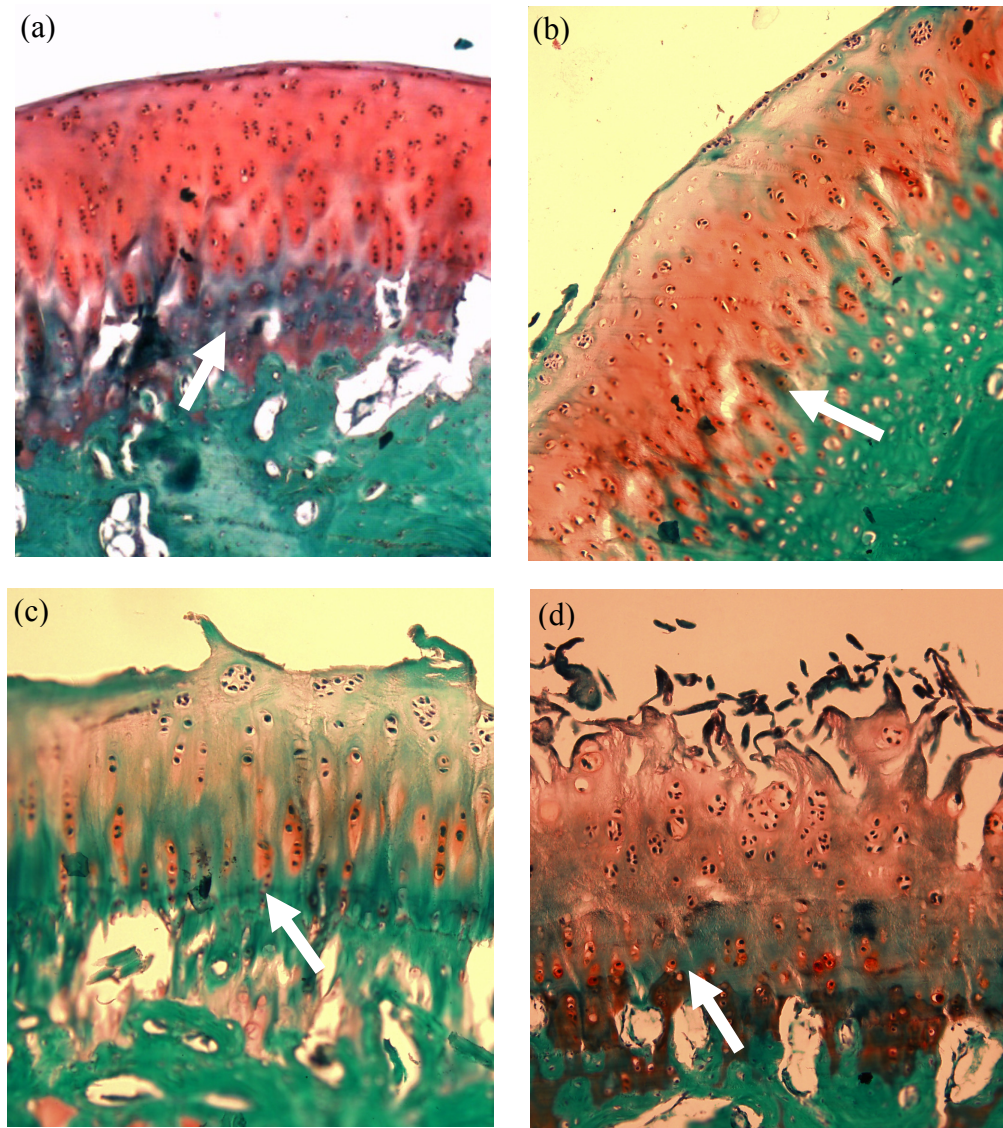


Figure 3-6 Typical histological images showing the Safranin O red and fast green staining for different cartilage samples. (a) Normal cartilage mainly stained with Safranin O red; (b) Grade 1 with uneven surface and loss of Safranin O staining in the superficial layer of cartilage; (c) Grade 2 with surface fibrillation and loss of Safranin O staining in the superficial and middle layers of cartilage; (d) Grade 3 with defect of partial cartilage thickness and loss of Safranin O staining in the superficial and middle layers of cartilage. The arrow indicates the cartilage-bone interface.

3.3.2. Changes of parameters with post-surgery time

The change of the measured parameters with the post-surgery time is plotted in Figure 3-7. These results are also listed in Table 3-2 and Table 3-3. For the

pathological grade, its distribution at different post-surgery time points is further plotted in Figure 3-8. Along with the post-surgery time, the mean pathological grade shifted from a low grade to a high grade due to the effect of ACL transection surgery. There was a significant difference detected among the four groups (Kruskal-Wallis test) both at the femoral side ($p < 0.001$) and at the tibial side ($p < 0.001$). Therefore, further comparisons were made between the unpaired two groups (Mann-Whitney test) and the results are shown in Table 3-2 and Table 3-3. Generally, the pathological grade increased along with the post-surgery time indicating that the ACL transection surgery was a proper model to induce a natural degeneration to the knee articular cartilage. The degeneration at the femoral side seemed to be larger than that at the tibial side but the difference did not reach the significant level ($p > 0.05$, Wilcoxon signed ranks test). For the thickness, no general trend of change was found with the post-surgery time, although significant difference was detected among the groups ($p < 0.01$). The thickness at the femoral side was significantly smaller than that at the tibial side for all the four groups ($p < 0.001$). For URI, a general trend of increase with the post-surgery time was found and significant difference was detected among the groups ($p < 0.001$ for the femoral side and $p < 0.05$ for the tibial side). For the comparison of femoral and tibial sides, significant difference was found only for the Week-9 group ($p < 0.05$). For IRC, a general trend of decrease was observed along with the post-surgery time and significant differences were found among the groups (both $p < 0.001$ for the femoral and tibial sides). No significant difference was revealed between the femoral and tibial sides ($p > 0.05$) except for the Week-9 group ($p < 0.01$). For SC, a general trend of decrease was also found to be associated with the post-surgery time. However, significant difference among the groups was observed only at the tibial side ($p < 0.001$). A significant difference of SC between the femoral side and the tibial side was found for all the groups ($p < 0.001$). Similar trend was also found for the reference parameter – the Young's modulus (E) and significant difference of this parameter among groups was found for both the femoral side ($p < 0.05$) and the tibial side ($p < 0.001$). Significant difference of E was also found between the femoral side and the tibial side for all the groups ($p < 0.01$). The detailed comparisons between two different post-surgery groups are listed in Table 3-2 and Table 3-3, for the femoral and tibial side, respectively. It should be noted that each value of the table refers a comparison of an

item in the row to that in the column. All the results showed that the measured parameters could demonstrate an increase of the level of cartilage degeneration with time.

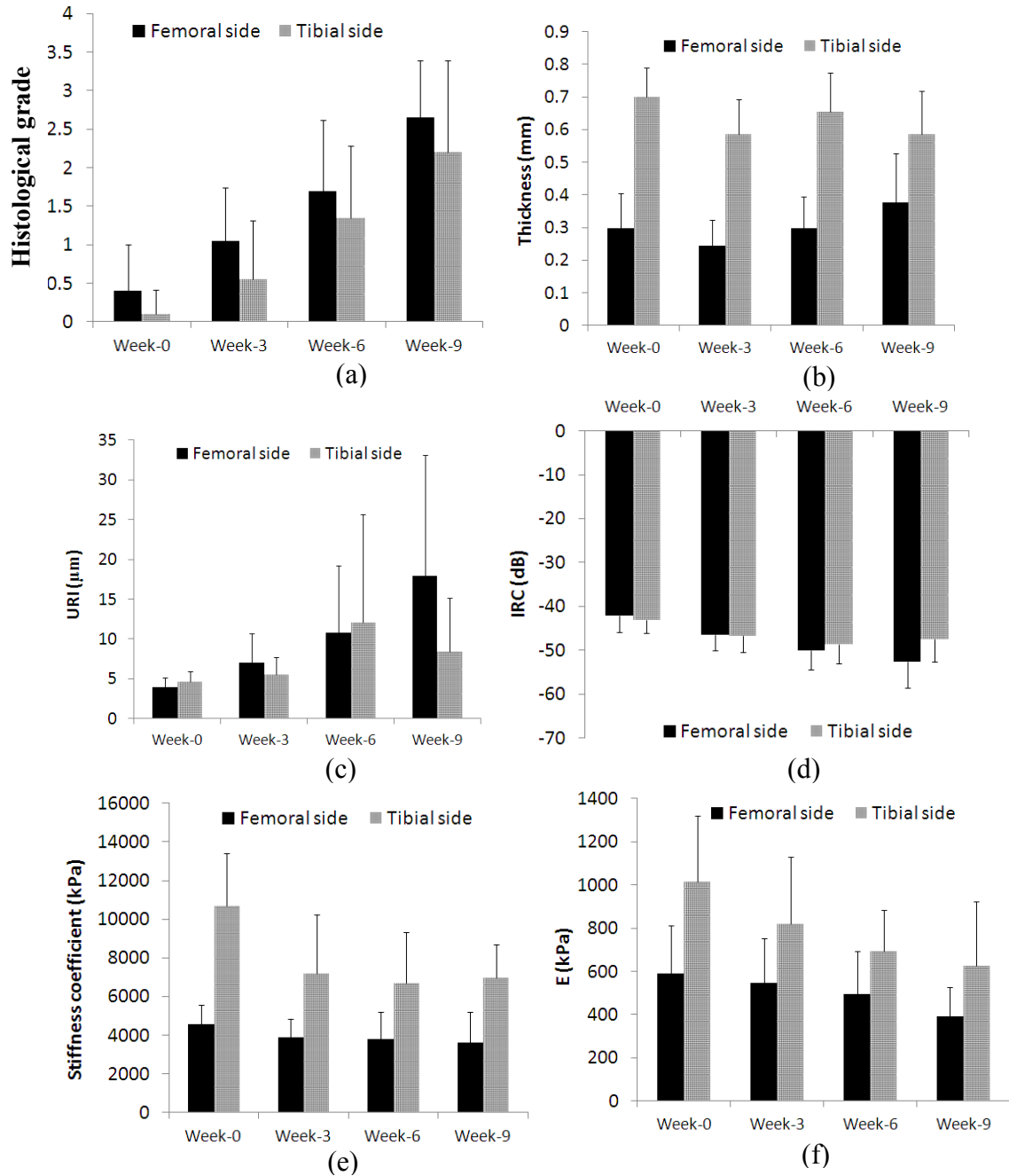


Figure 3-7 The change of various parameters: (a) Pathological grade, (b) thickness, (c) URI, (d) IRC, (e) Stiffness coefficient, (f) Young's modulus E along with the post-surgery time.

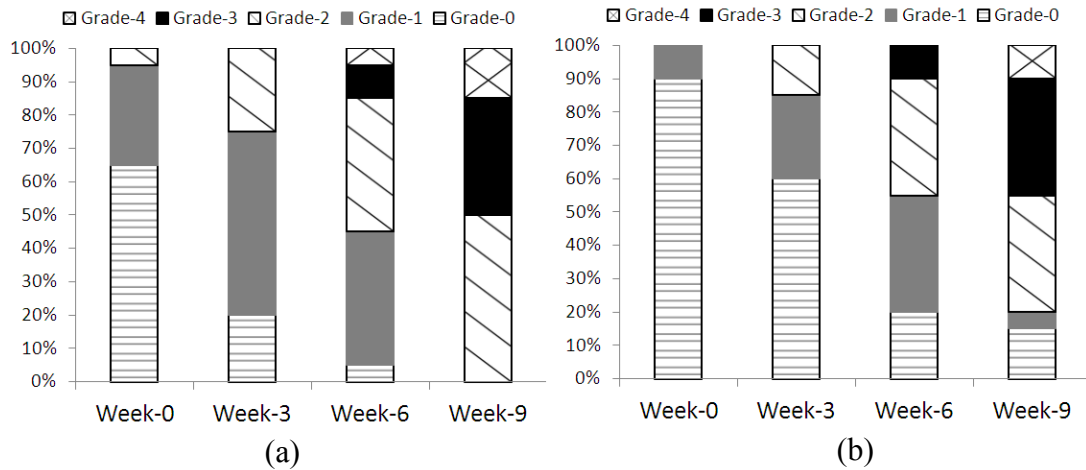


Figure 3-8 Distribution of the pathological grade of cartilage lesions (a) at the femoral side and (b) at the tibial side. An overall increase of the histological grades from Week-0 to Week-9 for the cartilage lesion could be observed in the figure, which indicated the progression of OA in the rabbit knee.

3.3.3. Changes of parameters with pathology

As the histological grade was a good indicator of the cartilage lesion, the cartilage was also divided into different groups according to its histological grade. The measured parameters were then compared among the groups and the results are shown in Figure 3-9. The test points were $n = 18, 25, 24, 9$ and 4 for the five groups at the femoral side and $n = 37, 15, 17, 9, 2$ at the tibial side, respectively. As the number of test points was too small for Group Grade-4 and for a reason of mismatch (discussed in Subsection 4.2.3.2 of the Discussion chapter), this group was not included in the statistical analysis. Therefore, comparisons were only made in the other four groups from Grade 0 to Grade 3. At the femoral side, significant differences were found for URI, IRC and E ($p < 0.001$). The post-hoc analysis results are shown in Table 3-4. At the tibial side, significant differences were found only for SC and E ($p < 0.01$) and post-hoc analysis results are shown in Table 3-5.

Table 3-2 The various parameters among different post-surgery groups and comparisons at the femoral side.

		W0 (n = 20)	W3 (n = 20)	W6 (n = 20)	W9 (n = 20)
W0	Path-grade	0.40 ± 0.60	< *	< ***	< ***
	Thickness (mm)	0.30 ± 0.11			
	URI (μm)	3.9 ± 1.2			< ***
	IRC (dB)	-42.1 ± 3.8	> *	> ***	> ***
	SC (kPa)	4570 ± 999			> *
	E (kPa)	590 ± 222			
W3	Path-grade		1.05 ± 0.69		< ***
	Thickness (mm)		0.24 ± 0.08		< **
	URI (μm)		7.0 ± 3.7		< **
	IRC (dB)		-46.4 ± 3.6		> ***
	SC (kPa)		3893 ± 936		
	E (kPa)		546 ± 207		
W6	Path-grade			1.70 ± 0.92	< **
	Thickness (mm)			0.30 ± 0.10	
	URI (μm)			10.8 ± 8.4	
	IRC (dB)			-50.0 ± 4.3	
	SC (kPa)			3815 ± 1368	
	E (kPa)			496 ± 196	
W9	Path-grade				2.65 ± 0.75
	Thickness (mm)				0.38 ± 0.15
	URI (μm)				17.9 ± 15.2
	IRC (dB)				-52.7 ± 5.8
	SC (kPa)				3618 ± 1566
	E (kPa)				393 ± 134

Groups from “W0” to “G9” represent the groups with different post-surgery time from Week 0 to Week 9. “Week 0” indicates the normal group. For the post-hoc tests, “*” represents $p < 0.05$, “**” represents $p < 0.01$ and “***” represents $p < 0.001$.

Table 3-3 The various parameters among different post-surgery groups and comparisons at the tibial side.

		W0 (n = 20)	W3 (n = 20)	W6 (n = 20)	W9 (n = 20)
W0	Path-grade	0.10 ± 0.31		< ***	< ***
	Thickness (mm)	0.70 ± 0.09	> *		> *
	URI (μm)	4.7 ± 1.2		< *	
	IRC (dB)	-43.2 ± 2.8		> ***	> **
	SC (kPa)	10665 ± 2723	> ***	> ***	> ***
	E (kPa)	1016 ± 303		> ***	> **
W3	Path-grade		0.55 ± 0.76	< *	< ***
	Thickness (mm)		0.58 ± 0.11		
	URI (μm)		5.5 ± 2.1		
	IRC (dB)		-46.6 ± 3.8		
	SC (kPa)		7194 ± 3048		
	E (kPa)		820 ± 311		
W6	Path-grade			1.35 ± 0.93	
	Thickness (mm)			0.65 ± 0.12	
	URI (μm)			12.1 ± 13.6	
	IRC (dB)			-48.6 ± 4.4	
	SC (kPa)			6706 ± 2610	
	E (kPa)			695 ± 188	
W9	Path-grade				2.20 ± 1.20
	Thickness (mm)				0.59 ± 0.13
	URI (μm)				8.4 ± 6.7
	IRC (dB)				-47.5 ± 5.2
	SC (kPa)				6952 ± 1732
	E (kPa)				626 ± 296

Groups from “W0” to “G9” represent the groups with different post-surgery time from Week 0 to Week 9. “Week 0” indicates the normal group. For the post-hoc tests, “*” represents $p < 0.05$, “**” represents $p < 0.01$ and “***” represents $p < 0.001$.

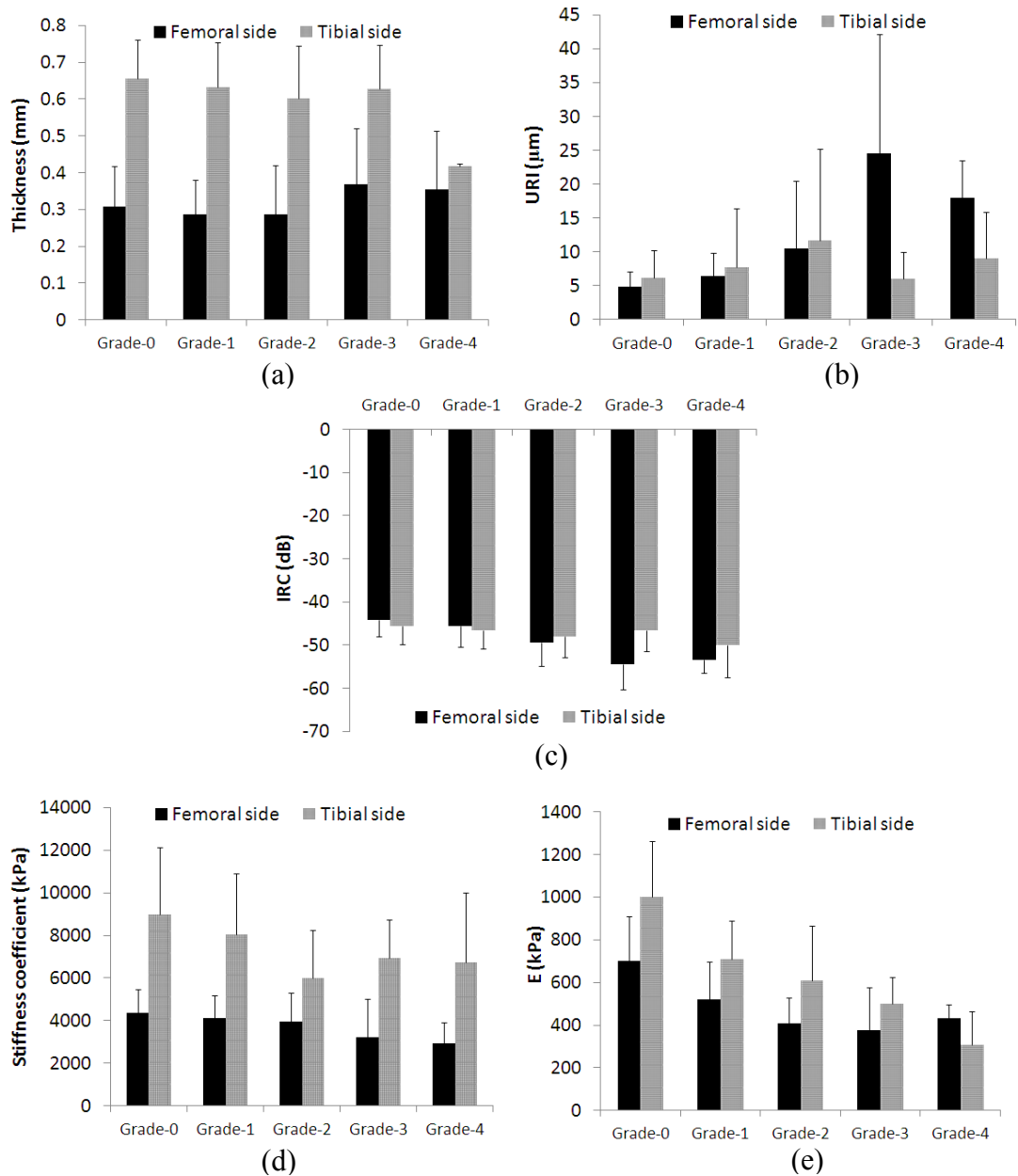


Figure 3-9 Comparisons of various measured parameters among groups classified according to the pathological grade. (a) Thickness; (b) URI; (c) IRC; (d) Stiffness coefficient and (e) Young's modulus E . The number of tested points was 18, 25, 24, 9 and 4 for the 5 groups at the femoral side and 37, 15, 17, 9, 2 for the 5 groups at the tibial side, respectively.

Table 3-4 The comparison of parameters for samples with different pathological grades at the femoral side.

		G0 (n = 18)	G1 (n = 25)	G2 (n = 24)	G3 (n = 9)
G0	Thickness (mm)	0.31 ± 0.11			
	URI (μm)	4.8 ± 2.2			< ***
	IRC (dB)	-44.1 ± 3.9		> **	> ***
	SC (kPa)	4357 ± 1107			
	E (kPa)	702 ± 208	> **	> ***	> ***
G1	Thickness (mm)		0.29 ± 0.09		
	URI (μm)		6.4 ± 3.4		< ***
	IRC (dB)		-45.6 ± 4.8		> ***
	SC (kPa)		4136 ± 1027		
	E (kPa)		520 ± 175		
G2	Thickness (mm)			0.29 ± 0.13	
	URI (μm)			10.4 ± 10.0	< ***
	IRC (dB)			-49.5 ± 5.5	
	SC (kPa)			3965 ± 1348	
	E (kPa)			407 ± 122	
G3	Thickness (mm)				0.37 ± 0.15
	URI (μm)				24.6 ± 17.5
	IRC (dB)				-54.4 ± 5.9
	SC (kPa)				3239 ± 1763
	E (kPa)				376 ± 200

Groups from “G0” to “G4” represent the groups with different pathological grades from Grade 0 to Grade 4. For the post-hoc tests, “*” represents $p < 0.05$, “**” represents $p < 0.01$ and “***” represents $p < 0.001$.

Table 3-5 The comparison of parameters for samples with different pathological grades at the tibial side.

		G0 (n = 18)	G1 (n = 25)	G2 (n = 24)	G3 (n = 9)
G0	Thickness (mm)	0.66 ± 0.10			
	URI (μm)	6.1 ± 4.1			
	IRC (dB)	-45.6 ± 4.3			
	SC (kPa)	8967 ± 3182		> **	
	E (kPa)	1001 ± 263	> ***	> ***	> ***
G1	Thickness (mm)		0.63 ± 0.12		
	URI (μm)		7.8 ± 8.6		
	IRC (dB)		-46.5 ± 4.4		
	SC (kPa)		8049 ± 2867		
	E (kPa)		710 ± 178		
G2	Thickness (mm)			0.60 ± 0.14	
	URI (μm)			11.7 ± 13.5	
	IRC (dB)			-48.0 ± 4.8	
	SC (kPa)			5993 ± 2260	
	E (kPa)			607 ± 259	
G3	Thickness (mm)				0.63 ± 0.12
	URI (μm)				6.1 ± 3.9
	IRC (dB)				-46.5 ± 4.8
	SC (kPa)				6945 ± 1783
	E (kPa)				501 ± 123

Groups from “G0” to “G4” represent the groups with different pathological grades from Grade 0 to Grade 4. For the post-hoc tests, “*” represents $p < 0.05$, “**” represents $p < 0.01$ and “***” represents $p < 0.001$.

3.3.4. Inter-correlations among measured parameters

The inter-correlations among the measured parameters are listed in Table 3-6 and shown in Figure 3-10. There was no significant correlation between thickness and URI ($p > 0.05$). Neither was the correlation significant for the relationship between thickness and IRC ($p > 0.05$). Moderate correlation was found between URI and SC ($r = -0.275$, $p < 0.001$), and between IRC and SC ($r = 0.257$, $p < 0.01$). The highest correlation was observed between URI and IRC ($r = -0.727$, $p < 0.001$) and between thickness and SC ($r = 0.638$, $p < 0.001$). The correlation between SC from the water-jet indentation and E from the Instron indentation was also analyzed and a moderate but significant correlation of $r = 0.55$ ($p < 0.001$) was found for the two parameters (Figure 3-11). This correlation verified that the water-jet indentation was effective to measure the stiffness of the articular cartilage.

Table 3-6 The correlations among different parameters measured in the study of rabbit cartilage.

Correlations	Thickness	URI	IRC	SC
Thickness	1	0.011	-0.095	0.638 ***
URI		1	-0.727 ***	-0.275 ***
IRC			1	0.257 **
SC				1

The significance level of the Pearson correlation: “**” represents $p < 0.01$; “***” represents $p < 0.001$.

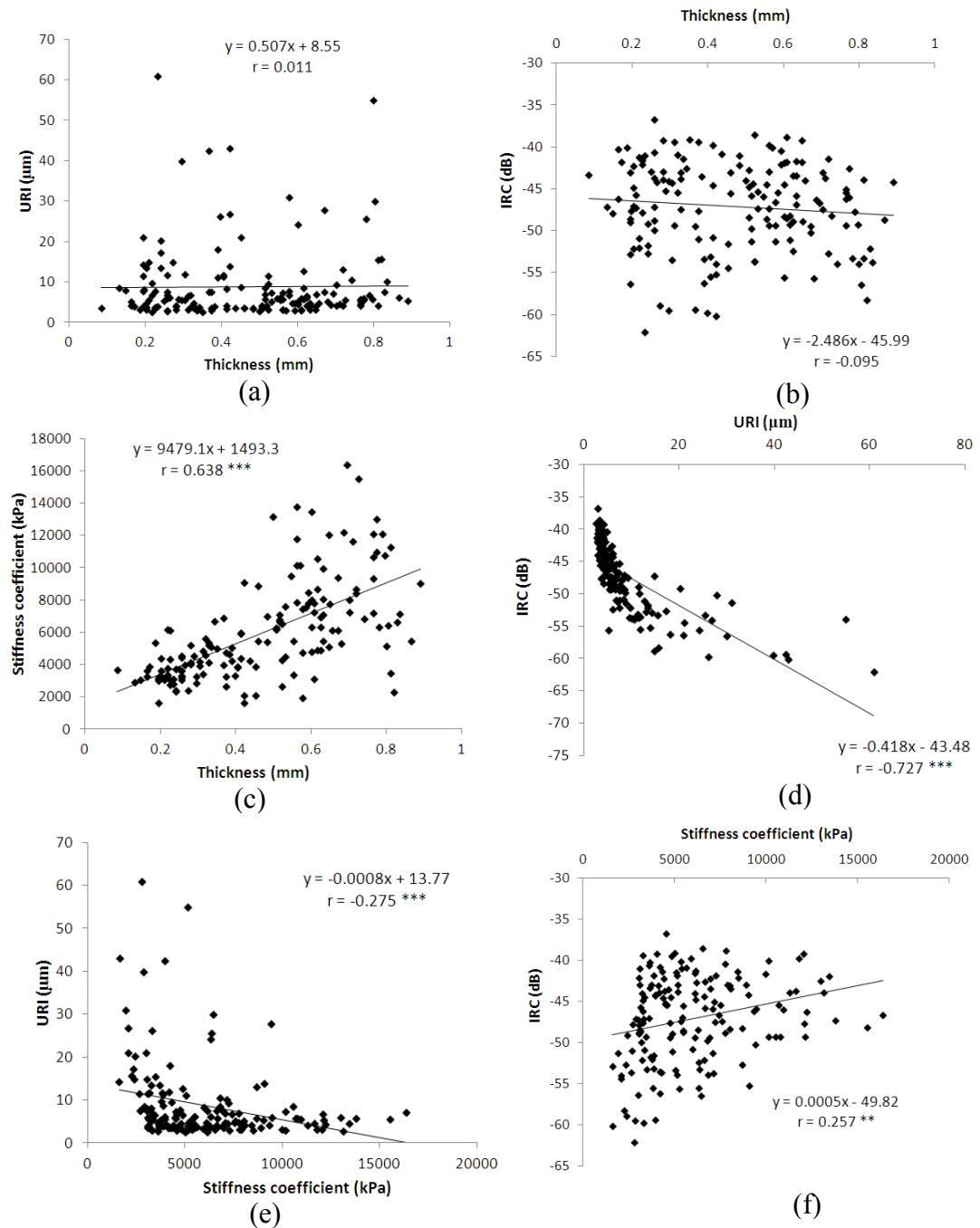


Figure 3-10 The correlations among different parameters measured in the current study. (a) Thickness vs. URI; (b) Thickness vs. IRC; (c) Thickness vs. SC; (d) URI vs. IRC; (e) SC vs. URI and (f) SC vs. IRC. “*” represents $p < 0.05$, “***” represents $p < 0.01$ and “***” represents $p < 0.001$.

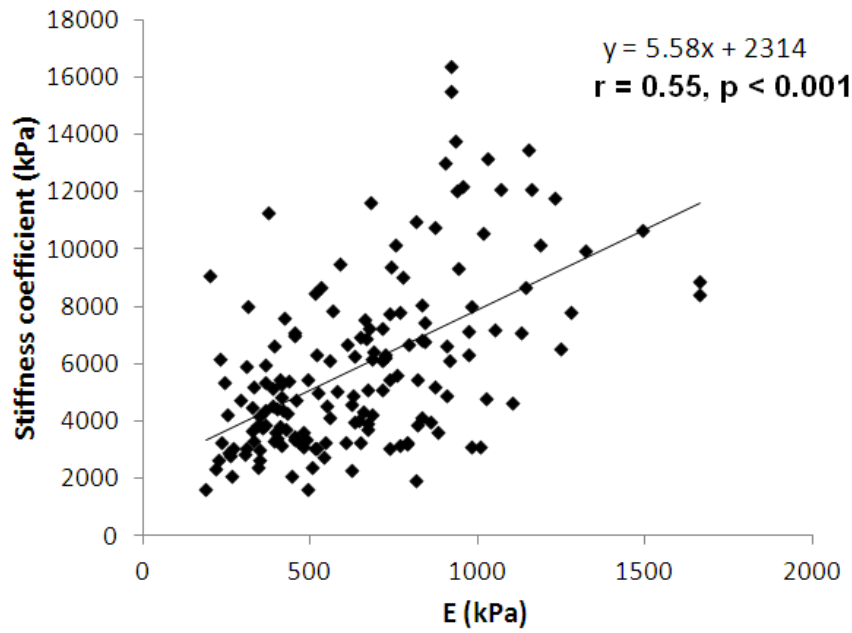


Figure 3-11 The correlation between Young's modulus (E) from the Instron indentation and stiffness coefficient from the water-jet indentation (the total sample number for correlation analysis: $n = 160$).

3.4. Results of tests using the arthroscopy-based probe

3.4.1. Results of IAUS for detection of cartilage degeneration

To have a sense of the reliability of the measurement, 8 repeated tests on one specimen were conducted and a mean thickness of 1.90 ± 0.03 mm (CV = 1.7%) was obtained, demonstrating that the measurement of thickness was very repeatable. For the surface reflection measurement, a similar test using 8 repeated measures on one specimen harvested a value of 179.7 ± 6.9 (arbitrary unit) with a CV of 3.9%. The thickness values for all the 16 samples (Groups 1 and 2) before enzyme treatment were compared between IAUS and Vevo measurements. The thickness obtained using the two methods was highly correlated ($r = 0.985$, $p < 0.001$, Figure 3-12), indicating that the IAUS had a comparable performance with Vevo for cartilage thickness measurement. The mean thickness measured by IAUS and Vevo was 1.83 ± 0.28 mm and 1.80 ± 0.29 mm, respectively.

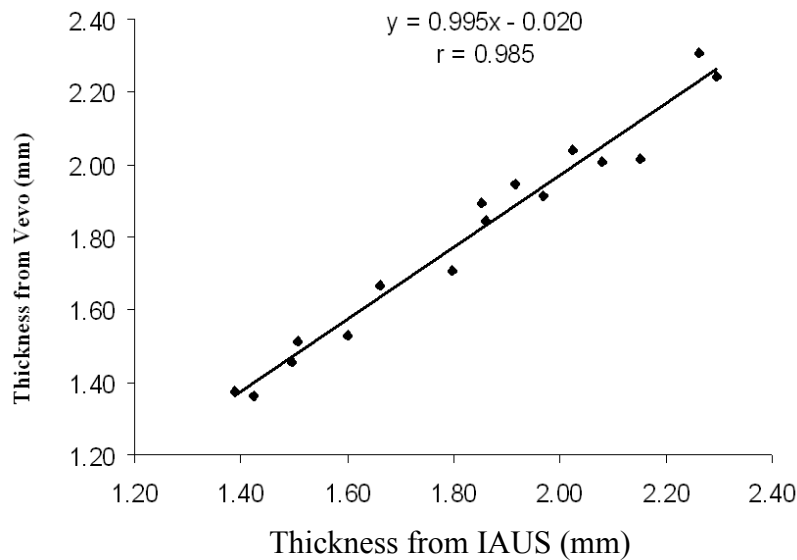


Figure 3-12 The correlation of thickness measured from IAUS and Vevo ultrasound imaging for cartilage specimens before enzyme digestion ($n = 16$).

Table 3-7 and Table 3-8 list the results of the thickness and surface reflection amplitude obtained by the IAUS after the treatments of trypsin and collagenase enzymes, respectively. The mean thickness value before and after treatment was 1.68 ± 0.25 mm and 1.68 ± 0.23 mm for the trypsin treatment group, respectively. It was 1.98 ± 0.27 mm and 1.99 ± 0.26 mm for the collagenase treatment group. Statistical analysis revealed no significant change in the sample thickness (both $p > 0.05$) after both the enzymatic treatments. However, the surface reflection amplitude showed a significant decrease for both the treatments ($p < 0.01$). The averaged decrease was $16.2 \pm 11.4\%$ after trypsin digestion and $52.1 \pm 10.3\%$ with collagenase treatment, respectively. Collagenase treatment appeared to have exerted a more significant effect on the surface reflection amplitude ($p < 0.001$). The corresponding measurement using Vevo showed similar results: the mean pre- and post-treatment thickness for trypsin treatment and collagenase treatment was 1.64 ± 0.22 vs. 1.65 ± 0.22 mm ($p > 0.05$) and 1.96 ± 0.29 vs. 1.95 ± 0.25 mm ($p > 0.05$), respectively. The corresponding surface reflection coefficient was 3.61 ± 0.57 vs. 2.66 ± 0.85 ($p < 0.01$) and 3.64 ± 1.11 vs. 0.52 ± 0.13 ($p < 0.001$), respectively. The surface reflection coefficient decreased by $26.9 \pm 19.5\%$ and $84.7 \pm 4.1\%$ ($p < 0.001$), respectively, after trypsin and collagenase treatments according to the results obtained by Vevo, which was consistent with the results by IAUS measurement.

Table 3-7 Effect of trypsin treatment on cartilage measured by IAUS.

Samples	Thickness (mm)		Surface reflection amplitude	
	Pre-treatment	Post-treatment	Pre-treatment	Post-treatment **
1	1.80	1.79	175.9	162.2
2	1.60	1.58	187.4	156.4
3	1.39	1.43	164.4	137.3
4	1.66	1.71	172.3	99.6
5	2.15	2.06	173.5	148.6
6	1.50	1.46	188.4	155.1
7	1.85	1.94	156.6	143.6
8	1.51	1.49	143.2	153.0
Mean	1.68	1.68	170.2	144.5
SD	0.25	0.23	15.2	19.7

**: $p < 0.01$ for paired t-test compared to pre-treatment value.

Table 3-8 Effect of collagenase treatment on cartilage measured by IAUS.

Samples	Thickness (mm)		Surface reflection amplitude	
	Pre-treatment	Post-treatment	Pre-treatment	Post-treatment ***
1	2.02	2.09	153.8	97.0
2	2.26	2.26	135.9	73.7
3	1.86	1.80	195.5	84.9
4	1.91	1.91	175.2	85.0
5	2.08	2.11	175.2	50.8
6	2.29	2.22	192.3	78.3
7	1.42	1.46	148.4	77.7
8	1.97	2.08	160.1	83.1
Mean	1.98	1.99	167.0	78.8
SD	0.27	0.26	21.1	13.3

***: $p < 0.001$ for paired t-test compared to pre-treatment value.

3.4.2. Results of tests on cartilage in intact porcine knees

The water-jet indentation experiment was successfully conducted in the intact porcine knee. The initial thickness and SC were measured from the cartilage of the femoral groove and the results are shown in Figure 3-13. There was no significant change of the cartilage thickness after the trypsin digestion ($p > 0.05$). However, for the stiffness, there was a significant decrease after the trypsin digestion ($p < 0.001$). Percentage change of the cartilage stiffness was also calculated and a mean decrease of $53.6 \pm 18.0\%$ was revealed after the treatment, which was similar to that disclosed in Subsection 3.2.2. The newly developed arthroscopy-based water-jet indentation probe was successfully applied in the intra-articular measurement of the mechanical properties of the knee cartilage.

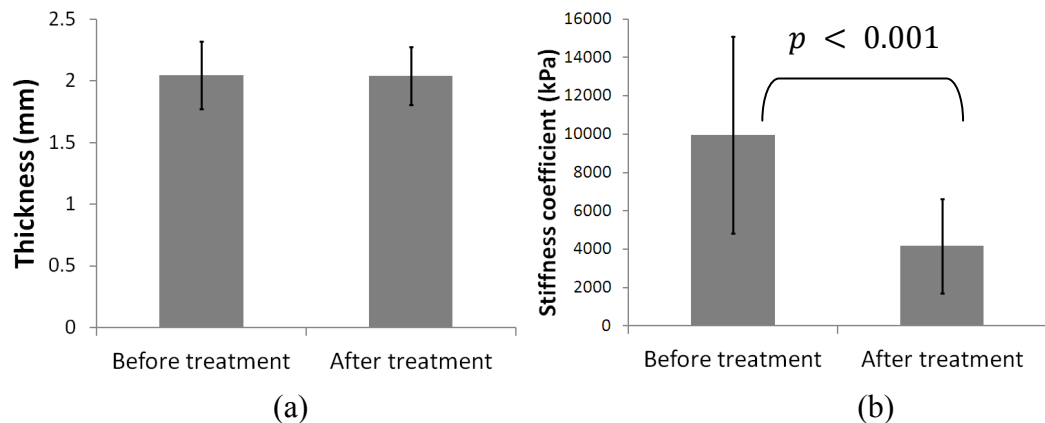


Figure 3-13 A comparison of (a) thickness and (b) stiffness coefficient for the cartilage before and after the trypsin digestion in the intact porcine knee. No significant change of thickness ($p > 0.05$), but significant decrease of the cartilage stiffness ($p < 0.001$) were detected after the trypsin digestion.

4. Discussion

This thesis describes the development of an arthroscopy-based water-jet ultrasound indentation probe and related experiments on evaluating the applicability of the newly developed probe for the assessment of articular cartilage degeneration. The successful design and fabrication of the probe through a two-step realization scheme have demonstrated it is feasible to develop such an arthroscopic probe. The results of the validation experiments have also showed that the ultrasound-based measurement of multiple tissue properties (including morphological, acoustic and mechanical properties) is an effective way to quantify the change of articular cartilage in degeneration, induced either by enzymatic digestions or by surgeries in an animal model of OA. The detailed discussion is divided into two parts: Subsection 4.1 is related to the instrumentation side of the current study, i.e., the design of the probe; in Subsection 4.2, discussion on the related experiment is given, for which to apply the developed instrument for clinical diagnosis and evaluation is the final goal.

4.1. Instrumental development

4.1.1. Development of miniaturized probe

Two steps of miniaturization were used in this study to develop the arthroscopic probe for the assessment of cartilage degeneration. At the first step, the probe was designed in a metal rod with a diameter of 12 mm. The successful design of the probe was mainly based on a small size single element ultrasound transducer and a compact design of the water-jet passage. Compared with the dimensions of the previous prototype water-jet indentation probe (Lu et al. 2005) (Figure 2-1), a significant decrease of the profile was achieved for the current miniaturized probe. Although the diameter of the ultrasound transducer (3 mm) was slightly larger than that of the exit orifice (2 mm), experimental data showed that the design did not block the ultrasound signal for the quantitative analysis. However, it was recognized that this probe was yet not small enough for real arthroscopic measurement.

Previous investigators have used either low or high frequency ultrasound to assess the articular cartilage status. A low spatial resolution was inherent with the low frequency ultrasound used externally on the skin for examining the articular cartilage in joints. For high frequency ultrasound, in previous reports it was mostly used for the study of articular cartilage in vitro because of a big profile of the transducer. There is a lack of specifically designed high frequency ultrasound transducer for arthroscopic measurement of articular cartilage in vivo. In the second step development of this study, a mature technique from the cardiovascular field – intravascular ultrasound was adopted as a type of intra-articular ultrasound (IAUS) for the intra-articular measurement to acquire quantitative information of articular cartilage. IAUS catheter has both the advantages of a small profile and the use of high frequency ultrasound. The results demonstrated that the IAUS was capable of measuring the thickness and surface reflection amplitude, with similar performance to those reported in the literature using the conventional single element ultrasound transducer (Hattori et al. 2003; Laasanen et al. 2002; Toyras et al. 1999). Compared to previous arthroscopic single ultrasound transducer measurement, the current IAUS catheter provided an extra function of tissue imaging for the cartilage. Together with its small size, it no doubt is advantageous to incorporate this imaging facility in the space-limited intra-articular applications.

With the availability of small IAUS catheter, a second step of miniaturization was conducted and a real arthroscopic probe was designed and fabricated for preliminary experimental test. A special adaptor was designed and installed at the tip of an arthroscopic working channel. The IAUS catheter could be fixed inside the adaptor and an exit was excavated in front of the active ultrasonic elements for effective data collection. At the same time, the exit was also connected to the water pipe and could be used as the passage for water-jet. The whole design was achieved in an arthroscopic channel with an outer diameter of 5.5 mm and therefore the probe was possible to be used in intra-articular operation such as that in minimally invasive surgeries.

The developed probe fulfilled the requirement of measurement of versatile tissue properties of the articular cartilage in an arthroscopic operation. The specific information that could be obtained from the probe was limited by the ultrasound frequency and the orifice size. Based on the geometrical size of the adaptor and the

position of the IAUS catheter, the angle that could be imaged for the external tissue was $40^\circ/360^\circ$ of the IAUS catheter in the current design. The total RF line number that can be viewed for external tissue was $\approx 602/9$ which was enough for calculating tissue material properties. On the other hand, the spatial resolution of the imaging was only limited by the ultrasound frequency. According to the manufacturer's webpage information, the frequency can be as high as 45 MHz for the intravascular ultrasound catheter, and therefore, if higher spatial resolution is needed, a higher frequency IAUS catheter can be adopted for the intra-articular measurement. However, it should be noted that the penetration depth will be compensated when higher frequency is used. Based on practical requirements of spatial resolution and penetration depth, a proper frequency can be selected for the design of probes and for convenient studies of cartilages from different species.

4.1.2. Limitations and future development of the arthroscopic probe

The current instrumental development has some limitations. Firstly, only A-line signal was used for the current IAUS-based arthroscopic probe, and therefore some morphological information of the cartilage such as the roughness cannot be obtained directly by processing the RF signal. Although the B-mode image directly obtained from the IAUS machine could be used for this purpose, its spatial resolution is not as high as the raw RF signal because some spatial information has been lost during the construction of the B-mode image based on the RF signals. The 2D imaging of the cartilage has several advantages for the qualitative and quantitative assessment including comparison of lesions between B-mode images and histology (Foster et al. 2000), spatial averaging of calculated parameters such as IRC to improve measurement reliability and studying regional variation of the tissue properties such as the surface roughness (Saarakkala et al. 2004; Wang et al. 2010a). For future development, data collection of 2D RF signals will be considered to calculate more material properties of the cartilage for diagnosis or to improve the measurement reliability. The 2D RF signals are available in the current IAUS system. A real problem that may be encountered is the massive data storage required for 2D acquisition. This can be solved by faster hardware or recently developed data processing method such as the graphic processing unit (GPU) computing. So the next step of development of the probe is to integrate the 2D RF data acquisition in the

software with appropriate resource allocation, where advanced signal processing is possible for the cartilage characterization.

Secondly, the design of the probe tip can also be further improved in order to provide more flexibility in adjustment when it is used in practical measurement. For example, when the insertion direction of the whole probe is fixed, the tip can be made in such a way that the angle of the water-jet can be adjusted in order to get better signals from the cartilage surface. In that case, a scissor-like handle can be designed at the proximal side of the probe to adjust the angle of the water-jet in a convenient way. After adjustment, the optimal angle can be locked so that a reliable measurement can still be conducted. With the adjustment flexibility of the water-jet angle, optimal operation could be more easily achieved. Another aspect of the design that may be optimized is the water-jet channel including the shape and size. It is expected that nozzles with different shapes will produce different types of water-jet so that the effect of water-jet on the tissue may be different. Under this situation, a calibration process is necessary for a specific nozzle shape before the real clinical measurement. Whether a nozzle shape is optimal for cartilage test depends on conditions including the size, beam uniformity and simplicity to calculate intrinsic material properties from the test. Therefore, optimal shape of the nozzle for producing the water-jet should be considered in further development.

Finally, the positioning of the probe on the cartilage in the intact knee operations was guided by an arthroscopic view in the current study. No quantitative space information was available for analyzing the spatial distribution of the measured parameters. In order to tackle this problem, spatial sensor may be considered in future design to synchronize the ultrasound-based measurement with its positional information registered so that a spatial mapping of the tissue properties could be possible for analyzing the pattern of change of cartilaginous properties in an osteoarthritic joint under the arthroscopic operation. Proper choice for such kind of positional localization can be the magnetic spatial sensor with a tiny profile, which can be installed at the end of the probe. The spatial sensor would be better to have anti-interference capability for metal material so that accurate measurement could be obtained. Spatial signal will be incorporated with the ultrasound-based measurement so that the mechanical material properties could be registered with spatial positions for a better analysis of the results.

4.2. Experimental validation studies

In this study, the experimental validation was arranged in an order of increased similarity with respect to a real intra-articular measurement in vivo. The silicone phantom was assumed to be a type of simplistic mimicking material of the soft tissue with homogeneous and isotropic material properties. However, it was recognized to be too simple to be a realistic model of the articular cartilage. For the experiments on real cartilage samples, the bovine cartilage sample was cored out from one quadrant of the patella; rabbit cartilage sample was attached on intact bone but the joint was opened; and for the porcine cartilage, it was on the intact knee but not opened. An increased similarity to in vivo cartilage situation indicates that the operation condition is more and more approaching the real situation on living cartilage and the developed probe is ready to be extended to in vivo clinical applications in future studies.

4.2.1. Phantom tests

In the silicone phantom test, the f/d coefficient was obtained as a parameter to compare the results from the miniaturized probe with those from the contact indentation device. Silicone is one of the most convenient categories of material to mimic soft tissues in the study of tissue elasticity (Lamouche et al. 2012; Lu et al. 2005; Lu et al. 2007) and therefore it was adopted in the current study as a simple model of the soft tissue for validation study. As the SOS of silicone phantom was significantly different from that of soft tissue, a specimen insertion method was firstly used to measure the sound speed. As a first step of the validation study, a good correlation of results between the water-jet ultrasound indentation method and the contact indentation method was obtained. This relationship would not be significantly affected by the indentation speed as the viscosity was small this silicone material. Neither the difference of testing conditions (in water for water-jet test and in air for contact indentation test) would affect mechanical properties of the phantoms as the material was impermeable. The good correlation demonstrated that the developed probe could be used to effectively quantify the stiffness of the phantoms. However, the silicone phantom used in the current study was relatively softer than that of the articular cartilage and the thickness was significantly larger than that of articular

cartilage in most animals, further study was necessary for study of real articular cartilage and its degeneration.

4.2.2. Tests on bovine cartilage in vitro

After the phantom experiment, further test was conducted on real bovine cartilage samples in vitro using the enzymatic digestion as a model to simulate the degeneration of articular cartilage. Disruption of collagen network and depletion of PGs are the most significant changes of extracellular matrix firstly observed in degenerated articular cartilage with OA (Hollander et al. 1994; LeRoux et al. 2000). Therefore, in this study, two specific enzymes, i.e. trypsin and collagenase were used to digest the two main components in cartilage to simulate the degeneration. The results by Safranin O staining showed that most of the PGs had been digested in the trypsin treatment. Only partial PGs were digested in the collagenase treated samples and the lost might be due to the porous structure formed after collapse of the collagen network, which was observable under SEM (Wang et al. 2010a). The histological study confirmed that enzymatic digestion could be practically used as model to simulate the complete or partial breakdown of the main components of cartilage.

For the specific analysis, the reproducibility study showed comparable or even better reproducibility of the current system compared to the previous system in terms of SCV (Wang et al. 2010a) and it was demonstrated that the quantitative parameters obtained from the miniaturized probe could be used to characterize the morphological, acoustic and mechanical properties of the cartilage and its change after enzymatic degeneration. In detail, the cartilage thickness was calculated from the two peak signals reflected from the two interfaces of the cartilage, i.e., the cartilage surface and cartilage-bone interface, respectively. The reflection from the surface of the cartilage originates directly from the difference of acoustic impedance between water and soft tissue. Therefore, it serves not only as a reference for the thickness measurement but also as a reference reflecting the acoustic impedance of the cartilage, which changes significantly after its compositional change, such as in the collagenase digestion process. The thickness was found to have no significant change after both enzymatic digestions. This was expected as an in-vitro degeneration model was used in the current study. In living cartilage, the tissue may adapt to the disruption of extracellular matrix components exhibiting the symptom of thickness reduction.

However, in the in-vitro model, the tissue loses the capability in adaption and therefore, immediately after the enzymatic digestion, the change of thickness is hardly detectable (Niemenen et al. 2002; Toyras et al. 1999). It is well known that the cartilage may become significantly thinner with the progression of OA, showing a significantly narrowed joint space (Agnesi et al. 2008). However, it should be noted in the early stage of degeneration, the cartilage thickness may increase instead of decrease because of hypertrophic repair and swelling of the cartilage (Brandt et al. 1991; Calvo et al. 2001). Therefore, the measurement of thickness will be helpful for the differentiation between the early and late stage of the cartilage degeneration.

With regard to the amplitude of the acoustic reflection from the cartilage surface, the results of IRC showed that the trypsin digestion induced no significant effect while collagenase treatment significantly reduced this parameter (Niemenen et al. 2009). Collagenase digestion caused the cleavage of the superficial collagen network. This reduced the acoustic impedance and increased the surface roughness of the cartilage, both of which caused the decrease of the ultrasound reflection from the cartilage surface (Chiang et al. 1994; Toyras et al. 1999). However, the PG content is small in the superficial layer of the cartilage (Mow et al. 2005) and change of the acoustic impedance and surface roughness is neglectable after the trypsin digestions. Accordingly, no significant change of surface reflection was observed from the group with the trypsin digestion. Therefore, the acoustic reflection from the cartilage surface could be practically used as an indicator to differentiate between degenerations induced by loss of PGs or breakdown of collagen fiber network.

The results of the water-jet ultrasound indentation test on the cartilage showed that the cartilage stiffness significantly decreased after the two enzymatic digestions. After trypsin digestion, the cartilage lost the PGs as shown in histology and the fixed charge density decreased, which significantly reduced the repulsive force during the compression and led to a much smaller stiffness (Sun et al. 2004). For the collagenase digestion, the breakdown of collagen fibers would form pores in the cartilage and some PGs would then easily move out of the extracellular matrix, both of which would reduce the mechanical quality of the cartilage. However, it seemed that in the current model the effect of collagenase digestion was smaller than that of trypsin treatment in reducing the stiffness of the cartilage (Table 3-1), which might be due to

the fact that most of PGs were depleted in the trypsin digestion while only partial PGs and the superficial network were affected by the collagenase treatment.

Viscosity is another important mechanical property of the biological soft tissue and in this study, the energy dissipation ratio (EDR) was used to investigate the change of cartilage viscosity before and after enzymatic digestion. From the typical indentation curve shown in Figure 2-13, the cartilage before enzymatic digestion behaved more like an elastic material with little hysteresis and preconditioning effect. However, the effects of hysteresis and preconditioning were more obvious after the digestion. It is well known that the hysteresis phenomenon observed in the mechanical testing of cartilage is mainly caused by the content of interstitial fluid. EDR of cartilage test is shown to be loading rate dependent (Varga et al. 2007). However, the same indentation speed was used for all the mechanical tests in the current study, and therefore the change of EDR after enzymatic digestion was not supposed to be caused by the difference of loading rate. The change of EDR might come from the alteration of hydration or the solid/fluid interactions in the cartilage. After digestion, the water content in the cartilage might become higher (Basalo et al. 2004) and the water might become easier to move with a higher permeability (Korhonen et al. 2003a). The combination of these changes together with the PG loss might make the tissue less capable of energy storage resulting in a larger EDR.

The combination of the parameters measured in the current study could also be used to differentiate between normal and degenerated cartilage and also between trypsin-digested and collagenase-digested cartilage. Figure 4-1 shows a 3D scatter plot of the three parameters in normal and degenerated cartilage samples, where the corresponding 2-D plots using two parameters among them are also presented. The normal group included the cartilage samples from both the groups before the enzymatic digestion. It can be easily observed from the figure that the three groups were clustered at different spatial locations. As the standard deviation of stiffness in the normal cartilage was quite large, the combination of IRC and EDR might have the best discrimination among the three groups. Therefore, this study has demonstrated that the multiple parameters measured by the probe could be used to discriminate between normal and degenerated cartilage samples and also to differentiate between trypsin and collagenase-digested cartilage samples.

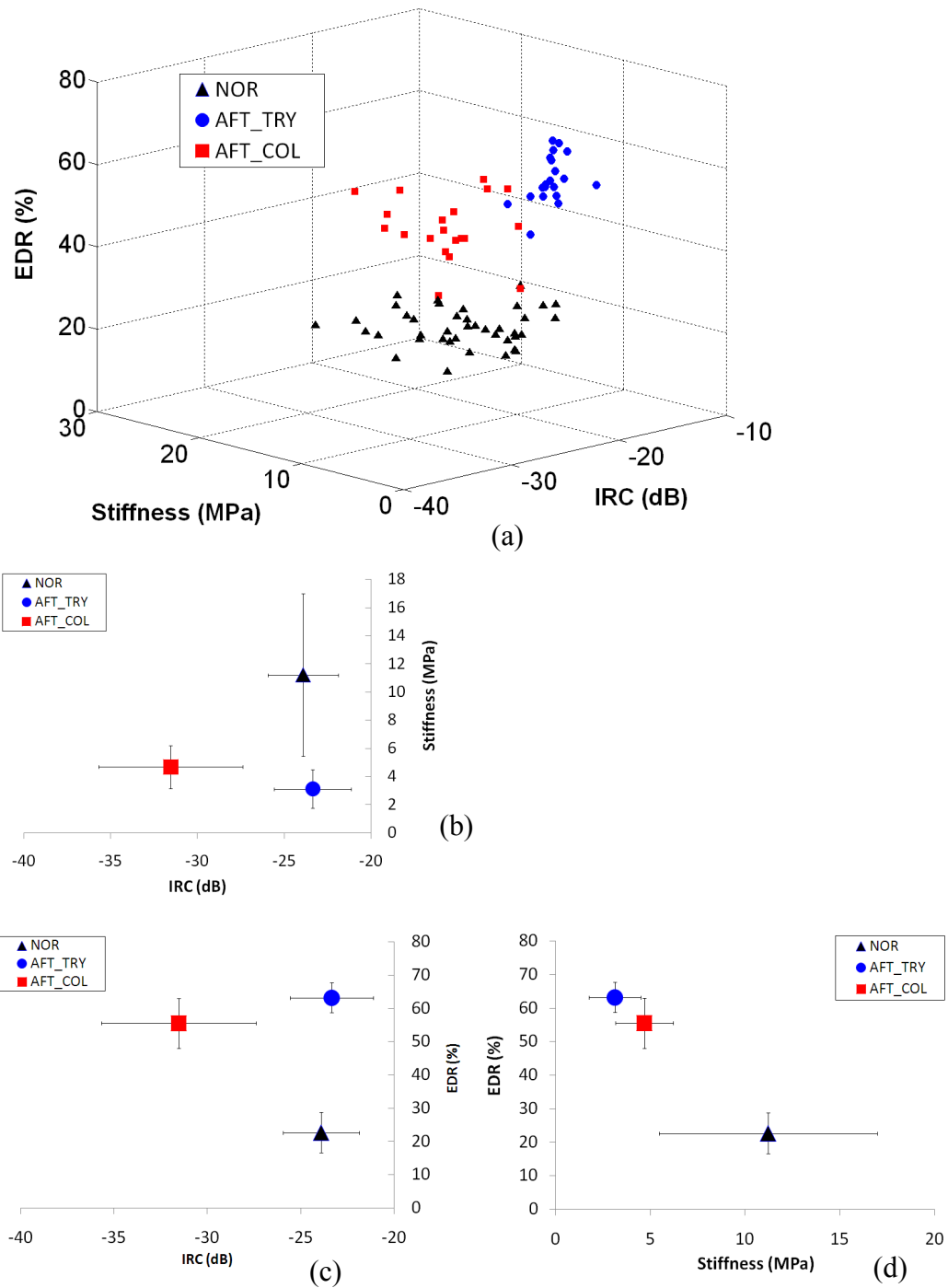


Figure 4-1 (a) A 3D scatter plot of three parameters IRC, stiffness and EDR in normal and degenerated cartilage before and after trypsin and collagenase digestion. The corresponding projection of the 3D data sets into 2-D plane in terms of mean and standard deviation of different groups is also plotted in (b) IRC vs. stiffness, (c) IRC vs. EDR and (d) stiffness vs. EDR. Normal cartilages included all those samples before trypsin digestion and before collagenase digestion. NOR: normal, AFT_TRY: trypsin-digested samples, AFT-COL: collagenase-digested samples.

Analysis of the results obtained from the water-jet indentation test and from the rigid indentation test showed that the mechanical parameters were highly correlated and the trend of change was consistent (Figure 3-3, Figure 3-4 and Table 3-1). Therefore, using the rigid indentation as a validated reference method, the results demonstrated that the mechanical test using the miniaturized water-jet ultrasound indentation probe was effective to study the biomechanical properties of the articular cartilage. Both methods showed a significantly decreased stiffness and an increased EDR of the cartilage after enzymatic digestions. With respect to extent of change, it was found that the decrease of Young's modulus measured from the rigid indentation induced by the two enzymatic digestions was smaller than that of stiffness coefficient from the water-jet indentation, especially for the collagenase treatment. In order to study the detailed relationship of stiffness from the two methods, the Bland-Altman test was performed for the water-jet indentation and contact indentation tests (not shown here). Through this test, it was found the difference of the two methods was relatively larger for a larger stiffness value. Therefore, it was recognized there was some nonlinearity for the relationship between the results of the two methods. With respect to EDR, its value from the water-jet indentation was generally smaller than that by the rigid indentation. These differences might originate from the two intrinsically different mechanical test methods. Interactions between the cartilage and indenter depend on the indenter material and therefore even with the same force level of indentation, the behavior of deformation may be quite different for the two indentation methods, which is further discussed in Subsection 4.2.5. Future investigation using experimental or simulation methods is necessary to explain the differences of results from the two methods and extract the intrinsic material parameters from the water-jet indentation. For the current study, a simplistic model of enzymatic digestion was used to simulate the cartilage degeneration. The extent of component destruction using this model may not be so easy to control to simulate an early degeneration of the cartilage. Furthermore, the destruction to the cartilage using these enzymes is quite specific and the model is quite simple with respect to the very complicated etiology and pathology of the cartilage degeneration in an osteoarthritic change. Therefore, further study was conducted on naturally degenerated articular cartilage in a rabbit mode of OA based on ACL transection.

4.2.3. Tests on rabbit cartilage in situ

ACL transection is a popular model used to study the change of articular cartilage in the knee joint in animal model studies of OA (Bendele 2001; Vignon et al. 1987). The surgery creates biomechanical instability to the joint and the varied loading pattern progressively causes the structural changes of the tissues inside the joint (Kaab et al. 2000), which finally lead to osteoarthritis. In this study, the combined ultrasound-based method was introduced to study the change of various properties in the rabbit knee cartilage using the ACL transection model of OA and to assess the potential application of this method in quantitatively assessing the cartilage degeneration. Matured rabbits were used in the study to assure that the degeneration was similar to adult human model of OA and the model was not affected by the maturation process. It should be noted that the morphological parameter URI and acoustic parameter IRC were obtained from a separate high frequency ultrasound imaging system, which was different from that of mechanical properties measured by the water-jet indentation system. This is not so convenient or even impossible for future studies in living tissues as the probe of the high frequency ultrasound system is too big and it takes time to use multiple devices for measurement during surgical operations. This problem can be solved by using the IAUS catheter, as used in the arthroscopic probe design. In this situation, all the parameters can be measured through a single device operation so that the developed device can be more attractive for clinical applications. Detailed discussion of the related results is presented as follows.

4.2.3.1. Change of various parameters with post-surgery time

There was a significant increase of the histological grade for the cartilage lesions along with the post-surgery time (Figure 3-7). The distribution of histological grades at different post-surgery time points also showed the gradual increase of the degeneration level (Figure 3-8), which has been reported in previous studies (Batiste et al. 2004; Yoshioka et al. 1996). The results of histological grades showed that there was real degenerative change of the articular cartilage and the change was progressive with time. Therefore, ACL transection model was an effective model to simulate the degenerative change of the articular cartilage. An interesting observation of the comparison between lesions at two sides revealed that the grade was generally higher

at the femoral side than that at the tibial side. The possible reason might come from the different loading pattern between the inspection sides. The average stress endured at the femoral sites might be larger in general than that at the tibial plateau so that the lesion at the femoral side was severer than that at the tibial side. The averaged grade was generally less than 2 for Groups Week-0, Week-3 and Week-6, except for Week-9, so the lesion was generally considered to be at the early stage, which served as a proper model for the purpose of detection of early cartilage degeneration using the ultrasound-based measurement method.

The ultrasound-based multi-modality measurement could obtain morphological, acoustic and mechanical properties from the articular cartilage. Except the thickness, all other parameters showed some general trend for the cartilage lesion along with the post-surgery time. The URI generally increased along with the post-surgery time, which was caused by fibrillation of the cartilage at the early degeneration. Fibrillation is characterized by splitting of the cartilage surface and therefore the surface roughness is increased after fibrillation. Yoshioka et al. (1996) also reported an increase of the RMS roughness for the cartilage after ACL transection when compared to the cartilage in the sham knee. The URI of cartilage with lesion at Week-9 post surgery was about 3~4 fold larger than that of the control sample; however, the URI had a slight decrease at the tibial side between Week-6 and Week-9, although the difference was not significant ($p > 0.05$). Possible reason might be due to the non-uniform change of the structural changes with time after the ACL transection surgery, which should be further investigated. The results of IRC showed that the acoustic reflection from the cartilage surface generally decreased with post-surgery time. A general decrease of 10 dB was found for IRC between the control and samples at 9 week post surgery. The decrease was caused by both the increase of the surface roughness and that of the cartilage physical properties including the acoustic impedance (Adler et al. 1992). However, similar to the situation of URI, the trend of IRC change between Week-6 and Week-9 was slightly different at the tibial side. It slightly increased rather than decreased after Week-6, for which the reason was uncertain and should be investigated in future studies. The stiffness of the cartilage measured from the water-jet ultrasound indentation showed a general decrease after the ACL transection surgery. A general difference of 20.8% was found for the stiffness between Group Week-9 and control at the femoral side and the

corresponding value was 34.8% at the tibial side. The decrease was generally smaller than that induced by the enzymatic digestion (Table 3-1). Similar results on the change of mechanical properties after ACL transection were reported in a previous study which disclosed a decrease of 18% for the aggregate modulus at 9 weeks post surgery (Sah et al. 1997). The decrease of the stiffness after surgery was assumed to be caused by the material degeneration in the articular cartilage including the breakdown of the collagen network and the loss of proteoglycans. Although there were significant differences between control and the post-surgery groups, the difference among the different post-surgery groups was not significant, suggesting that the degradation of the mechanical properties in the cartilage was quite subtle. In this situation, the change of other properties such as morphological and acoustic properties could be complementary to the mechanical properties as reliable indicators of early degeneration of cartilage.

4.2.3.2. Association of parameters with histology and inter-correlations

The association of the various parameters with the pathological grade was also analyzed to see whether the measured parameters could be used as good indicators to reflect the severity of the cartilage degeneration. The results were quite similar to those post-surgery time related results, which might be due to a good correlation between the histological grade and post-surgery time. A Spearman rank correlation analysis showed that the correlation between the histological grade and post-surgery time was 0.77 and 0.68 at the femoral side and at the tibial side (both $p < 0.001$), respectively. The histological grade was given based on the OARSI grading method and served as a gold standard for assessing the cartilage quality. The histological scale was specifically given at the test position so that there was one-to-one correspondence between the measured parameters and the histological grade, except Grade 4. In Grade-4 samples, the pathological grade might not represent the real situation of the tested cartilage because the ultrasound-based measurement could not be conducted on bone directly. In this situation, the ultrasound measurement was performed on the nearest position where cartilage was still there. Therefore, this part of results with Grade 4 was not included for comparisons in the statistical analyses. In future studies, a better control of the correspondence between sites for pathological grading and ultrasound measurement should be planned for a better correspondence of the results.

No obvious association was found between the cartilage thickness and the pathological grade. Until at the very late stage, the thickness of cartilage might not be a reliable parameter to indicate the severity of cartilage degeneration. In order to observe the trend of change of different parameters with respect to the pathological grade, a linear regression of the parameters with respect to the grade was analyzed. A general trend was significant or nearly significant for almost all the parameters except the thickness at the femoral side: for URI, a trend of 6.3 μm per one grade increase ($y = 6.3x - 4.2, r = 0.91, p = 0.092$); for IRC, a trend of -3.46 dB per one grade increase ($y = -3.46x - 39.76, r = -0.98, p = 0.024$); for SC, a trend of -353 kPa per one grade increase ($y = -353x + 4806, r = -0.94, p = 0.060$) and for E, a trend of -109 kPa per one grade increase ($y = -109x + 774, r = -0.96, p = 0.045$) were obtained. At the tibial side, the trend was not obvious for the URI and IRC; for SC, a trend of -812 kPa per one grade increase ($y = -812x + 9519, r = -0.81, p = 0.19$) and for E, a trend of -160 kPa per one grade increase ($y = -160x + 1106, r = -0.96, p = 0.038$) were obtained. More consistent change along with the progression of degeneration seemed to happen at the femoral side than at the tibial side, for which the reason should be further investigated. The multiple parameters from the ultrasound-based measurement provide the opportunity to study the progressive change of the cartilage in terms of change of different material properties. How to combine these multi-modality parameters into an integral indicator to reflect the severity of cartilage degeneration needs to be further investigated.

The inter-correlations among the measured parameters were analyzed and the results showed that the maximum correlation came from negative relationship between the URI and the IRC ($r = -0.73$), and followed by that between the stiffness and stiffness coefficient ($r = 0.64$). The high correlation between URI and IRC was understandable, because when the surface is rougher, the energy is scattered in a larger angle range so that the reflection at the 180° backscattering direction with respect to the incident ultrasound beam becomes smaller. The linear relationship was more obvious when the URI was small and it became more scattered when the URI was large (Figure 3-10d). A more detailed explanation and theoretical models related to ultrasound scattering can be found in previous studies (Thorsos 1988; Thorsos and Jackson 1989; Yang and Broschat 1992). The URI was a direct physical parameter

reflecting the cartilage surface condition while the IRC was an indirect indicator of the cartilage surface. The correlation between the thickness and stiffness of the rabbit cartilage was also demonstrated in a previous study (Rasanen and Messner 1996). The correlation showed that in rabbit the elasticity of the stifle cartilage was closely related to its thickness, which might be related to a distribution of the loading inside the knee joint. However, it should be noted that the correlation between thickness and cartilage stiffness was controversial as some studies denied the existence of such a correlation (Athanasίου et al. 1991; Simon 1970; Simon 1971) and the correlation was different among different species (Niederauer et al. 2004), which warrants further studies. The relationship between the morphological (URI) and mechanical properties (stiffness) was also determined. The results showed that when the surface roughness became sufficiently large (e.g., $URI > 30 \mu\text{m}$), the stiffness was significantly reduced because of the degradation of the collagen network. However, in a small range of URI, the relationship between stiffness and surface roughness was not so obvious. The situation was similar for the relationship between IRC and stiffness coefficient. Further studies are necessary to more clearly identify the relationship between the surface roughness and the mechanical properties of articular cartilage.

Finally, a significant correlation between the stiffness coefficient measured from the water-jet indentation and Young's modulus from the intact indentation demonstrated that the water-jet indentation method was an effective method to measure the mechanical properties of the cartilage, as also showed in the previous experiment on the bovine cartilage test *in vitro*. However, it was found that the correlation ($r = 0.55$, Figure 3-11) was not so high. There were several possible reasons for the intermediate correlation value. The first one was the high aspect ratio (indenter radius/cartilage thickness ≈ 2) in the rabbit cartilage test. When aspect ratio was high, the results of Young's modulus calculated from the Hayes' equation (1972) would be more dependent on the test condition and other material properties (such as the Poisson's ratio and cartilage thickness), inducing larger errors in calculation for different samples if the specific parameters were uncertain. The second might be the large inhomogeneity of cartilage especially the thickness under the large indenter so that the conditions of using Hayes' equation could not be met in this situation. The third reason was the relatively lower accuracy in measuring the deformation during indentation due to the small thickness of cartilage so that the error of final results

might become relatively larger in this case. In future studies, it is necessary to use a smaller indenter or increase the ultrasound frequency in order to improve the measurement accuracy and reliability. The last one came from the equation used for calculating the stiffness coefficient in water-jet indentation. It was just used as a reference measurement of the cartilage elasticity. Further investigation is necessary to extract the intrinsic material properties from the water-jet indentation test, as discussed in Subsection 4.2.5.

4.2.4. Arthroscopic tests on cartilage in intact porcine knees

After the arthroscopy-based probe was developed, preliminary experiment was conducted on the cartilage of the intact knee using the trypsin digestion model to simulate the degeneration of the articular cartilage. With the guidance of arthroscopic view, the probe could be properly positioned inside the intact knees in order to achieve good imaging of the cartilage. A good fixation of the probe using a clamp could facilitate the operation and a reliable measurement could be conducted using this setup. Based on the current setup, the thickness and stiffness of the cartilage were measured for comparison before and after the trypsin digestion. As expected, the experimental results showed that the cartilage thickness did not change after the trypsin treatment, as trypsin does not cause any significant change on the tissue structure. However, for the mechanical properties, the stiffness significantly decreased after the trypsin digestion ($p < 0.001$). It was uncertain whether the decrease of stiffness might come from the natural degeneration of the material quality with time even without the effect of enzymatic digestion. In order to measure the time (about 4 hours) effect on the cartilage stiffness, two extra tests were conducted in two extra intact knees to measure the change of cartilage stiffness along with time. The original stiffness for the two control samples was 4445 kPa and 4154 kPa, respectively. The knees were kept hydrated and then the cartilage was re-tested after 4 hours of hydration. The corresponding stiffness became 4029 kPa and 3863 kPa. There was only a 9.4% and 7.0% decrease of stiffness for the two samples. This might suggest that the main decrease of stiffness came from the enzymatic digestion, which was mainly caused by the depletion of proteoglycans, but not from the pure time effect.

Through the preliminary tests inside the intact porcine knees, the basic concept and feasibility of using the arthroscopic probe for characterizing the degeneration of the articular cartilage through arthroscopic measurement was demonstrated. The developed probe has a proper size which can be inserted into the joint of big animals for direct measurement of the cartilage material properties. In order to make this tool ready for clinical applications, further improvement of the probe design and fabrication is needed and more pre-clinical trials should be planned in future studies.

4.2.5. Limitations of experimental studies and future research directions

There were some limitations for the current experimental study of detection of early cartilage degeneration using the probe developed in the current study, in addition to those that have been separately discussed in previous subsections.

The water-jet was successfully applied as an indentation medium to compress the cartilage in this study. However, as the purpose of the water-jet is to indent rather than destroy the tissue, the pressure used in my study was far smaller and the nozzle size was much larger than those used in surgical cutting applications. For the current system, when the maximal pressure was set to be larger than 550 kPa (5.5 bar), the water-jet became quite turbulent, which greatly affected the acquisition of ultrasound signal and made the signal void for quantitative analysis. Therefore, a maximal pressure smaller than this value (about 330 kPa) was used in the current study. Specialized design may be necessary in future study if a larger water pressure is needed to induce certain large enough amount of deformation in the tissue. In the case of high pressure, it is necessary to use high resistant material for the tube and connectors to prevent the whole system from being broken for a normal operation. On the other hand, in our study the maximal pressure loading of 330 kPa was quite small compared to the peak loading stress of cartilage endured in a normal physiological loading condition; for example, a high pressure up to 18 MPa may be induced in the hip joint cartilage (Hodge et al. 1986). Therefore, it was hypothesized that the potential deleterious effect of the water-jet indentation on the cell viability and matrix quality on the cartilage samples either with normal condition or early degeneration in the current study could be neglected. However, if a larger water-jet pressure was needed in future studies, labeling methods such as the TUNEL staining (Loening et al.

2000) can be introduced to study its detrimental effects on the cell viability in the normal, pre-osteoarthritic and severely degenerated cartilage.

The second limitation is related to the technical aspect of the water-jet ultrasound indentation method. With respect to the mechanical properties, a very simple model of the mechanical behavior of cartilage under water-jet indentation was adopted in the current study. The slope of the loading phase of the force-deformation curve was used to represent the elastic properties of the cartilage under certain test protocols together with the cartilage's initial thickness as shown in the definition of stiffness coefficient. The stiffness coefficient is not an intrinsic parameter of the tissue material. In order to extract intrinsic material parameters such as Young's modulus from the water-jet indentation, the interaction of water-jet with the soft tissue should be further studied. This could be started from the finite element analysis with modern software which can handle the analysis of solid-fluid interaction (such as Ansys). Tissue model will be created first and then the water-jet will be used to indent the tissue with their interface defined by specific solid-fluid interaction (FSI) model. The robustness of the simulation will be verified by experimental study. After verification, finally a specific calculation method (most likely, an equation) will be derived from the simulation results to calculate the Young's modulus from the data of pressure and deformation. Furthermore, it is well known that cartilage is a complex multiple-phasic tissue (for example, including the solid, fluid and ion states in a triphasic model (Lai et al. 1991; Mow et al. 1980) and it has various characteristics of a typical biological soft tissue under mechanical test: inhomogeneity induced by hierarchical structure, anisotropy induced by fiber orientation, strain and strain-rate dependence induced by tissue fluid. The interaction between water-jet and cartilage is of great importance for analyzing the experimental data. For example, a continuous water-jet was adopted in the current study to indent the cartilage. The rebound force might induce positional change in the tissue if the probe was not fixed during the operation. To solve this problem, pulsatile water-jet may be adopted in further studies to reduce the effect of rebound. Otherwise, some balancing mechanism needs to be incorporated to reduce the effect from the rebounding force. How those more realistic and practical models such as biphasic or triphasic model (Lai et al. 1991; Mow et al. 1980) together with a detailed analysis of the water-jet indentation data can be used to get intrinsic properties from the cartilage warrants further research. Only intrinsic parameters of the cartilage are obtained from

the measurement, comparisons of results from different research groups and centers are possible for better studies of this tissue.

Another limitation for the application of the developed probe is the invasiveness of the operation. Although an arthroscopic operation can be thought to be minimally invasive, the invasiveness may limit the operation to those subjects for whom arthroscopic operation is suggested by the doctors as necessary and unavoidable. This may be the main hurdle which prevents the current technique from being accepted as a clinical routinely used diagnostic method. This is also the main disadvantage of the current technique compared to those truly non-invasive methods such as MRI imaging of articular cartilage. Traditional ultrasonographic detection of articular cartilage is possible as introduced in the Introduction part of the thesis. However, it suffers from a low spatial resolution because of low frequency used for a deep enough penetration. To improve the spatial resolution, relatively high frequency was used but it needs a near distance operation so that more accurate measurement could be performed. The near distance operation made the requirement of minimal invasive arthroscopic operation unavoidable. On the other side, minimal invasive operation is acceptable for some patients. Nowadays, hundreds of thousands of arthroscopies are performed in each year on those patients who have problems with their knees. According to Rutkow's report, there were 632,000 procedures of knee arthroscopy which was the 7th most frequent operation in United States in 1994 (Rutkow 1997). These patients receive the operation of knee arthroscopy probably because of pathologies such as meniscus tear or ligament injuries. However, they may also have signs of early OA and the developed arthroscopic probe can be used to detect the change of tissue properties of the articular cartilage. The use of the arthroscopic probe would not significantly be different from the use of other arthroscopic instruments but these patients can benefit from the early detection of cartilage degeneration. Treatment schemes can be prescribed to those patients to prevent or delay the progression of OA. On the other hands, for those patients who receive cartilage repair surgeries, the developed probe can also be used to monitor the recovery of the cartilage under different treatment schemes such as laser or ultrasound stimulations (Gur et al. 2003; Loyola-Sanchez et al. 2012). For the purpose of screening of early cartilage degeneration, low-cost and noninvasive examination methods are needed to be developed in future.

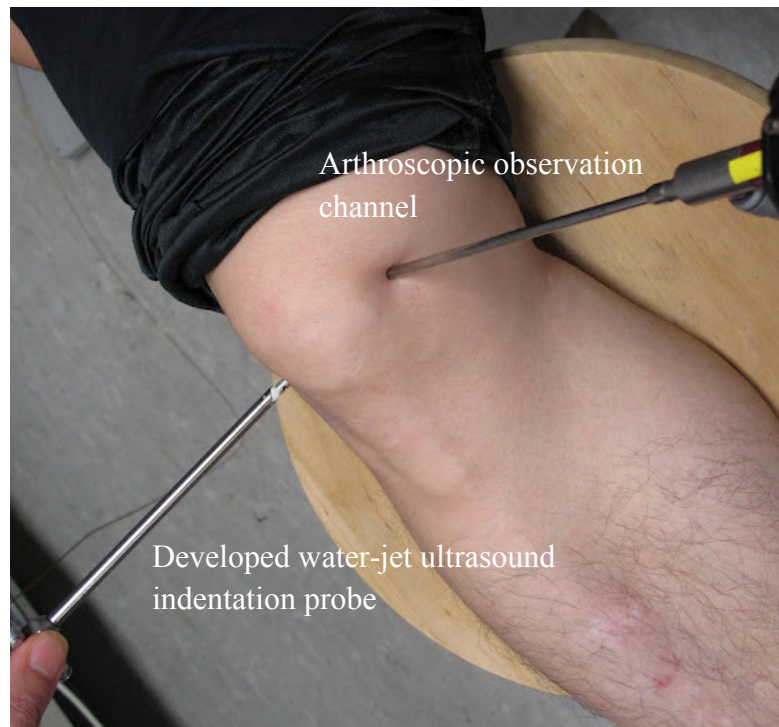


Figure 4-2 A simple demonstration of the arthroscopic operation of the developed probe in the human knee test in vivo.

Lastly, the usefulness of the rabbit OA model for study of adult human subjects is still of concern and further studies on using the multi-modality measurement for assessment of human cartilage degeneration are needed to demonstrate the potential of the developed probe. When the probe with further improvement meets the general standards of operation on human subjects such as easy disinfection, biological compatibility and reliable measurement, the probe can be inserted into the joint for in vivo test as shown in Figure 4-2. The viewing arthroscopy then can be used to guide the positioning of the developed probe and related measurement will be conducted after the probe is placed at a proper position in the joint. Furthermore, 3D positional sensing device can be installed at the tip of the probe for locating the exact test site so that a coarse mapping of the cartilage properties can be possible. The distribution of the material properties can be used to study the regional difference of the degeneration in the osteoarthritic joint. The ultimate goal of the development of arthroscopic is to help the diagnosis of early cartilage degeneration or the monitoring of cartilage repair in a quantitative and objective way, for those patients as mentioned in the above paragraph.

5. Conclusions and Suggestions on Future Work

In this study, the development of an arthroscopy-based water-jet ultrasound indentation and corresponding experiments to test the feasibility and applicability of the ultrasound-based measurement for detecting the degeneration of articular cartilage were described. Based on the successful design of the probe and corresponding experimental results, the following conclusions can be drawn:

- 1) An arthroscopy-based water-jet ultrasound indentation probe has been successfully designed and fabricated through a two-step development scheme;
- 2) The developed miniaturized probe could be used to detect the degeneration of bovine articular cartilage in vitro induced by enzymatic digestions;
- 3) The experiment on rabbit knee cartilage in situ using an osteoarthritis model induced by ACL transection surgery showed that the ultrasound-based measurement technique was effective to detect the natural degeneration of the articular cartilage;
- 4) The pre-clinical trials in intact porcine knees using the arthroscopy-based probe demonstrated it was feasible to be applied for intra-articular characterization of cartilage degeneration.

To continue this study, I propose the following topics as suggestions for the future research:

- 1) To study the profile of deformation induced by the water-jet on the soft tissue and the interactions, so that intrinsic material properties such as Young's modulus can be extracted from this type of non-contact indentation test;
- 2) To further develop the IAUS-based water-jet indentation probe in aspects such as shape optimization, operation optimization, 2D RF data collection, and possibilities in integration with other sensors, e.g., spatial sensor or optical sensor, so that more effective operation can be achieved and more mechano-acoustic parameters can be obtained within one probe;
- 3) To further test the developed probe using naturally degenerated human osteoarthritic cartilage samples in vitro or even human cartilages in joints in vivo to demonstrate its usefulness in clinical practice.

References

- Adam C, Eckstein F, Milz S, Schulte E, Becker C, Putz R. The distribution of cartilage thickness in the knee-joints of old-aged individuals - measurement by A-mode ultrasound. *Clin. Biomech.* 1998;13:1-10.
- Adler RS, Dedrick DK, Laing TJ, Chiang EH, Meyer CR, Bland PH, Rubin JM. Quantitative assessment of cartilage surface roughness in osteoarthritis using high frequency ultrasound. *Ultrasound Med. Biol.* 1992;18:51-58.
- Agnesi F, Amrami KK, Frigo CA, Kaufman KR. Comparison of cartilage thickness with radiologic grade of knee osteoarthritis. *Skeletal Radiol.* 2008;37:639-643.
- Aisen AM, McCune WJ, MacGuire A, Carson PL, Silver TM, Jafri SZ, Martel W. Sonographic evaluation of the cartilage of the knee. *Radiology* 1984;153:781-784.
- Altman R, Asch E, Bloch D, Bole G, Borenstein D, Brandt K, Christy W, Cooke TD, Greenwald R, Hochberg M, Howell D, Kaplan D, Koopman W, Longley S, Mankin H, McShane DJ, Medsger T, Meenan R, Mikkelsen W, Moskowitz R, Murphy W, Rothschild B, Segal M, Sokoloff L, Wolfe F. Development of criteria for the classification and reporting of osteoarthritis - classification of osteoarthritis of the knee. *Arthritis Rheum.* 1986;29:1039-1049.
- Armstrong CG, Mow VC. Variations in the intrinsic mechanical properties of human articular cartilage with age, degeneration, and water-content. *J. Joint Bone Surg. Am.* 1982;64A:88-94.
- Ateshian GA, Mow VC. Friction, lubrication, and wear of articular cartilage and diarthrodial joints, In: Mow VC and Huiskes R, ed. *Basic Orthopaedic Biomechanics and Mechano-biology*. Philadelphia: Lippincott Williams & Wilkins, 2005. pp. 447-494.
- Athanasίου KA, Rosenwasser MP, Buckwalter JA, Malinin TI, Mow VC. Interspecies comparisons of in situ intrinsic mechanical properties of distal femoral cartilage. *J. Orthop. Res.* 1991;9:330-340.
- Bae WC, Lewis CW, Levenston ME, Sah RL. Indentation testing of human articular cartilage: effects of probe tip geometry and indentation depth on intra-tissue strain. *J. Biomech.* 2006;39:1039-1047.

- Bae WC, Temple MM, Amiel D, Coutts RD, Niederauer GG, Sah RL. Indentation testing of human cartilage: sensitivity to articular surface degeneration. *Arthritis Rheum.* 2003;48:3382-3394.
- Bansal PN, Joshi NS, Entezari V, Grinstaff MW, Snyder BD. Contrast Enhanced Computed Tomography can predict the glycosaminoglycan content and biomechanical properties of articular cartilage. *Osteoarthritis Cartilage* 2010;18:184-191.
- Basalo IP, Mauck RL, Kelly TAN, Nicoll SB, Chen FH, Hung CT, Ateshian GA. Cartilage interstitial fluid load support in unconfined compression following enzymatic digestion. *J. Biomech. Eng.-Trans. ASME* 2004;126:779-786.
- Batiste DL, Kirkley A, Laverty S, Thain LMF, Spouge AR, Holdsworth DW. Ex vivo characterization of articular cartilage and bone lesions in a rabbit ACL transection model of osteoarthritis using MRI and micro-CT. *Osteoarthritis Cartilage* 2004;12:986-996.
- Bear DM, Szczodry M, Kramer S, Coyle CH, Smolinski P, Chu CR. Optical coherence tomography detection of subclinical traumatic cartilage injury. *J. Orthop. Trauma* 2010;24:577-582.
- Bendele AM. Animal models of osteoarthritis. *J Musculoskelet Neuronal Interact* 2001;1:363-376.
- Berkenblit SI, Frank EH, Salant EP, Grodzinsky AJ. Nondestructive detection of cartilage degeneration using electromechanical surface spectroscopy. *J. Biomech. Eng.-Trans. ASME* 1994;116:384-392.
- Bhandari M, Adili A, Lachowski RJ. High pressure pulsatile lavage of contaminated human tibiae: an in vitro study. *J. Orthop. Trauma* 1998;12:479-484.
- Bi XH, Yang X, Bostrom MPG, Camacho NP. Fourier transform infrared imaging spectroscopy investigations in the pathogenesis and repair of cartilage. *Biochim. Biophys. Acta-Biomembr.* 2006;1758:934-941.
- Blankevoort L, Kuiper JH, Huiskes R, Grootenboer HJ. Articular contact in a 3-dimensional model of the knee. *J. Biomech.* 1991;24:1019-1031.
- Brandt KD, Myers SL, Burr D, Albrecht M. Osteoarthritic changes in canine articular cartilage, subchondral bone, and synovium 54 months after transection of the anterior cruciate ligament. *Arthritis Rheum.* 1991;34:1560-1570.
- Brittberg M, Winalski CS. Evaluation of cartilage injuries and repair. *J. Bone Joint Surg. Am.* 2003;85A Suppl 2:58-69.

- Brown CP, Bowden JC, Rintoul L, Meder R, Oloyede A, Crawford RW. Diffuse reflectance near infrared spectroscopy can distinguish normal from enzymatically digested cartilage. *Phys. Med. Biol.* 2009;54:5579-5594.
- Brown CP, Hughes SW, Crawford RW, Oloyede A. Ultrasound assessment of articular cartilage: analysis of the frequency profile of reflected signals from naturally and artificially degraded samples. *Connect. Tissue Res.* 2007;48:277-285.
- Brown CP, Jayadev C, Glyn-Jones S, Carr AJ, Murray DW, Price AJ, Gill HS. Characterization of early stage cartilage degradation using diffuse reflectance near infrared spectroscopy. *Phys. Med. Biol.* 2011;56:2299-2307.
- Buckwalter JA, Mankin HJ. Articular cartilage .1. Tissue design and chondrocyte-matrix interactions. *J. Joint Bone Surg. Am.* 1997;79A:600-611.
- Byrick RJ, Bell RS, Kay JC, Waddell JP, Mullen JB. High-volume, high-pressure pulsatile lavage during cemented arthroplasty. *J. Bone Joint Surg. Am.* 1989;71A:1331-1336.
- Calvo E, Palacios I, Delgado E, Ruiz-Cabello J, Hernandez P, Sanchez-Pernaute O, Egido J, Herrero-Beaumont G. High-resolution MRI detects cartilage swelling at the early stages of experimental osteoarthritis. *Osteoarthritis Cartilage* 2001;9:463-472.
- Camacho NP, West P, Torzilli PA, Mendelsohn R. FTIR microscopic imaging of collagen and proteoglycan in bovine cartilage. *Biopolymers* 2001;62:1-8.
- Caprise PA, Miclau T, Dahners LE, Dirschl DR. High-pressure pulsatile lavage irrigation of contaminated fractures: effects on fracture healing. *J. Orthop. Res.* 2002;20:1205-1209.
- Castriota-Scanderbeg A, DeMicheli V, Scarale MG, Bonetti MG, Cammisa M. Precision of sonographic measurement of articular cartilage: Inter- and intraobserver analysis. *Skeletal Radiol.* 1996;25:545-549.
- Chao J, Kalunian K. Ultrasonography in osteoarthritis: recent advances and prospects for the future. *Curr. Opin. Rheumatol.* 2008;20:560-564.
- Chen SS, Falcovitz YH, Schneiderman R, Maroudas A, Sah RL. Depth-dependent compressive properties of normal aged human femoral head articular cartilage: relationship to fixed charge density. *Osteoarthritis Cartilage* 2001;9:561-569.
- Cherin E, Saied A, Laugier P, Netter P, Berger G. Evaluation of acoustical parameter sensitivity to age-related and osteoarthritic changes in articular cartilage using 50-MHz ultrasound. *Ultrasound Med. Biol.* 1998;24:341-354.

- Chiang EH, Adler RS, Meyer CR, Rubin JM, Dedrick DK, Laing TJ. Quantitative assessment of surface-roughness using backscattered ultrasound - the effect of finite surface curvature. *Ultrasound Med. Biol.* 1994;20:123-135.
- Chiang EH, Laing TJ, Meyer CR, Boes JL, Rubin JM, Adler RS. Ultrasonic characterization of in vitro osteoarthritic articular cartilage with validation by confocal microscopy. *Ultrasound Med. Biol.* 1997;23:205-213.
- Chu CR, Lin D, Geisler JL, Chu CT, Fu FH, Pan YT. Arthroscopic microscopy of articular cartilage using optical coherence tomography. *Am. J. Sports Med.* 2004;32:699-709.
- Conaghan PG, Hunter DJ, Maillefert JF, Reichmann WM, Losina E. Summary and recommendations of the OARSI FDA osteoarthritis Assessment of Structural Change Working Group. *Osteoarthritis Cartilage* 2011;19:606-610.
- Cooperberg PL, Tsang I, Truelove L, Knickerbocker J. Gray scale ultrasound in evaluation of rheumatoid arthritis of knee. *Radiology* 1978;126:759-763.
- Dashefsky JH. Arthroscopic measurement of chondromalacia of patella cartilage using a microminiature pressure transducer. *Arthroscopy* 1987;3:80-85.
- Disler DG, Raymond E, May DA, Wayne JS, McCauley TR. Articular cartilage defects: in vitro evaluation of accuracy and interobserver reliability for detection and grading with US. *Radiology* 2000;215:846-851.
- Duda GN, Kleemann RU, Bluecher U, Weiler A. A new device to detect early cartilage degeneration. *Am. J. Sports Med.* 2004;32:693-698.
- Eckstein F, Burstein D, Link TM. Quantitative MRI of cartilage and bone: degenerative changes in osteoarthritis. *NMR Biomed.* 2006;19:822-854.
- Foster FS, Pavlin CJ, Harasiewicz KA, Christopher DA, Turnbull DH. Advances in ultrasound biomicroscopy. *Ultrasound Med. Biol.* 2000;26:1-27.
- Fournier C, Bridal SL, Berger G, Laugier P. Reproducibility of skin characterization with backscattered spectra (12-25 MHz) in healthy subjects. *Ultrasound Med. Biol.* 2001;27:603-610.
- Friedman L, Finlay K, Jurriaans E. Ultrasound of the knee. *Skeletal Radiol.* 2001;30:361-377.
- Fuchs KH. Minimally invasive surgery. *Endoscopy* 2002;34:154-159.
- Gardner DL, Salter DM, Oates K. Advances in the microscopy of osteoarthritis. *Microsc. Res. Tech.* 1997;37:245-270.

- Gefen A, Megido-Ravid M, Azariah M, Itzhak Y, Arcan M. Integration of plantar soft tissue stiffness measurements in routine MRI of the diabetic foot. *Clin. Biomech.* 2001;16:921-925.
- Giurea M, Aichroth PM, Duri Z. Classification of articular cartilage lesions of the knee at arthroscopy. *Knee* 1998;5:159-164.
- Gluer CC, Blake G, Lu Y, Blunt BA, Jergas M, Genant HK. Accurate assessment of precision errors - how to measure the reproducibility of bone densitometry techniques. *Osteoporos. Int.* 1995;5:262-270.
- Grassi W. Clinical evaluation versus ultrasonography: Who is the winner? *J. Rheumatol.* 2003;30:908-909.
- Grassi W, Filippucci E, Farina A. Ultrasonography in osteoarthritis. *Semin. Arthritis Rheum.* 2005;34:19-23.
- Grassi W, Lamanna G, Farina A, Cervini C. Sonographic imaging of normal and osteoarthritic cartilage. *Semin. Arthritis Rheum.* 1999;28:398-403.
- Guilak F, Ratcliffe A, Lane N, Rosenwasser MP, Mow VC. Mechanical and biochemical changes in the superficial zone of articular cartilage in canine experimental osteoarthritis. *J. Orthop. Res.* 1994;12:474-484.
- Gur A, Cosut A, Sarac AJ, Cevik R, Nas K, Uyar A. Efficacy of different therapy regimes of low-power laser in painful osteoarthritis of the knee: A double-blind and randomized-controlled trial. *Lasers Surg. Med.* 2003;33:330-338.
- Han LH, Noble JA, Burcher M. A novel ultrasound indentation system for measuring biomechanical properties of *in vivo* soft tissue. *Ultrasound Med. Biol.* 2003;29:813-823.
- Harris ED, Radin EL, Krane SM, Parker HG. Effects of proteolytic-enzymes on structural and mechanical properties of cartilage. *Arthritis Rheum.* 1972;15:497-503.
- Hasler EM, Herzog W, Wu JZ, Muller W, Wyss U. Articular cartilage biomechanics: theoretical models, material properties, and biosynthetic response. *Crit. Rev. Biomed. Eng.* 1999;27:415-488.
- Hattori K, Mori K, Habata T, Takakura Y, Ikeuchi K. Measurement of the mechanical condition of articular cartilage with an ultrasonic probe: quantitative evaluation using wavelet transformation. *Clin. Biomech.* 2003;18:553-557.

- Hattori K, Takakura Y, Ishimura M, Habata T, Uematsu K, Ikeuchi K. Quantitative arthroscopic ultrasound evaluation of living human cartilage. *Clin. Biomech.* 2004;19:213-216.
- Hayes WC, Herrmann G, Mockros LF, Keer LM. A mathematical analysis for indentation tests of articular cartilage. *J. Biomech.* 1972;5:541-551.
- Herrmann JM, Pitris C, Bouma BE, Boppart SA, Jesser CA, Stamper DL, Fujimoto JG, Brezinski ME. High resolution imaging of normal and osteoarthritic cartilage with optical coherence tomography. *J. Rheumatol.* 1999;26:627-635.
- Herzog W. Articular Cartilage. *Wiley Encyclopedia of Biomedical Engineering* 2006;DOI: 10.1002/9780471740360.ebs0233.
- Hodge WA, Fijan RS, Carlson KL, Burgess RG, Harris WH, Mann RW. Contact pressures in the human hip joint measured in vivo. *Proc. Natl. Acad. Sci. USA* 1986;83:2879-2883.
- Hollander AP, Heathfield TF, Webber C, Iwata Y, Bourne R, Rorabeck C, Poole AR. Increased damage to type-II collagen in osteoarthritic articular cartilage detected by a new immunoassay. *J. Clin. Invest.* 1994;93:1722-1732.
- Honl M, Rentzsch R, Uebeyli H, Hille E, Morlock M, Louis H. Water-jet cutting in medical use - an overview, In: Ciccu R, ed. *Jet Cutting Technology, Proceedings of the 15th International Conference on Jetting Technology*. Westminster: Professional Engineering Publishing Ltd., 2000. pp. 183-196.
- Hsu CC, Tsai WC, Chen CPC, Shau YW, Wang CL, Chen MJL, Chang KJ. Effects of aging on the plantar soft tissue properties under the metatarsal heads at different impact velocities. *Ultrasound Med. Biol.* 2005;31:1423-1429.
- Hsu DK, Hughes MS. Simultaneous ultrasonic velocity and sample thickness measurement and application in composites. *J. Acoust. Soc. Am.* 1992;92:669-675.
- Hsu TC, Wang CL, Tsai WC, Kuo JK, Tang FT. Comparison of the mechanical properties of the heel pad between young and elderly adults. *Arch. Phys. Med. Rehabil.* 1998;79:1101-1104.
- Huang YP, Saarakkala S, Toyras J, Wang LK, Jurvelin JS, Zheng YP. Effects of optical beam angle on quantitative optical coherence tomography (OCT) in normal and surface degenerated bovine articular cartilage. *Phys. Med. Biol.* 2011;56:491-509.

- Huang YP, Zheng YP, Leung SF. Quasi-linear viscoelastic properties of fibrotic neck tissues obtained from ultrasound indentation tests in vivo. *Clin. Biomech.* 2005;20:145-154.
- Huang YP, Zheng YP, Wang SZ, Chen ZP, Huang QH, He YH. An optical coherence tomography (OCT)-based air jet indentation system for measuring the mechanical properties of soft tissues. *Meas. Sci. Technol.* 2009;20:015805.
- Hunter DJ, Lo GH, Gale D, Grainger AJ, Guermazi A, Conaghan PG. The reliability of a new scoring system for knee osteoarthritis MRI and the validity of bone marrow lesion assessment: BLOKS (Boston-Leeds Osteoarthritis Knee Score). *Ann. Rheum. Dis.* 2008;67:206-211.
- Ishihara M, Sato M, Kaneshiro N, Mitani G, Sato S, Mochida J, Kikuchi M. Development of a diagnostic system for osteoarthritis using a photoacoustic measurement method. *Lasers Surg. Med.* 2006;38:249-255.
- Jacobson JA. The knee, In: O'Neill J, ed. *Musculoskeletal ultrasound*: Springer, 2008. pp. 199-222.
- Ju JH, Kang KY, Kim IJ, Yoon JU, Kim HY, Park SH. Three-dimensional ultrasonographic application for analyzing synovial hypertrophy of the knee in patients with osteoarthritis. *J. Ultrasound Med.* 2008;27:729-736.
- Jurvelin JS, Rasanen T, Kolmonen P, Lyyra T. Comparison of optical, needle probe and ultrasonic techniques for the measurement of articular-cartilage thickness. *J. Biomech.* 1995;28:231-235.
- Kaab MJ, Ito K, Clark JM, Notzli HP. The acute structural changes of loaded articular cartilage following meniscectomy or ACL-transection. *Osteoarthritis Cartilage* 2000;8:464-473.
- Kaleva E, Saarakkala S, Jurvelin JS, Viren T, Toyras J. Effects of ultrasound beam angle and surface roughness on the quantitative ultrasound parameters of articular cartilage. *Ultrasound Med. Biol.* 2009;35:1344-1351.
- Kallioniemi AS, Jurvelin JS, Nieminen MT, Lammi MJ, Toyras J. Contrast agent enhanced pQCT of articular cartilage. *Phys. Med. Biol.* 2007;52:1209-1219.
- Kane D, Balint PV, Sturrock R, Grassi W. Musculoskeletal ultrasound--a state of the art review in rheumatology. Part 1: Current controversies and issues in the development of musculoskeletal ultrasound in rheumatology. *Rheumatology* 2004a;43:823-828.

- Kane D, Grassi W, Sturrock R, Balint PV. Musculoskeletal ultrasound--a state of the art review in rheumatology. Part 2: Clinical indications for musculoskeletal ultrasound in rheumatology. *Rheumatology* 2004b;43:829-838.
- Karvonen RL, Negendank WG, Teitge RA, Reed AH, Miller PR, Fernandezmadrid F. Factors affecting articular-cartilage thickness in osteoarthritis and aging. *J. Rheumatol.* 1994;21:1310-1318.
- Kawchuk GN, Elliott PD. Validation of displacement measurements obtained from ultrasonic images during indentation testing. *Ultrasound Med. Biol.* 1998;24:105-111.
- Kempson GE. Relationship between the tensile properties of articular cartilage from the human and age. *Ann. Rheum. Dis.* 1982;41:508-511.
- Kempson GE, Freeman MAR, Swanson SAV. Tensile properties of articular cartilage. *Nature* 1968;220:1127-1128.
- Kerdok AE, Ottensmeyer MP, Howe RD. Effects of perfusion on the viscoelastic characteristics of liver. *J. Biomech.* 2006;39:2221-2231.
- Kim J, Ahn B, De S, Srinivasan MA. An efficient soft tissue characterization algorithm from in vivo indentation experiments for medical simulation. *Int. J. Med. Robot. Comput. Assist. Surg.* 2008;4:277-285.
- Kim YH, Song SJ, Lee JK. Simultaneous measurements of the ultrasonic wave velocity and thickness of a solid plate made from one side of the plate. *Meas. Sci. Technol.* 2003;14:N13-N16.
- Kiviranta P, Lammentausta E, Toyras J, Kiviranta I, Jurvelin JS. Indentation diagnostics of cartilage degeneration. *Osteoarthritis Cartilage* 2008;16:796-804.
- Klaesner JW, Hastings MK, Zou DQ, Lewis C, Mueller MJ. Plantar tissue stiffness in patients with diabetes mellitus and peripheral neuropathy. *Arch. Phys. Med. Rehabil.* 2002;83:1796-1801.
- Knecht S, Vanwanseele B, Stussi E. A review on the mechanical quality of articular cartilage - implications for the diagnosis of osteoarthritis. *Clin. Biomech.* 2006;21:999-1012.
- Korhonen RK, Laasanen MS, Toyras J, Lappalainen R, Helminen HJ, Jurvelin JS. Fibril reinforced poroelastic model predicts specifically mechanical behavior of normal, proteoglycan depleted and collagen degraded articular cartilage. *J. Biomech.* 2003a;36:1373-1379.

- Korhonen RK, Saarakkala S, Toyras J, Laasanen MS, Kiviranta K, Jurvelin JS. Experimental and numerical validation for the novel configuration of an arthroscopic indentation instrument. *Phys. Med. Biol.* 2003b;48:1565-1576.
- Kornaat PR, Ceulemans RYT, Kroon HM, Riyazi N, Kloppenburg M, Carter WO, Woodworth TG, Bloem JL. MRI assessment of knee osteoarthritis: Knee Osteoarthritis Scoring System (KOSS) - inter-observer and intra-observer reproducibility of a compartment-based scoring system. *Skeletal Radiol.* 2005;34:95-102.
- Kuettner K, Goldberg VM. Introduction, In: Kuettner K and Goldberg VM, ed. Osteoarthritic disorders. Rosemont: American Academy of Orthopaedic Surgeons, 1995. pp. xxi-xxv.
- Laasanen MS, Saarakkala S, Toyras J, Hirvonen J, Rieppo J, Korhonen RK, Jurvelin JS. Ultrasound indentation of bovine knee articular cartilage in situ. *J. Biomech.* 2003a;36:1259-1267.
- Laasanen MS, Saarakkala S, Toyras J, Rieppo J, Jurvelin JS. Site-specific ultrasound reflection properties and superficial collagen content of bovine knee articular cartilage. *Phys. Med. Biol.* 2005;50:3221-3233.
- Laasanen MS, Toyras J, Hirvonen J, Saarakkala S, Korhonen RK, Nieminen MT, Kiviranta I, Jurvelin JS. Novel mechano-acoustic technique and instrument for diagnosis of cartilage degeneration. *Physiol. Meas.* 2002;23:491-503.
- Laasanen MS, Toyras J, Vasara A, Saarakkala S, Hyttinen MM, Kiviranta I, Jurvelin JS. Quantitative ultrasound imaging of spontaneous repair of porcine cartilage. *Osteoarthritis Cartilage* 2006;14:258-263.
- Laasanen MS, Toyras J, Vasara AI, Hyttinen MM, Saarakkala S, Hirvonen J, Jurvelin JS, Kiviranta I. Mechano-acoustic diagnosis of cartilage degeneration and repair. *J. Bone Joint Surg. Am.* 2003b;85A Suppl 2:78-84
- Lai WM, Hou JS, Mow VC. A triphasic theory for the swelling and deformation behaviors of articular cartilage. *J. Biomech. Eng.-Trans. ASME* 1991;113:245-258.
- Lamouche G, Kennedy BF, Kennedy KM, Bisailon CE, Curatolo A, Campbell G, Pazos V, Sampson DD. Review of tissue simulating phantoms with controllable optical, mechanical and structural properties for use in optical coherence tomography. *Biomed. Opt. Express* 2012;3:1381-1398.

- Landes CA, Goral W, Mack MG, Sader R. 3-D sonography for diagnosis of osteoarthritis and disk degeneration of the temporomandibular joint, compared with MRI. *Ultrasound Med. Biol.* 2006;32:627-632.
- Lau JCM, Li-Tsang CWP, Zheng YP. Application of tissue ultrasound palpation system (TUPS) in objective scar evaluation. *Burns* 2005;31:445-452.
- Lawrence RC, Helmick CG, Arnett FC, Deyo RA, Felson DT, Giannini EH, Heyse SP, Hirsch R, Hochberg MC, Hunder GG, Liang MH, Pillemer SR, Steen VD, Wolfe F. Estimates of the prevalence of arthritis and selected musculoskeletal disorders in the United States. *Arthritis Rheum.* 1998;41:778-799.
- Le Graverand MPH, Mazzuca S, Lassere M, Guermazi A, Pickering E, Brandt K, Peterfy C, Cline G, Nevitt M, Woodworth T, Conaghan P, Vignon E, Radiography Working G. Assessment of the radioanatomic positioning of the osteoarthritic knee in serial radiographs: comparison of three acquisition techniques. *Osteoarthritis Cartilage* 2006;14:A37-A43.
- Le Pen C, Reygrobelle C, Gerentes I. Financial cost of osteoarthritis in France - the "COART" France study. *Joint Bone Spine* 2005;72:567-570.
- Lee CL, Huang MH, Chai CY, Chen CH, Su JY, Tien YC. The validity of in vivo ultrasonographic grading of osteoarthritic femoral condylar cartilage: a comparison with in vitro ultrasonographic and histologic gradings. *Osteoarthritis Cartilage* 2008;16:352-358.
- Lefebvre F, Graillat N, Cherin E, Berger G, Saied A. Automatic three-dimensional reconstruction and characterization of articular cartilage from high-resolution ultrasound acquisitions. *Ultrasound Med. Biol.* 1998;24:1369-1381.
- LeRoux MA, Arokoski J, Vail TP, Guilak F, Hyttinen MM, Kiviranta I, Setton LA. Simultaneous changes in the mechanical properties, quantitative collagen organization, and proteoglycan concentration of articular cartilage following canine meniscectomy. *J. Orthop. Res.* 2000;18:383-392.
- Leung KS, Qin L, Leung MCT, Fu LLK, Chan CW. Partial patellectomy induces a decrease in the proteoglycan content in the remaining patellar articular cartilage. An experimental study in rabbits. *Clin. Exp. Rheumatol.* 1999;17:597-600.
- Leung SF, Zheng YP, Choi CYK, Mak SSS, Chiu SKW, Zee B, Mak AFT. Quantitative measurement of post-irradiation neck fibrosis based on the young modulus - description of a new method and clinical results. *Cancer* 2002;95:656-662.

- Ling HY, Zheng YP, Patil SG. Strain dependence of ultrasound speed in bovine articular cartilage under compression *in vitro*. *Ultrasound Med. Biol.* 2007;33:1599-1608.
- Loehne HB. Pulsatile lavage with suction, In: Sussman C and Bates-Jensen B, ed. *Wound Care: A Collaborative Practice Manual for Health Professionals*. Philadelphia, PA: Lippincott Williams & Wilkins, 2007. pp. 665-682.
- Loening AM, James IE, Levenston ME, Badger AM, Frank EH, Kurz B, Nuttall ME, Hung HH, Blake SM, Grodzinsky AJ, Lark MW. Injurious mechanical compression of bovine articular cartilage induces chondrocyte apoptosis. *Arch. Biochem. Biophys.* 2000;381:205-212.
- Loyola-Sanchez A, Richardson J, Beattie KA, Otero-Fuentes C, Adachi JD, MacIntyre NJ. Effect of low-intensity pulsed ultrasound on the cartilage repair in people with mild to moderate knee osteoarthritis: a double-blinded, randomized, placebo-controlled pilot study. *Arch. Phys. Med. Rehabil.* 2012;93:35-42.
- Lu MH, Zheng YP, Huang QH. A novel noncontact ultrasound indentation system for measurement of tissue material properties using water jet compression. *Ultrasound Med. Biol.* 2005;31:817-826.
- Lu MH, Zheng YP, Huang QH. A novel method to obtain modulus image of soft tissues using ultrasound water jet indentation: a phantom study. *IEEE Trans. Biomed. Eng.* 2007;54:114-121.
- Lu MH, Zheng YP, Huang QH, Ling C, Wang Q, Bridal L, Qin L, Mak A. Noncontact evaluation of articular cartilage degeneration using a novel ultrasound water jet indentation system. *Ann. Biomed. Eng.* 2009;37:164-175.
- Lu XL, Sun DDN, Guo XE, Chen FH, Lai WM, Mow VC. Indentation determined mechanoelectrochemical properties and fixed charge density of articular cartilage. *Ann. Biomed. Eng.* 2004;32:370-379.
- Lyyra-Laitinen T, Niinimäki M, Toyras J, Lindgren R, Kiviranta I, Jurvelin JS. Optimization of the arthroscopic indentation instrument for the measurement of thin cartilage stiffness. *Phys. Med. Biol.* 1999;44:2511-2524.
- Lyyra T, Arokoski JPA, Oksala N, Vihko A, Hyttinen M, Jurvelin JS, Kiviranta I. Experimental validation of arthroscopic cartilage stiffness measurement using enzymatically degraded cartilage samples. *Phys. Med. Biol.* 1999a;44:525-535.

- Lyyra T, Jurvelin J, Pitkanen P, Vaatainen U, Kiviranta I. Indentation instrument for the measurement of cartilage stiffness under arthroscopic control. *Med. Eng. Phys.* 1995;17:395-399.
- Lyyra T, Kiviranta I, Vaatainen U, Helminen HJ, Jurvelin JS. In vivo characterization of indentation stiffness of articular cartilage in the normal human knee. *J. Biomed. Mater. Res.* 1999b;48:482-487.
- Mak AF, Lai WM, Mow VC. Biphasic indentation of articular cartilage. I. Theoretical analysis. *J. Biomech.* 1987;20:703-714.
- Makhsous M, Venkatasubramanian G, Chawla A, Pathak Y, Priebe M, Rymer WZ, Lin F. Investigation of soft-tissue stiffness alteration in denervated human tissue using an ultrasound indentation system. *J. Spinal Cord. Med.* 2008;31:88-96.
- Mankin HJ, Dorfman H, Lippiell L, Zarins A. Biochemical and metabolic abnormalities in articular cartilage from osteo-arthritic human hips. 2. Correlation of morphology with biochemical and metabolic data. *J. Bone Joint Surg. Am.* 1971;53A:523-537.
- Mann RW. Comment on 'ultrasonic measurement of the thickness of human articular cartilage in situ' by Yao and Seedhom. *Rheumatology* 2001;40:829-831.
- Marticke JK, Hosselbarth A, Hoffmeier KL, Marintschev I, Otto S, Lange M, Plettenberg HKW, Spahn G, Hofmann GO. How do visual, spectroscopic and biomechanical changes of cartilage correlate in osteoarthritic knee joints? *Clin. Biomech.* 2010;25:332-340.
- Martino F, Ettorre GC, Patella V, Macarini L, Moretti B, Pesce V, Resta L. Articular cartilage echography as a criterion of the evolution of osteoarthritis of the knee. *Int. J. Clin. Pharmacol. Res.* 1993;13:35-42.
- McCune WJ, Dedrick DK, Aisen AM, Macguire A. Sonographic evaluation of osteoarthritic femoral condylar cartilage - correlation with operative findings. *Clin. Orthop. Relat. Res.* 1990;254:230-235.
- Meenagh G, Filippucci E, Iagnocco A, Delle Sedie A, Riente L, Bombardieri S, Valesini G, Grassi W. Ultrasound imaging for the rheumatologist - VIII. Ultrasound imaging in osteoarthritis. *Clin. Exp. Rheumatol.* 2007;25:172-175.
- Modest VE, Murphy MC, Mann RW. Optical verification of a technique for in-situ ultrasonic measurement of articular-cartilage thickness. *J. Biomech.* 1989;22:171-176.

- Moller I, Bong D, Naredo E, Filippucci E, Carrasco I, Moragues C, Iagnocco A. Ultrasound in the study and monitoring of osteoarthritis. *Osteoarthritis Cartilage* 2008;16 Suppl 3:S4-7.
- Mouritz AP, Townsend C, Khan MZS. Non-destructive detection of fatigue damage in thick composites by pulse-echo ultrasonics. *Compos. Sci. Technol.* 2000;60:23-32.
- Mow VC, Gibbs MC, Lai WM, Zhu WB, Athanasiou KA. Biphasic indentation of articular cartilage. II. A numerical algorithm and an experimental study. *J. Biomech.* 1989;22:853 - 861.
- Mow VC, Gu WY, Chen FH. Structure and function of articular cartilage and meniscus, In: Mow VC and Huiskes R, ed. *Basic Orthopaedic Biomechanics and Mechano-Biology*: Lippincott Williams & Wilkins, 2005. pp. 181-258.
- Mow VC, Kuei SC, Lai WM, Armstrong CG. Biphasic creep and stress-relaxation of articular cartilage in compression - theory and experiments. *J. Biomech. Eng.-Trans. ASME* 1980;102:73-84.
- Myers SL, Dines K, Brandt DA, Brandt KD, Albrecht ME. Experimental assessment by high-frequency ultrasound of articular cartilage thickness and osteoarthritic changes. *J. Rheumatol.* 1995;22:109-116.
- Niederauer GG, Niederauer GM, Cullen LC, Athanasiou KA, Thomas JB, Niederauer MQ. Correlation of cartilage stiffness to thickness and level of degeneration using a handheld indentation probe. *Ann. Biomed. Eng.* 2004;32:352-359.
- Nieminen HJ, Julkunen P, Toyras J, Jurvelin JS. Ultrasound speed in articular cartilage under mechanical compression. *Ultrasound Med. Biol.* 2007;33:1755-1766.
- Nieminen HJ, Saarakkala S, Laasanen MS, Hirvonen J, Jurvelin JS, Toyras J. Ultrasound attenuation in normal and spontaneously degenerated articular cartilage. *Ultrasound Med. Biol.* 2004;30:493-500.
- Nieminen HJ, Toyras J, Rieppo J, Nieminen MT, Hirvonen J, Korhonen R, Jurvelin JS. Real-time ultrasound analysis of articular cartilage degradation *in vitro*. *Ultrasound Med. Biol.* 2002;28:519 - 525.
- Nieminen HJ, Zheng YP, Saarakkala S, Wang Q, Toyras J, Huang YP, Jurvelin J. Quantitative assessment of articular cartilage using high-frequency ultrasound: research findings and diagnostic prospects. *Crit. Rev. Biomed. Eng.* 2009;37:461-494.

- Nitta N, Shiina T. A visualization of nonlinear elasticity property of tissues by ultrasound. *Electron. Comm. Jpn. III - Fundam. Electron. Sci.* 2002;85:9-18.
- Oakley SP, Lassere MN. A critical appraisal of quantitative arthroscopy as an outcome measure in osteoarthritis of the knee. *Semin. Arthritis Rheum.* 2003;33:83-105.
- Outerbridge RE. The etiology of chondromalacia patellae. *J Bone Joint Surg Br* 1961;43-B:752 - 757.
- Paillet-Mattei C, Bec S, Zahouani H. In vivo measurements of the elastic mechanical properties of human skin by indentation tests. *Med. Eng. Phys.* 2008;30:599-606.
- Palmer AW, Guldberg RE, Levenston ME. Analysis of cartilage matrix fixed charge density and three-dimensional morphology via contrast-enhanced microcomputed tomography. *Proc. Natl. Acad. Sci. USA* 2006;103:19255-19260.
- Pan YT, Li ZG, Xie TQ, Chu CR. Hand-held arthroscopic optical coherence tomography for *in vivo* high-resolution imaging of articular cartilage. *J. Biomed. Opt.* 2003;8:648-654.
- Patil SG, Zheng YP, Wu JY, Shi J. Measurement of depth-dependence and anisotropy of ultrasound speed of bovine articular cartilage *in vitro*. *Ultrasound Med. Biol.* 2004;30:953-963.
- Pelletier JP, Martel-Pelletier J, Abramson SB. Osteoarthritis, an inflammatory disease - potential implication for the selection of new therapeutic targets. *Arthritis Rheum.* 2001;44:1237-1247.
- Peterfy CG, Guermazi A, Zaim S, Tirman PFJ, Miaux Y, White D, Kothari M, Lu Y, Fye K, Zhao S, Genant HK. Whole-organ magnetic resonance imaging score (WORMS) of the knee in osteoarthritis. *Osteoarthritis Cartilage* 2004;12:177-190.
- Piscaer TM, Waarsing JH, Kops N, Pavljasevic P, Verhaar JAN, van Osch G, Weinans H. In vivo imaging of cartilage degeneration using mu CT-arthrography. *Osteoarthritis Cartilage* 2008;16:1011-1017.
- Pritzker KPH, Gay S, Jimenez SA, Ostergaard K, Pelletier JP, Revell PA, Salter D, van den Berg WB. Osteoarthritis cartilage histopathology: grading and staging. *Osteoarthritis Cartilage* 2006;14:13-29.
- Rasanen T, Messner K. Regional variations of indentation stiffness and thickness of normal rabbit knee articular cartilage. *J. Biomed. Mater. Res.* 1996;31:519-524.

- Rogowska J, Bryant CM, Brezinski ME. Cartilage thickness measurements from optical coherence tomography. *J. Opt. Soc. Am. A - Opt. Image Sci. Vis.* 2003;20:357-367.
- Rome K, Webb P, Unsworth A, Haslock I. Heel pad stiffness in runners with plantar heel pain. *Clin. Biomech.* 2001;16:901-905.
- Rutkow IM. Surgical operations in the United States - then (1983) and now (1994). *Arch. Surg.* 1997;132:983-990.
- Saarakkala S, Jurvelin JS, Zheng YP, Nieminen HJ, Toyras J. Quantitative information from ultrasound evaluation of articular cartilage should be interpreted with care. *Arthroscopy* 2007;23:1137-1138.
- Saarakkala S, Laasanen MS, Jurvelin JS, Torronen K, Lammi MJ, Lappalainen R, Toyras J. Ultrasound indentation of normal and spontaneously degenerated bovine articular cartilage. *Osteoarthritis Cartilage* 2003;11:697-705.
- Saarakkala S, Laasanen MS, Jurvelin JS, Toyras J. Quantitative ultrasound imaging detects degenerative changes in articular cartilage surface and subchondral bone. *Phys. Med. Biol.* 2006;51:5333-5346.
- Saarakkala S, Toyras J, Hirvonen J, Laasanen MS, Lappalainen R, Jurvelin JS. Ultrasonic quantitation of superficial degradation of articular cartilage. *Ultrasound Med. Biol.* 2004;30:783-792.
- Saarakkala S, Wang SZ, Huang YP, Zheng YP. Quantification of optical surface reflection and surface roughness of articular cartilage using optical coherence tomography. *Phys. Med. Biol.* 2009;54:6837-6852.
- Sachs JR, Grodzinsky AJ. Electromechanical spectroscopy of cartilage using a surface probe with applied mechanical displacement. *J. Biomech.* 1995;28:963-976.
- Sah RL, Yang AS, Chen AC, Hant JJ, Halili RB, Yoshioka M, Amiel D, Coutts RD. Physical properties of rabbit articular cartilage after transection of the anterior cruciate ligament. *J. Orthop. Res.* 1997;15:197-203.
- Samani A, Plewes D. A method to measure the hyperelastic parameters of ex vivo breast tissue samples. *Phys. Med. Biol.* 2004;49:4395-4405.
- Schinagl RM, Gurskis D, Chen AC, Sah RL. Depth-dependent confined compression modulus of full-thickness bovine articular cartilage. *J. Orthop. Res.* 1997;15:499-506.

- Scott WW, Lethbridgecejku M, Reichle R, Wigley FM, Tobin JD, Hochberg MC. Reliability of grading scales for individual radiographic features of osteoarthritis of the knee - the Blatimore longitudinal study of aging atlas of knee osteoarthritis. *Invest. Radiol.* 1993;28:497-501.
- Setton LA, Mow VC, Muller FJ, Pita JC, Howell DS. Mechanical properties of canine articular cartilage are significantly altered following transection of the anterior cruciate ligament. *J. Orthop. Res.* 1994;12:451-463.
- Sharma L, Kapoor D, Issa S. Epidemiology of osteoarthritis: an update. *Curr. Opin. Rheumatol.* 2006;18:147-156.
- Shingleton WD, Hodges DJ, Brick P, Cawston TE. Collagenase: a key enzyme in collagen turnover. *Biochem. Cell Biol.* 1996;74:759-775.
- Silver-Thorn MB. In vivo indentation of lower extremity limb soft tissues. *IEEE Trans. Rehabil. Eng.* 1999;7:268-277.
- Simon BR, Liable JP, Pflaster D, Yuan Y, Krag MH. A poroelastic finite element formulation including transport and swelling in soft tissue structures. *J. Biomech. Eng.-Trans. ASME* 1996;118:1-9.
- Simon WH. Scale effects in animal joints. 1. Articular cartilage thickness and compressive stress. *Arthritis Rheum.* 1970;13:244-255.
- Simon WH. Scale effects in animal joints. 2. Thickness and elasticity in deformability of articular cartilage. *Arthritis Rheum.* 1971;14:493-502.
- Spahn G, Klinger HM, Baums M, Hoffmann M, Plettenberg H, Kroker A, Hofmann GO. Near-Infrared spectroscopy for arthroscopic evaluation of cartilage lesions results of a blinded, prospective, interobserver study. *Am. J. Sports Med.* 2010;38:2516-2521.
- Spahn G, Klinger HM, Baums M, Pinkepank U, Hofmann GO. Reliability in arthroscopic grading of cartilage lesions: results of a prospective blinded study for evaluation of inter-observer reliability. *Arch. Orthop. Trauma Surg.* 2011;131:377-381.
- Spahn G, Klinger HM, Hofmann GO. How valid is the arthroscopic diagnosis of cartilage lesions? Results of an opinion survey among highly experienced arthroscopic surgeons. *Arch. Orthop. Trauma Surg.* 2009;129:1117-1121.
- Spahn G, Plettenberg H, Hoffmann M, Pfeiffer B, Klinger HM, Kirschbaum S. Semiquantitative evaluation of chondral damages by near infrared spectroscopy. *Osteoarthritis Cartilage* 2004;12:S121.

- Spahn G, Plettenberg H, Kahl E, Klinger HM, Muckley T, Hofmann GO. Near-infrared (NIR) spectroscopy. A new method for arthroscopic evaluation of low grade degenerated cartilage lesions. Results of a pilot study. BMC Musculoskelet. Disord. 2007;8:47.
- Spahn G, Plettenberg H, Nagel H, Kahl E, Klinger HM, Muckley T, Gunther M, Hofmann GO, Mollenhauer JA. Evaluation of cartilage defects with near-infrared spectroscopy (NIR): an *ex vivo* study. Med. Eng. Phys. 2008;30:285-292.
- Spriet MP, Girard CA, Foster SF, Harasiewicz K, Holdsworth DW, Lavery S. Validation of a 40 MHz B-scan ultrasound biomicroscope for the evaluation of osteoarthritis lesions in an animal model. Osteoarthritis Cartilage 2005;13:171-179.
- Suh JKF, Youn I, Fu FH. An in situ calibration of an ultrasound transducer: a potential application for an ultrasonic indentation test of articular cartilage. J. Biomech. 2001;34:1347-1353.
- Sun DD, Guo XE, Likhitpanichkul M, Lai WM, Mow VC. The influence of the fixed negative charges on mechanical and electrical behaviors of articular cartilage under unconfined compression. J. Biomech. Eng.-Trans. ASME 2004;126:6-16.
- Thorsos EI. The validity of the Kirchhoff approximation for rough surface scattering using a Gaussian roughness spectrum. J. Acoust. Soc. Am. 1988;83:78-92.
- Thorsos EI, Jackson DR. The validity of the perturbation approximation for rough surface scattering using a Gaussian spectrum. J. Acoust. Soc. Am. 1989;86:261-277.
- Tiderius CJ, Olsson LE, Leander P, Ekberg O, Dahlberg L. Delayed gadolinium-enhanced MRI of cartilage (dGEMRIC) in early knee osteoarthritis. Magn. Reson. Med. 2003;49:488-492.
- Tonuk E, Silver-Thorn MB. Nonlinear elastic material property estimation of lower extremity residual limb tissues. IEEE Trans. Neural Syst. Rehabil. Eng. 2003;11:43-53.
- Toyras J, Korhonen RK, Voutilainen T, Jurvelin JS, Lappalainen R. Improvement of arthroscopic cartilage stiffness probe using amorphous diamond coating. J. Biomed. Mater. Res. B Appl. Biomater. 2005;73B:15-22.
- Toyras J, Laasanen MS, Saarakkala S, Lammi MJ, Rieppo J, Kurkijarvi J, Lappalainen R, Jurvelin JS. Speed of sound in normal and degenerated bovine articular cartilage. Ultrasound Med. Biol. 2003;29:447-454.

- Toyras J, Rieppo J, Nieminen MT, Helminen HJ, Jurvelin JS. Characterization of enzymatically induced degradation of articular cartilage using high frequency ultrasound. *Phys. Med. Biol.* 1999;44:2723-2733.
- Treuting R. Minimally invasive orthopedic surgery: arthroscopy. *The Ochsner Journal* 2000;2:158-163.
- Tsai CY, Lee CL, Chai CY, Chen CH, Su JY, Huang HT, Huang MH. The validity of in vitro ultrasonographic grading of osteoarthritic femoral condylar cartilage - a comparison with histologic grading. *Osteoarthritis Cartilage* 2007;15:245-250.
- Vannah WM, Childress DS. Indentor tests and finite element modeling of bulk muscular tissue in vivo. *J. Rehabil. Res. Dev.* 1996;33:239-252.
- Varga F, Drzik M, Handl M, Chlpik J, Kos P, Filova E, Rampichova M, Necas A, Trc T, Amler E. Biomechanical characterization of cartilages by a novel approach of blunt impact testing. *Physiol. Res.* 2007;56:S61-S68.
- Vignon E, Bejui J, Mathieu P, Hartmann JD, Ville G, Evreux JC, Descotes J. Histological cartilage changes in a rabbit model of osteoarthritis. *J. Rheumatol.* 1987;14:104-106.
- Wakefield RJ, Gibbon WW, Emery P. The current status of ultrasonography in rheumatology. *Rheumatology* 1999;38:195-198.
- Walther M, Harms H, Krenn V, Radke S, Faehndrich TP, Gohlke F. Correlation of power Doppler sonography with vascularity of the synovial tissue of the knee joint in patients with osteoarthritis and rheumatoid arthritis. *Arthritis Rheum.* 2001;44:331-338.
- Wang Q, Zheng YP, Niu HJ, Mak AFT. Extraction of mechanical properties of articular cartilage from osmotic swelling behavior monitored using high frequency ultrasound. *J. Biomech. Eng.-Trans. ASME* 2007;129:413-422.
- Wang Q, Zheng YP, Qin L, Huang QH, Lam WL, Leung G, Guo X, Lu HB. Real-time ultrasonic assessment of progressive proteoglycan depletion in articular cartilage. *Ultrasound Med. Biol.* 2008;34:1085-1092.
- Wang SZ, Huang YP, Saarakkala S, Zheng YP. Quantitative assessment of articular cartilage with morphologic, acoustic and mechanical properties obtained using high frequency ultrasound. *Ultrasound Med. Biol.* 2010a;36:512-527.
- Wang SZ, Huang YP, Wang Q, Zheng YP, He YH. Assessment of depth and degeneration dependences of articular cartilage refractive index using optical coherence tomography *in vitro*. *Connect. Tissue Res.* 2010b;51:36-47.

- Wang YX, Guo YZ, Zhang LH, Niu HJ, Xu M, Zhao B, Wan WB. Ultrasound biomicroscopy for the detection of early osteoarthritis in an animal model. *Acad. Radiol.* 2011;18:167-173.
- Watson PJ, Carpenter TA, Hall LD, Tyler JA. Cartilage swelling and loss in a spontaneous model of osteoarthritis visualized by magnetic resonance imaging. *Osteoarthritis Cartilage* 1996;4:197-207.
- West PA, Bostrom MPG, Torzilli PA, Camacho NP. Fourier transform infrared spectral analysis of degenerative cartilage: an infrared fiber optic probe and imaging study. *Appl. Spectrosc.* 2004;58:376-381.
- Williams A, Gillis A, McKenzie C, Po B, Sharma L, Micheli L, McKeon B, Burstein D. Glycosaminoglycan distribution in cartilage as determined by delayed gadolinium-enhanced MRI of cartilage (dGEMRIC): Potential clinical applications. *Am. J. Roentgenol.* 2004;182:167-172.
- Woo J, Lau E, Lau CS, Lee P, Zhang J, Kwok T, Chan C, Chiu P, Chan KM, Chan A, Lam D. Socioeconomic impact of osteoarthritis in Hong Kong: utilization of health and social services, and direct and indirect costs. *Arthritis Rheum.* 2003;49:526-534.
- Wu JZ, Herzog W, Epstein M. Evaluation of the finite element software ABAQUS for biomechanical modelling of biphasic tissues. *J. Biomech.* 1998;31:165-169.
- Xie L, Lin ASP, Levenston ME, Guldberg RE. Quantitative assessment of articular cartilage morphology via EPIC-mu CT. *Osteoarthritis Cartilage* 2009;17:313-320.
- Yang TQ, Broschat SL. A comparison of scattering model results for 2-dimensional randomly rough surfaces. *IEEE Trans. Antennas Propag.* 1992;40:1505-1512.
- Yao JQ, Seedhom BB. Ultrasonic measurement of the thickness of human articular cartilage *in situ*. *Rheumatology* 1999;38:1269-1271.
- Yoshioka M, Coutts RD, Amiel D, Hacker SA. Characterization of a model of osteoarthritis in the rabbit knee. *Osteoarthritis Cartilage* 1996;4:87-98.
- Zhang M, Zheng YP, Mak AFT. Estimating the effective Young's modulus of soft tissues from indentation tests - nonlinear finite element analysis of effects of friction and large deformation. *Med. Eng. Phys.* 1997;19:512-517.
- Zheng YP, Choi YKC, Wong K, Chan S, Mak AFT. Biomechanical assessment of plantar foot tissue in diabetic patients using an ultrasound indentation system. *Ultrasound Med. Biol.* 2000a;26:451-456.

- Zheng YP, Huang YP. More intrinsic parameters should be used in assessing degeneration of articular cartilage with quantitative ultrasound. *Arthritis Res. Ther.* 2008;10:125.
- Zheng YP, Huang YP, Zhu YP, Wong M, He JF, Huang ZM. Development of a foot scanner for assessing the mechanical properties of plantar soft tissues under different bodyweight loading in standing. *Med. Eng. Phys.* 2012;34:506-511.
- Zheng YP, Leung SF, Mak AFT. Assessment of neck tissue fibrosis using an ultrasound palpation system: a feasibility study. *Med. Biol. Eng. Comput.* 2000b;38:497-502.
- Zheng YP, Li ZM, Choi APC, Lu MH, Chen X, Huang QH. Ultrasound palpation sensor for tissue thickness and elasticity measurement - assessment of transverse carpal ligament. *Ultrasonics* 2006;44:E313-E317.
- Zheng YP, Mak AFT. An ultrasound indentation system for biomechanical properties assessment of soft tissues *in-vivo*. *IEEE Trans. Biomed. Eng.* 1996;43:912-918.